Nutrient-dependent regulation of histone homeostasis in *Saccharomyces cerevisiae*

Dissertation

DER FAKULTÄT FÜR BIOLOGIE
DER LUDWIG-MAXIMILIANS-UNIVERSITÄT MÜNCHEN

Zur Erlangung des Doktorgrades der Naturwissenschaften
Doctor rerum naturalium (Dr. rer. nat.)

vorgelegt von

Dimitra Chatzitheodoridou

München, Mai 2023

This work was carried out in the laboratory of Dr. Kurt Schmoller at the Institute of Functional Epigenetics, Helmholtz Centre Munich.

First examiner:	Prof. Dr. Pascal Falter-Braun
Second examiner:	Prof. Dr. Christof Osman
Day of submission:	Mai 31, 2023
Day of oral examination:	February 8, 2024

Eidesstattliche Erklärung

Ich versichere hiermit an Eides statt, dass die vorliegende Dissertation mit dem Titel „Nutrient-dependent regulation of histone homeostasis in *Saccharomyces cerevisiae*“ von mir selbstständig und ohne unerlaubte Hilfe angefertigt ist.

München, 31.05.2023 ……

(Dimitra Chatzitheodoridou)

Erklärung

Ich erkläre hiermit, dass die vorliegende Dissertation mit dem Titel „Nutrient-dependent regulation of histone homeostasis in *Saccharomyces cerevisiae*“ weder ganz noch in wesentlichen Teilen einer anderen Prüfungskommission vorgelegt worden ist. Weiterhin, habe ich mich nicht anderweitig ohne Erfolg einer Doktorprüfung unterzogen.

München, 31.05.2023 ……

(Dimitra Chatzitheodoridou)

Parts of this study have been published in:

1) K.-L. Claude, D. Bureik, D. Chatzitheodoridou, P. Adarska, A. Singh, K. M. Schmoller, Transcription coordinates histone amounts and genome content. *Nat Commun*. **12**, 4202 (2021).

2) D. Chatzitheodoridou, D. Bureik, F. Padovani, K. V. Nadimpalli, K. M. Schmoller, Decoupling of transcript and protein concentrations ensures budding yeast histone homeostasis in different nutrient conditions. *bioRxiv* (2023), doi:10.1101/2023.01.26.525696.

Acknowledgements

I would like to acknowledge and extend my sincere thanks to my supervisor Dr. Kurt Schmoller, who offered me the opportunity to work on this exciting project and embark on a four-year journey of learning, self-discovery and professional growth. With his expertise, scientific knowledge and remarkably positive attitude, Kurt motivated me to ask the right questions, think outside the box and find my own path as a researcher. I am also grateful for the great discussions and brainstorming sessions, which helped shape the course of this project.

My special thanks go to the members of the thesis advisory committee, Prof. Dr. Pascal Falter-Braun and Prof. Dr. Christof Osman who have accompanied me through this journey, sharing their expertise and providing invaluable scientific advice. I would like to express my gratitude to Prof. Dr. Pascal Falter-Braun for his guidance as my official doctoral supervisor and to Prof. Dr. Christof Osman for taking on the role of second examiner of this thesis.

I owe many thanks to Daniela Bureik, Kora-Lee Claude, and Francesco Padovani for their excellent scientific collaboration. I will always be grateful to Daniela and Kora-Lee for sharing their knowledge and helping me navigate the early stages of my PhD. I also thank Francesco for making data analysis much more enjoyable and for patiently answering all my questions.

Furthermore, I would like to thank all the members of the Schmoller research group as well as the IFE institute for all their support and the welcoming environment they provided. From the very beginning, I felt part of a driven scientific community that helped me grow and develop as a scientist. Special thanks to Yagya Chadha, Alissa Finster, Arohi Khurana, Benedikt Mairhörmann and Magdalena Valenta for all the fruitful discussions and good times we have shared over the years. Last, but not least, I would like to express my gratitude to Anika Seel for her scientific advice, moral support and friendship.

Finally, I have been blessed with incredibly supportive friends and family who have always encouraged me to pursue my goals in life. I am deeply grateful to my partner Zacharias for always being my rock, supporting me and lighting up the room with his presence.
From the bottom of my heart I would like to thank my parents for their love and unwavering faith in me. They are my greatest role models, and have made this journey possible. I am also eternally grateful to my sister Melina for her wisdom and heartfelt encouragement over the years. Her drive and creativity have always motivated me to stay curious and embark on new adventures.

Abstract

Regulation of cellular protein homeostasis in response to environmental challenges such as nutrient availability is essential for maintaining cell function and viability. The surrounding nutrients strongly influence cell growth and biosynthetic capacity, dictating, among others, cellular growth rate, cell size and cell cycle progression. Ensuring protein homeostasis therefore requires cells to tightly control RNA and protein concentrations, even when cell growth and the cell cycle are significantly modulated by nutrient conditions. This poses a challenge, especially for genes whose expression is highly regulated throughout the cell cycle. A comprehensive picture of how cells achieve nutrient-dependent homeostasis of periodically expressed genes remains elusive.

In this work, I study histone biogenesis in the model organism *Saccharomyces cerevisiae* to investigate how cells produce the appropriate amount of histones in different nutrient environments. Histones constitute an ideal model to understand differential regulation of cell cycle-regulated proteins, as their synthesis is strongly coordinated with the DNA replication during S-phase. Moreover, as building blocks of chromatin, histones are produced in proportion to the genome content, which requires accurate control of histone concentrations. To understand the regulatory processes underlying nutrient-dependent histone homeostasis, I perform population and single-cell analyses of histone expression at the protein and mRNA level.

Using western blots, flow cytometry and live-cell imaging, I first show that cells maintain constant amounts of the core histone H2B in rich and poor nutrients, independent of changes in cell growth and cell cycle. As a result, H2B concentrations increase in poor growth media, due to the smaller cell volumes. Surprisingly, however, I find that histone mRNA concentrations are downregulated in poor compared to rich nutrients. smFISH analysis of histone promoter-driven *mCitrine* expression further reveals that the promoter can confer this nutrient-dependent transcript regulation, which depends on regulatory elements within the promoter, as well as the transcriptional activator Spt10. Furthermore, my results suggest that cells in poor growth media are more sensitive to excess histone accumulation than cells in rich growth media. By keeping histone transcript levels low, they may therefore minimize the risk of histone overexpression. Finally, I propose that cells compensate for the

differentially regulated histone transcript concentrations by modulating the relative translation efficiency according to the nutrient conditions. Thereby, they can finely tune histone protein abundance across nutrients, while preventing high histone accumulation in poor growth media. Overall, I show that the decoupling of mRNA and protein concentrations enables nutrient-dependent histone homeostasis despite changes in cell growth and cell cycle phases. This work could lay the foundation for a deeper understanding of the differential regulation of cell cycle-regulated genes across changing nutrient environments.

List of Figures

List of Abbreviations

°C	Degree Celsius
3D	Three dimensions
A	Ampere
Acetyl-CoA	Acetyl coenzyme A
arb. u.	Arbitrary unit
bp	Base pair
cDNA	Complementary DNA
Cq	Quantification cycle
D	Dextrose/Glucose
Da	Dalton
DAPI	4′,6-diamidino-2-phenylindole
DNA	Deoxyribonucleic acid
E. coli	*Escherichia coli*
EDTA	Ethylenediaminetetraacetic acid
g	Gram
Gal	Galactose
GE	Glycerol ethanol
HRP	Horseradish peroxidase
k	Kilo
L	Litre
LB	Lysogeny broth
LDS	Lithium dodecyl sulphate
LED	Light emitting diode
LiOAc	Lithium acetate
m	Milli
M	Molar
min	Minute
mRNA	Messenger RNA

n	Nano
NAD	Nicotinamide adenine dinucleotide
OD	Optical density
ORF	Open reading frame
PCR	Polymerase chain reaction
PEG	Polyethylene glycol
RNA	Ribonucleic acid
rpm	Revolutions per minute
rRNA	Ribosomal RNA
RT	Room temperature
RT-qPCR	Reverse transcription quantitative PCR
s	Second
S. cerevisiae	*Saccharomyces cerevisiae*
SC	Synthetic complete
SD	Synthetic defined
SDS	Sodium dodecyl sulphate
smFISH	Single-molecule fluorescence in situ hybridization
SOC	Super optimal broth with catabolite repression
T	Temperature
TBS	Tris-buffered saline
TCA	Tricarboxylic acid
TE	Tris-EDTA
UTR	Untranslated region
V	Volt
v/v	Volume per volume
w/v	Weight per volume
WT	Wild-type
x g	Times gravity
YP	Yeast extract peptone
Δ	Delta
µ	Micro

Table of Contents

1 Introduction

1.1 Cellular protein homeostasis

Cellular protein homeostasis, or ‘proteostasis’, refers to the regulation of proteins from biosynthesis to degradation through highly interacting biological pathways *(1)*. The proteostasis network maintains a balanced and functional proteome by controlling protein concentrations, folding, trafficking, binding interactions and translocation to various cellular compartments (*1*–*6*). For this purpose the network is coordinated by integrated signaling pathways that respond to imbalances in proteome integrity (*2*, *5*). The complexity of the eukaryotic proteostasis network can vary significantly across different species. In higher eukaryotes, it is more complex in order to meet the requirements of cell- and tissue-specific proteomes and regulatory processes (*5*–*7*). Protein homeostasis is also regulated at the transcript level, as transcription, mRNA degradation and localisation all determine the availability of mRNA, and ultimately affect the biosynthesis of the encoded protein (*8*, *9*).

As proteins drive nearly all biological processes, accurate proteostasis is important for cell function and viability. A deficient or lost homeostasis is linked to cellular dysfunction, various diseases and aging (*2*–*5*, *10*). In human, the accumulation of misfolded or aggregating proteins is often associated with loss-of-function disorders (e.g. cystic fibrosis, Gaucher disease) or gain-of-toxic-function disorders (e.g. Alzheimer’s, Huntington’s and Parkinson’s disease), respectively (*2*–*4*). Moreover, the ability of cells to restore proteostasis declines with age, thereby increasing the susceptibility to these pathologies (*2*, *3*, *5*). However even in the absence of disease, a progressive deterioration of protein homeostasis contributes to various aspects of aging, as observed in diverse aging models (*11*–*14*). For example, in yeast it was shown that proteostasis breakdown in aging cells was accompanied by impaired chaperone activity and G1-cyclin function, ultimately leading to irreversible G1 arrest (*15*). Another study reported that large yeast and human cells lose the ability to scale transcription and translation according to cell size. This biosynthesis breakdown causes cytoplasm dilution, which can contribute to cellular senescence (*16*).

1.2 Environmental challenges to protein homeostasis

Maintaining protein homeostasis is fundamental, especially in the face of internal and external challenges, such as cell differentiation, or metabolic and environmental changes (*3*, *4*, *17–19*). During development, cellular differentiation drastically alters gene expression and thus the composition of the proteome. Therefore, proteostasis enables differentiated cells to change their functional type, allowing successful organismal development (*6*, *17*). Furthermore, cells must precisely control protein concentrations across different environmental conditions in spite of changes in cell growth and morphology that are induced by external factors such as temperature, pH, osmotic pressure, oxygen levels or nutrient quality (*20–26*).

One of the most common environmental parameters is ambient temperature, which exerts a great impact on cell physiology, growth and cell cycle progression (*20*, *21*, *27–29*). Within a specific temperature range, the cellular growth rate of mammalian cells and single cell organisms increases with temperature to a certain maximum, before it starts decreasing (*20*, *30–32*). In addition, the duration of the different cell cycle phases changes in response to the temperature variations (*20*, *31*, *33*). As proteostasis is critical for proper cell function, cells adapt to the external temperature using global transcription and translation strategies. A study in yeast has revealed that within the temperature range of 23°C to 37°C the overall protein concentration in cells remained constant (*34*). It was shown that cells sustain protein homeostasis by increasing global translation and protein degradation with temperature. Thereby decreased protein stability compensated for the increased translation rates at higher temperatures. However, an abnormal rise in environmental temperature eventually results in heat-induced protein denaturation, protein misfolding and aggregation, threatening proteome integrity and cellular fitness (*19*, *21*, *30*). To cope with thermal stress, cells employ a highly conserved survival mechanism termed the heat shock response (*21*, *35*, *36*). The heat shock transcription factor 1, HSF1, which is present as a monomer under normal conditions, trimerizes upon stress and promotes the expression of the heat shock proteins that refold misfolded or damaged proteins and prevent aggregation (*19*, *30*, *37*).

Other environmental challenges to proteostasis include fluctuations in oxygen concentration or osmotic pressure. Local oxygen levels affect cell growth, metabolism, signalling and differentiation (*17*, *24*, *38–42*). Studies in mammalian cells have shown that cell proliferation

and metabolic activity can decrease with increasing oxygen levels, potentially due to the formation of reactive oxygen species (*40*, *43*, *44*). Increased oxygen availability was also found to promote the differentiation of stem cells (*38*, *43*, *45*). On the other hand, low oxygen levels can induce cell cycle arrest in many cell types, preventing high oxygen consumption in hypoxic environments (*24*, *46*).

Furthermore, biophysical cues such as osmotic pressure have been studied for their effects on cell function and proliferation. Changes in osmotic pressure have been linked to variations in cell growth and cell cycle progression in different organisms and cell types (*23*, *47–49*). At the cellular level, elevated osmotic pressure can suppress proliferation (*23*, *50*). A recent study in human metastatic cells showed that mild hyperosmotic stress can lead to disturbed nuclear growth and cell cycle delay or arrest (*23*). Upon osmotic stress in *Saccharomyces cerevisiae*, the stress-activated protein kinase Hog1 modulates cell cycle progression through interaction with components of the cell cycle machinery. Specifically, it delays cell cycle-phase transitions to enable cells to adapt to hyperosmotic conditions (*49*, *51*, *52*). Moreover, external osmotic pressure has been reported to alter the volume and stiffness of stem cells, and ultimately affect stem cell differentiation (*53*).

Lastly, another major environmental challenge to protein homeostasis is the changing availability and quality of the surrounding nutrients. Effects of varying nutrient conditions on cell growth and cell cycle, as well as cellular responses maintaining proteostasis are discussed separately in the following section.

1.2.1 Protein homeostasis and cell growth under changing nutrient conditions

Nutrient availability exerts a great influence on cell growth and cell cycle progression, dictating cellular growth rate, cell size and the duration of the cell cycle phases. Unicellular organisms such as yeast or bacteria are limited by the extracellular nutritional environment, and are often growing as fast as the nutrient supply permits. Thus, in nutrient rich conditions, they tend to have higher growth rates than in nutrient-poor conditions (*54–56*). A landmark study conducted over six decades ago in the bacterium *Salmonella typhimurium* highlighted the coordination of cell size with growth rate and nutrient quality (*57*, *58*). When cultured in rich nutrients, the bacterial cells grew at a faster rate and were twice the size of the slower-growing

cells in poor nutrients. Eventually, the nutrient-dependent regulation of cell size and growth rate was further demonstrated in other types of bacteria (*59–61*). Similarly, yeast cells modulate their size and growth rate according to the nutrient environment, growing larger and faster in rich nutrients (*54*, *55*, *62*, *63*).

As the nutrient-dependent growth rate increases, cells produce higher concentrations of ribosomes to meet the demands of protein synthesis and allow for increased biosynthetic capacity (*54*, *64–66*). Thus, the nutrient environment not only dictates ribosome concentrations but also influences the rate of translation. Thereby, growth rate and protein synthesis are coordinated with nutrient availability ensuring cellular protein homeostasis. In eukaryotes, a central regulator of cell growth is TORC1, the target of the rapamycin complex 1 (*62*, *67–70*). TORC1 acts as a nutrient sensor, monitoring the availability of the surrounding nutrients and coupling it to cell growth. It also adjusts the balance between anabolic and catabolic processes in response to changing environments. In nutrient-rich conditions, TORC1 activates cell growth by promoting ribosome biogenesis and stimulating protein synthesis. The function of TORC1 is widely conserved among many eukaryotic organisms, from yeasts to mammals (*67*, *68*, *71*). However, unlike yeast, cells in multicellular organisms rely on multiple extracellular growth factors for proliferation (*54*, *70*, *72*).

Nutrients are also important determinants of cell cycle progression. Cells coordinate their cell cycle with external nutritional conditions by sensing and evaluating nutrient availability to decide whether it is appropriate to divide. Deprivation of nutrients or growth factors induces arrest of the cell cycle or prolongs the progression through G1 phase (*26*, *54*, *73*). A study by Hartwell et al. reported on the yeast START site in late G1, where cells commit to cell division (*74*). Later studies revealed that the commitment to cell cycle and hence passage through START is greatly influenced by the nutrient sensor TORC1 (*73*, *75*). While the mammalian equivalent to START, the restriction point, is strongly growth-factor dependent, studies also reported of late-G1 checkpoints regulated by amino acids and mTORC1, where mammalian cells assess their nutrient environment prior to committing to cell division (*73*, *76*).

Furthermore, nutrient regulation of cell cycle progression can result in the lengthening or shortening of G1. For example, yeast cells growing on rich medium move rapidly through G1, whereas cells on poor medium are delayed in their transition to S-phase. This allows them to reach the critical nutrient-specific cell size required for budding. Consequently, the fraction of unbudded cells increases in nutrient-poor conditions, leading to relatively smaller fractions of S and G2/M cells (*56*, *77–79*).

1.3 Aim of this study: Understanding histone protein homeostasis in different nutrients

Maintaining protein homeostasis is fundamental for normal cell function and requires cells to precisely control RNA and protein concentrations, especially in situations where cell growth and cell cycle progression are drastically modulated by environmental conditions. Nutrient availability is one of the most common environmental parameters, affecting, among others, cell size, growth rate and the length of cell cycle phases. Particularly, the nutrient-related cell cycle changes pose a major challenge to the homeostasis of cell cycle regulated proteins, whose expression profiles peak during short periods of the cell cycle. These periodically expressed proteins are involved in various cellular processes including DNA replication, DNA packaging and repair, protein biosynthesis, metabolism, cell cycle regulation and more (*80–84*). The total number of cycling genes in a cell varies considerably depending on the species. For example, 800 periodically expressed genes have been identified in the budding yeast *Saccharomyces cerevisiae*, representing >10% of all protein-coding genes (*83*). Other examples include the bacterium *Caulobacter crescentus*, which has been reported to contain 553 cell cycle-regulated genes (*85*), and primary human fibroblasts, which contain approximately 700 cycling genes (*86*). To maintain correct concentrations of the encoded proteins in different nutritional environments, cells need to coordinate gene expression with the nutrient-specific cell cycle. However, little is known about the nutrient-dependent regulation of periodically expressed proteins.

In this work, I will focus on histone biogenesis in the model organism *Saccharomyces cerevisiae* to investigate whether and how cells produce the right amount of histones in spite of the nutrient-induced changes in growth rate, cell volume, and cell cycle progression. Histones represent an ideal model to understand the differential regulation of cell cycle-regulated proteins in changing nutrients, as their expression is strongly coupled to the DNA replication and therefore restricted to late G1 and S-phase (*87*, *88*). As building blocks of chromatin, histones are also DNA-binding proteins, whose biosynthesis is coordinated with the genome content in constant environments (*89–91*). It is therefore important that histone concentrations are tightly controlled to avoid toxic effects such as genome instability caused by protein misregulation (*92*, *93*). By analyzing histone gene expression in different nutrient environments, I aim to uncover the regulatory processes underlying nutrient-dependent

histone homeostasis. This could further lay the groundwork for a better understanding of how cell cycle-regulated genes are regulated amidst nutrient-related changes in cell growth and cell cycle.

1.4 Yeast *Saccharomyces cerevisiae* as a model organism

Early yeast researchers realized that studies of yeast phenomena could provide key insights into various aspects of cell biology (*94*). The unicellular budding yeast *Saccharomyces cerevisiae* has since been widely used as a valuable model system for studying fundamental biological processes relevant to all eukaryotes, including gene expression, aging, cell cycle, cell division, metabolism and more (*94–96*). Despite being a simple eukaryote, budding yeast shares many conserved functional pathways with multicellular eukaryotes such as humans, and has contributed immensely to the understanding of several human diseases (*94*, *96*, *97*). For example, it has been estimated that the yeast genome contains orthologs of up to 22% of human genes associated with disease (*98*).

Budding yeast is a very popular model organism, as it is non-pathogenic, and inexpensive to grow in the laboratory due to its simple growth requirements. With a doubling time of about 90 min under optimal conditions, budding yeast can grow rapidly to high cell densities (Fig. 1). It can also be stored for weeks at 4°C or long-term in 15% glycerol at -80°C. Another important attribute is the easy and cost-effective genetic manipulation of yeast owing to the particularly efficient homologous recombination, which allows the integration, alteration or deletion of genes in the yeast genome (*94*, *97*, *99*). Budding yeast also offers many advances in live cell imaging, as it does not move during image acquisition and its simple shape allows for easy cell segmentation. Moreover, budding yeast cells can exist in both, haploid and diploid forms, facilitating genetic analyses such as the characterization of recessive mutations (*100*). In 1996, *S. cerevisiae* became the first eukaryote with a completely sequenced genome, which is composed of over 6,000 genes organized in 16 chromosomes (*97*, *101*). Subsequently, a functional genomics toolbox was developed, including strain libraries of yeast deletion and overexpression mutants as well as a comprehensive collection of green fluorescent protein (GFP)-labelled yeast strains (*96*, *102–104*). This in turn led to the emergence of many high-throughput technologies for genome-wide transcriptome, proteome or metabolome analysis and opened up new fields of computational biology, required to gain a systems view of a

eukaryotic cell (*96*, *105–108*). Finally, in the context of my research question, the relatively small number of eleven histone genes (*87*), whose regulation is fairly well studied, will be helpful in elucidating how cells maintain histone homeostasis in different nutrient conditions.

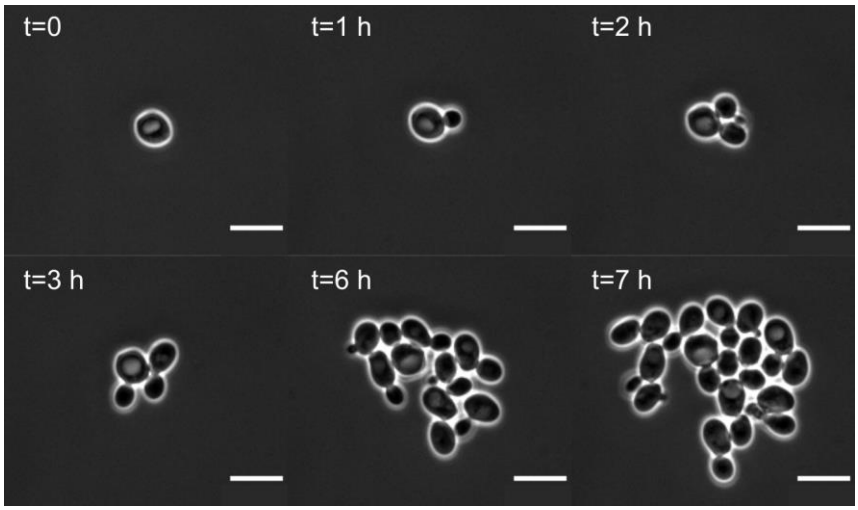

Figure 1. Growth of *S. cerevisiae* at 30°C on YPD (yeast peptone dextrose) medium. Representative phase-contrast images of rapidly dividing budding yeast cells were taken at different time points over the course of seven hours. Scale bar: 10 µm.

1.4.1 *S. cerevisiae* adapts to various nutrient conditions

Another key aspect of budding yeast that is advantageous for studying histone homeostasis across changing nutrient environments is its ability to easily adapt its growth and metabolism to a variety of available carbon sources. It is well established that *S. cerevisiae* utilizes glucose as the preferred carbon and energy source, as it can readily enter the glycolytic pathway (*109*, *110*). During glycolysis, glucose is then broken down into pyruvate by a set of enzyme-catalysed reactions. Pyruvate can further undergo two metabolic pathways, either fermentation or respiration. Alcoholic fermentation is considered an anaerobic process and generates ethanol, carbon dioxide and NAD+ in a two-step reaction. On the other hand, in the aerobic respiration pathway, pyruvate is oxidatively decarboxylated to acetyl-CoA, which is later oxidized to carbon dioxide in the tricarboxylic acid (TCA) cycle (*109*, *111*, *112*). While budding yeast is capable of both, alcoholic fermentation and respiration, the predominant pathway of glucose catabolism is fermentation, even under aerobic conditions. This is referred

to as the Crabtree effect, which states that in glucose-rich environments, fermentation overcomes respiration (*109*, *113*). Besides glucose, however, budding yeast cells can grow on a wide range of carbon sources, including fermentable and non-fermentable compounds. Alternative fermentable sugars are fructose, raffinose, galactose, maltose, and sucrose (*109*, *111*). For example, galactose is a monosaccharide that enters glycolysis after being converted into glucose-6-phosphate by enzymes of the Leloir pathway. In the presence of glucose, the GAL genes encoding the Leloir pathway enzymes are repressed, but become induced up to 1000-fold in glucose-starved cells that are growing on galactose (*109*, *114*). In addition to the fermentable carbon sources, budding yeast can also utilize non-fermentable compounds such as ethanol, glycerol, lactate or acetate through a major reprogramming of gene expression (*109*, *110*, *115*). For example, ethanol is aerobically metabolized in a three-step pathway to acetyl-CoA, which can subsequently enter the TCA cycle (*109*, *110*).

In the context of this work, the use of budding yeast makes it possible to test a great variety of nutrient changes that can result in different growth phenotypes challenging histone homeostasis. As mentioned in section 1.2.1, yeast cells respond to the nutrient environment by altering their growth rate and biosynthetic capacity, as well as their cell size and cell cycle (*54–56*, *64*, *78*, *79*). In rich nutrients, the cells are usually bigger, exhibiting higher growth rates and shorter cell cycles. They also tend to spend less time in G1, when grown on rich instead of poor growth media. A study of yeast growth under different nutritional conditions showed how cells adjusted their growth rate over a nearly sevenfold range, depending on the surrounding nutrients. At the same time, a more than two-fold change in cell size was measured across the cultures (*56*).

Along with the nutrient-related changes in cell growth and cell cycle, the transcriptome and proteome composition of budding yeast cells is adjusted in response to the nutrient environment (*64*, *116*, *117*). For example, Metzl-Raz et al. revealed that the fraction of translation-related proteins increased with the nutrient-dependent growth rate to support protein synthesis during faster growth. Specifically, it was found that the expression of ribosomal transcripts and proteins scales linearly with growth rate. On the other hand, slow-growing cells showed increased abundance of mitochondria and respiration-related proteins, as well as proteins involved in stress response (*64*).

1.4.2 Cell growth and cell cycle in budding yeast

S. cerevisiae cells divide asymmetrically through the process of budding, giving rise to a mother cell and a smaller daughter cell. The cell cycle can be divided into four consecutive stages, based on the chromosomal events (Fig. 2) (*118*). Cells first undergo the gap phase G1, growing to a critical size before they commit to cell division at START in late G1 (*77*). Passage through START is only possible if cellular and environmental conditions have been assessed appropriate for cell proliferation. Otherwise, cells may prolong the G1 period or even arrest in the nondividing, quiescent state G0 until conditions become favourable (*54*, *74*, *118*, *119*). After cell cycle commitment, cells replicate their DNA during S-phase and generate two copies of each chromosome. Moreover, a new bud emerges at the time they enter S-phase, which grows in size as they move through the cell cycle. In fact, the bud size can be a useful marker of cell cycle progression (*118*). The next phase of the cell cycle is the second gap phase, G2, which serves as a regulatory transition, ensuring that cells do not initiate nuclear division (mitosis) if DNA is damaged or replication is incomplete (*118*). Finally, in the following M-phase, mitosis and cell division (cytokinesis) occur. After the duplicated chromosomes are evenly distributed into the bud, the daughter cell separates from the mother, entering its own cell division cycle. Compared to other eukaryotic model systems, budding yeast undergoes a long G1 phase but has no clearly defined G2-phase, which is why the last cell cycle stages are often referred to as G2/M-phase (*118*). Haploid cells are also capable of mating, a process in which cells of the opposite mating type fuse into a diploid cell *(118)*. There are two mating types in *S. cerevisiae,* Mat a and Mat α, which release specific pheromones (a-factor and α-factor) causing the cells to arrest in G1 before they mate and form a stable Mat a/Mat α diploid cell (*118*, *120*). In response to stress such as nitrogen or carbon starvation, diploid budding yeast cells can undergo sporulation giving rise to four spores, two of each mating type, which can germinate once conditions become favourable (*118*, *121*).

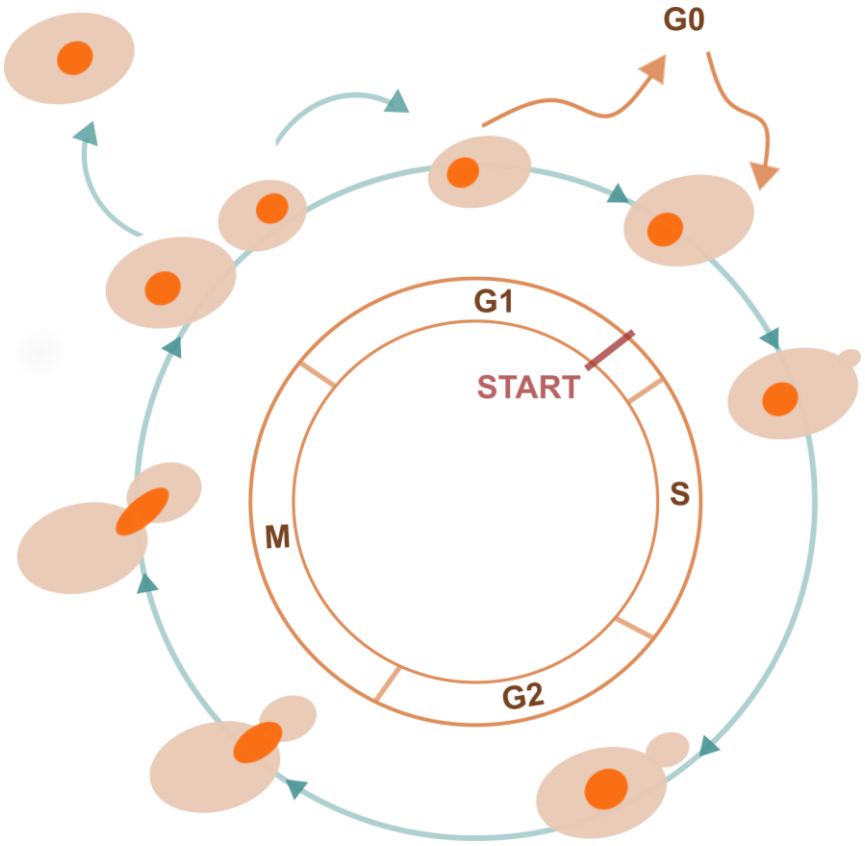

Figure 2. Cell cycle of *S. cerevisiae*. Schematic representation of a budding yeast cell as it progresses through the cell cycle phases. The cell first undergoes G1-phase, and grows in size before committing to the cell cycle. Afterwards, a new bud emerges and the cell enters S-phase, during which it replicates its DNA and duplicates the chromosomes. In the following stages, the chromosomes are evenly distributed into the bud and the cell divides asymmetrically, giving rise to a mother and a smaller daughter cell. Under unfavourable growth conditions, cells may refrain from entering the cell cycle and instead reside in G0 phase until conditions improve.

1.4.3 Histone regulation in budding yeast

Histones are evolutionary conserved positively charged proteins that associate with negatively charged DNA to form nucleosomes, which are the building blocks of chromatin *(87)*. Each nucleosome contains 147 bp of DNA wrapped around a histone octamer that is composed of eight histone proteins, two copies each of the four core histones—H2A, H2B, H3, and H4 *(118)*. In budding yeast, the histone octamers are arranged along the DNA with a repeat length of ~165 bp (*87*, *118*). The linker histone H1 binds the linker DNA between the nucleosomes and organizes the nucleosome arrays into a higher order chromatin structure. Yeast cells have

one H1 copy per 37 nucleosomes (*87*, *122*). Budding yeast also possesses two histone variants, H2A.Z (a H2A variant) and CenH3 (a H3 variant), which are expressed at low levels throughout the cell cycle (*87*, *123*). In contrast, the four core histones and the linker histone H1 are synthesized in a cell cycle-dependent manner, in parallel with DNA replication. Consequently, transcription of these histone genes is induced in late G1 to yield adequate histone amounts for efficient DNA packaging during S-phase (*88*, *124*). In fact, inhibition of DNA synthesis represses histone gene expression, highlighting the tight coupling between DNA replication and histone production (*87*, *123*).

In budding yeast, the four core histones are each encoded by two genes transcribed from divergent promoters *(87)* (Fig. 3). Specifically, histones H2A and H2B are encoded by the gene pairs, *HTA1-HTB1* and *HTA2-HTB2* (*125*), and histones H3 and H4 by the gene pairs *HHT1-HHF1* and *HHT2-HHF2* (*126*). Furthermore, the gene *HHO1* encodes the linker histone H1, whereas *HTZ1* and *CSE4* encode the variants H2A.Z and CenH3, respectively (*87*). In this work, I will focus on the core histone genes.

The core histone promoters contain positive and negative cis-acting regulatory elements that couple gene expression to DNA replication in S-phase *(87)*. For example, the cell cycle-dependent activation of core histone genes requires the four 16 bp upstream activating sequences (UASs), which provide binding sites for the transcriptional activators Spt10 and SBF (*87*, *123*). While SBF mediates a small initial expression peak of histone transcripts, Spt10 acts as a primary transcription activator, driving a major subsequent peak of histone transcript expression (*87*, *127*, *128*). Histone genes are further subject to negative regulation mediated by the HIR complex alongside Asf1 and Rtt106, which represses histone transcription outside of S-phase (*87*, *88*, *129*, *130*). The HIR-mediated regulation works via the NEG, a negative regulatory element located in three of the four core histone promoters, with the exception of the *HTA2–HTB2* promoter (*87*, *123*, *131*). Furthermore, at the post-transcriptional level, a Rad53-dependent pathway promotes degradation of excess histones to control cellular histone levels. Consequently, cells lacking the protein kinase Rad53 exhibit increased accumulation of histone proteins (*132*, *133*).

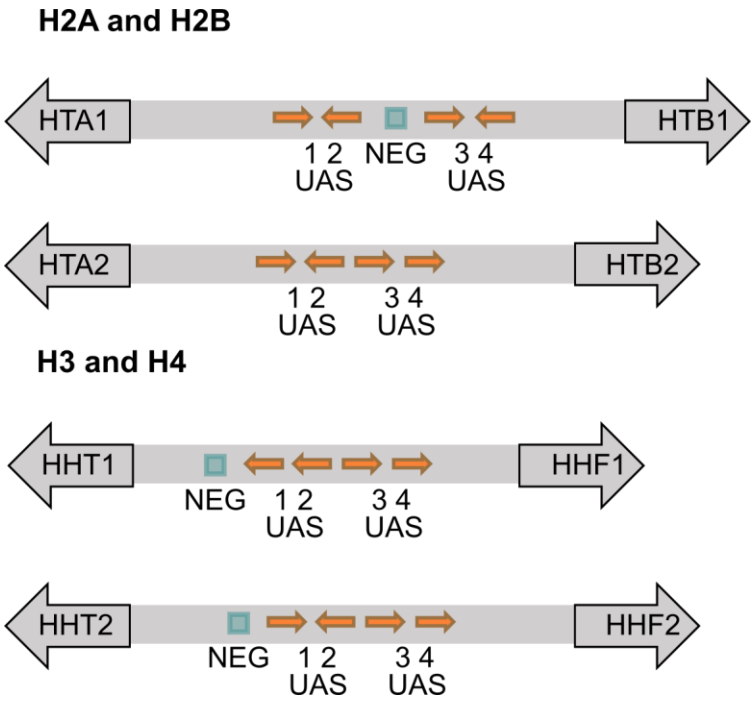

Figure 3. The *S. cerevisiae* core histone genes. Schematic representation of the gene pairs encoding the core histones H2A, H2B, H3 and H4. The orange arrows indicate the four UASs within the central histone promoters; the blue box shows the negative regulatory element NEG, which is present in three of the four core histone promoters (adapted from Eriksson et al. 2012, (*87*)).

1.4.4 Cell size-independent coordination of histones with genome content

Most proteins scale with cell size, ensuring constant protein concentrations as cells grow (Fig. 4A). This is because the biosynthesis of these proteins is typically limited by the transcription and translation machinery, which increases with cell size, leading to higher global transcription and translation rates in larger cells (*89*, *134–136*).

Given their significant role as building blocks of chromatin, histones must be tightly regulated throughout the cell cycle and their concentrations closely monitored. However, histone expression is tied to genome content rather than cell size *(89)*. Consequently, histone protein concentrations increase with ploidy, but decrease with cell size (Fig. 4B) *(89)*. Histones are coordinated with the genomic content already at the transcript level in a promoter-mediated manner (*89*). In fact, they have been described as a major group of sub-scaling mRNAs in yeast and other organisms (*90*, *91*). A possible explanation for the differential sub-scaling

behavior of histones is that their transcription is limited by the gene itself, rather than the transcriptional machinery, thereby linking the transcriptional output to genome content instead of cell volume (*89*). In this work, I will address the question of whether this distinct regulation of histones also occurs across changing nutrient environments by investigating the regulatory processes underlying nutrient-dependent histone homeostasis.

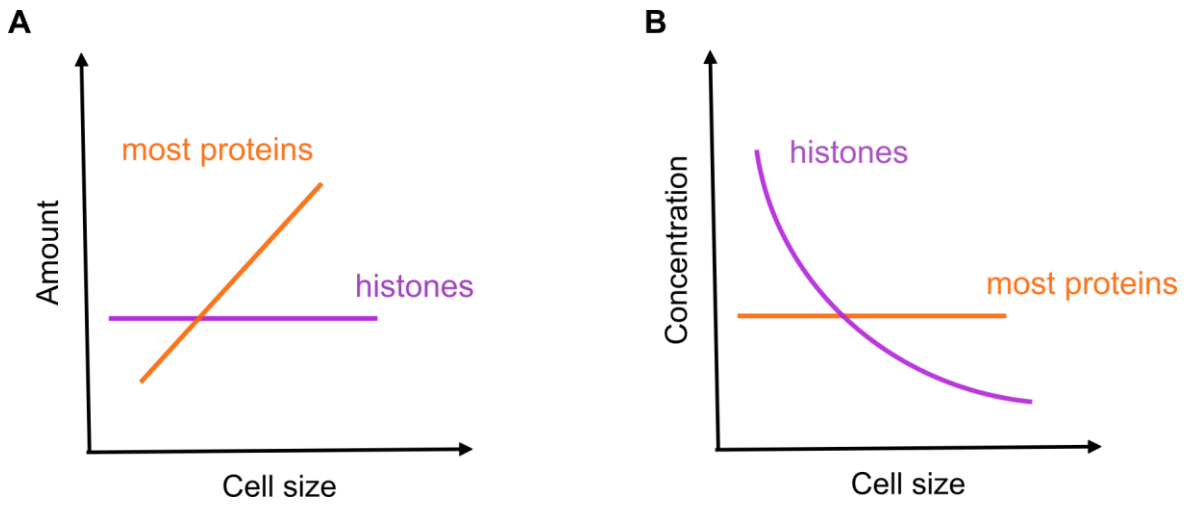

Figure 4. Histone proteins do not scale with cell size. (**A-B**) While the amount of most proteins increases with cell size to keep concentrations constant, histones are produced in a cell-size-independent manner, leading to reduced histone concentration with increasing cell size *(89)*.

1.5 Outline of this study

In this work, I will investigate the regulation of budding yeast histone homeostasis in changing environments and ask how cells maintain the right amount of histones in situations where cell growth and cell cycle progression are significantly altered by nutrients (Fig. 5). To this end, I will first select a set of rich and poor growth media with different compositions and characterize the induced phenotypic changes in wildtype cells, *i.e.* variations in doubling time, cell size and cell cycle phases. Next, I will perform population-level and single-cell protein analysis to quantify the histone H2B levels in varying nutrients. I will examine how the nutrient-dependent histone protein expression is coordinated with cell size, and ask if cells produce equal amounts of histones in all growth media. As a control, I will use the housekeeping protein actin, which is expected to scale with cell size (*89*, *90*). In a next step, I will test whether nutrient-dependent histone homeostasis occurs at the mRNA level. For this, I will measure histone mRNA

concentrations in rich and poor nutrients and disentangle the contribution of mRNA synthesis and degradation to the nutrient-dependent histone gene expression. To gain more insight, I will further investigate the role of the histone promoter in the transcriptional and post-transcriptional regulation of histones across the different nutrient conditions. For this, I will use population-level and single-cell techniques to measure the mRNA and protein levels of the reporter gene *mCitrine* driven by a histone promoter, in rich and poor growth media. Moreover, I will search for regulatory elements within the histone promoter that might contribute to the regulation of histone gene expression in the different nutrients.

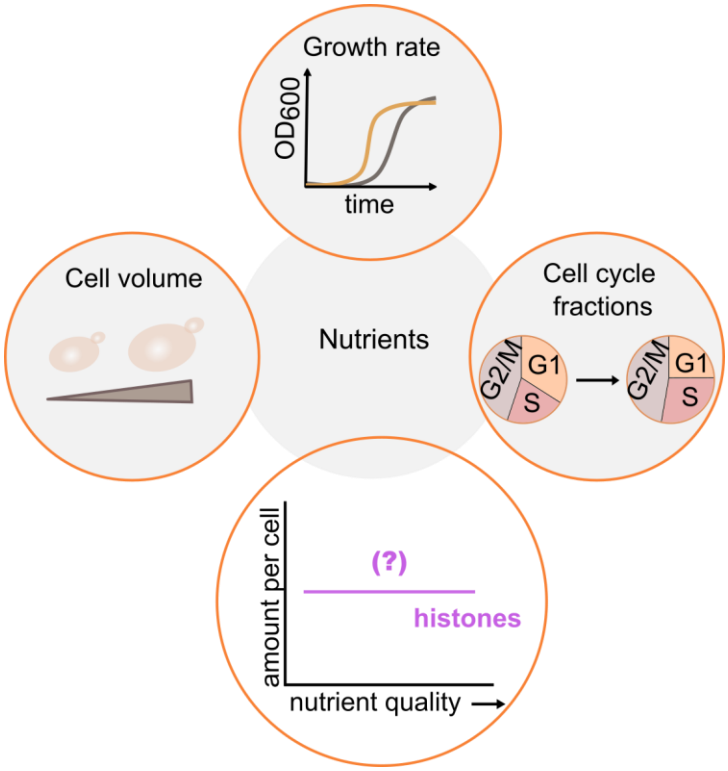

Figure 5. Budding yeast histone proteostasis in different nutritional environments. Nutrients are important determinants of growth rate, cell size and cell cycle. Therefore, fluctuations in nutrient availability pose a major challenge to the homeostasis of histone proteins, raising the questions of whether and how cells ensure a constant histone-to-DNA ratio regardless of the induced changes in cell growth and cell cycle.

2 Materials and Methods

2.1 Chemicals and Consumables

Table 1. Chemicals and consumables used in this work.

Chemicals and Consumables	Supplier
10X Bolt™ sample reducing agent	Invitrogen by Thermo Fisher Scientific, USA
1X Bolt™ MES SDS Running buffer	Invitrogen by Thermo Fisher Scientific, USA
4X Bolt™ LDS sample buffer	Invitrogen by Thermo Fisher Scientific, USA
Acetic acid, CH_3COOH	Honeywell Fluka, Germany
Alkaline phosphatase (CIP)	New England Biolabs, Germany
Amino acids	Sigma-Aldrich, USA
Ammonium sulfate	Sigma-Aldrich, USA
Ampicillin	Roth, Germany
Bolt™ 12% Bis-Tris plus mini-gels	Invitrogen by Thermo Fisher Scientific, USA
CellASIC® ONIX2 Y04C microfluidic plate	Merck Millipore, USA
Clarity™ western ECL substrate	Bio-Rad, USA
Coverslips (18 x 18 mm)	VWR International, USA
D(+) Glucose	Sigma-Aldrich, USA
Difco Agar, granulated	Th. Greyer, Germany
Dipotassium phosphate, K_2HPO_4	Sigma-Aldrich, USA
DNase I	Invitrogen by Thermo Fisher Scientific, USA
Ethanol, CH_3CH_2OH	Sigma-Aldrich, USA
EDTA	Sigma-Aldrich, USA
Formaldehyde 37%	PanReac AppliChem, Germany
Formamide	VWR International, USA
Galactose	Sigma-Aldrich, USA
Glass beads, acid-washed	Sigma-Aldrich, USA
Glycerol	Th. Greyer, Germany

High-capacity cDNA reverse transcription kit with RNase inhibitor	Applied biosystems by Thermo Fisher Scientific, USA
LB Broth (Lennox)	Sigma-Aldrich, USA
LB-Agar (Lennox)	Sigma-Aldrich, USA
LightCycler 480 Multiwell Plate 96	Roche, Schwitzerland
Lithium acetate dihydrate	Sigma-Aldrich, USA
Nitrocellulose membranes (0.2 µm pore size)	Invitrogen by Thermo Fisher Scientific, USA
Non-fat dried milk powder	PanReac AppliChem, Germany
NucleoSpin Gel and PCR Clean-up	Macherey-Nagel, Germany
NucleoSpin Plasmid kit	Macherey-Nagel, Germany
Peptone, BD Bacto™	Life Technologies, USA
Phenol:Chloroform:Isoamyl alcohol (25:24:1)	Thermo Fisher Scientific, USA
Phusion polymerase	Laboratory stock
Polyethylene glycol (PEG), BioXtra	Sigma-Aldrich, USA
Ponceau Red S	Sigma-Aldrich, USA
Proteinase K	Promega, USA
Restriction Enzymes	New England Biolabs, Germany
RNase A	Sigma-Aldrich, USA
RNAse-free water	Qiagen, Germany
Sodium chloride, NaCl	Supelco, USA
Sodium dodecyl sulfate (SDS)	Thermo Fisher Scientific, USA
Sodium hydroxide, NaOH	Thermo Fisher Scientific, USA
Sorbitol	Sigma-Aldrich, USA
SsoAdvanced™ universal SYBR® Green supermix	Bio-Rad, USA
Stellaris® smFISH probes	LGC Biosearch Technologies, UK
Stellaris® RNA FISH hybridization buffer	LGC Biosearch Technologies, UK
Stellaris® RNA FISH wash buffer A	LGC Biosearch Technologies, UK
SuperFrost Plus™ Adhesion slides (25x75x1mm)	Epredia, USA
SYBR® Green I	Sigma-Aldrich, USA
T4 DNA Ligase	Thermo Fisher Scientific, USA
Thiolutin	Biomol, Germany
Tris-HCl	Sigma-Aldrich, USA

Triton X 100	Roth, Germany
Tween 20	Roth, Germany
Vectashield® mounting medium	Vector Laboratories, US
Yeast extract, BD Bacto™	Biozol, Germany
Yeast nitrogen base	Becton Dickinson, USA
YeaStar RNA kit	Zymo Research, Germany
Zymolyase	Biomol, Germany
β-estradiol	Sigma-Aldrich, USA

2.2 Devices

Table 2. Devices used in this work.

Device	Supplier
Zeiss LSM 800 microscope	Zeiss, Germany
NanoDrop OneC	Thermo Fisher Scientific, USA
LightCycler® 96	Roche, Schwitzerland
CytoFlex S flow cytometer	Beckman Coulter, Germany
Ecotron shaking incubator	Infors HT, Switzerland
ChemiDocTM MP imaging system	Bio-Rad, USA
Mini gel tank	Invitrogen by Thermo Fisher Scientific, USA
Mini blot module	Invitrogen by Thermo Fisher Scientific, USA

2.3 Antibodies

Table 3. Primary and secondary antibodies used in this work.

Antibody	Host species	Supplier/Catalogue number	Dilution
Anti-histone H2B	rabbit	Abcam/ab188291	1:2000
Anti-β actin	mouse	Abcam/ab170325	1:10000
Goat Anti-Rabbit	goat	Abcam/ab205718	1:10000
Goat Anti-Mouse	goat	Abcam/ab205719	1:10000

2.4 Strains

Table 4. Yeast strains used in this work. All strains are derivatives of W303.

Name	Genotype	Description	Origin
ASY020-1	*Mat α/a; ADE2/ADE2, URA3/ura3, leu2/LEU2*	Diploid wildtype	Anika Seel, Schmoller Lab
CY14093	*Mat α; sml1Δ::hphMX3*	*sml1Δ* haploid strain	Christopher Bruhn
CY14098	*Mat α; sml1Δ::hphMX3, rad53Δ::natMX6*	*sml1Δrad53Δ* haploid strain	Christopher Bruhn
CY15164	*Mat α; sml1Δ::hphMX3, rad53Δ::natMX6, spt21Δ::kanMX6*	*sml1Δrad53Δspt21Δ* haploid strain	Christopher Bruhn
DBY020-2	*Mat α; ADE2, ura3::CglaTRP1-HTB1prom-mCitrine-ADH1term-URA3*	Haploid strain with *HTB1* promoter expressing mCitrine	Daniela Bureik, Schmoller Lab
DBY021-3	*Mat α; ADE2, ura3::CglaTRP1-HTB2prom-mCitrine-ADH1term-URA3*	Haploid strain with *HTB2* promoter expressing mCitrine	Daniela Bureik, Schmoller Lab
DBY052-2	*Mat a/α ; ADE2/ADE2, leu2-3/LEU2, URA3/ura3-1,htb1Δ::CglaTRP1/HTB1*	*HTB1/htb1Δ* diploid strain	
DBY053-4	*Mat a/α ; ADE2/ADE2, leu2-3/LEU2, URA3/ura3-1,htb1Δ::CglaTRP1/HTB1, htb2Δ::HIS3 /HTB2*	*HTB1/htb1Δ, htb2Δ/HTB2* diploid strain	Daniela Bureik, Schmoller Lab
DBY054-8	*Mat a/α ; ADE2/ADE2, leu2-3/LEU2, URA3/ura3-1, htb1Δ::CglaTRP1/HTB1, htb2Δ::HIS3 /htb2Δ::NatMX6*	*HTB1/htb1Δ, htb2Δ/htb2Δ* diploid strain	Daniela Bureik, Schmoller Lab
DCY001-1	*Mat α; ADE2, htb2::Htb2-linker-mCitrine-ADH1term-CglaTRP1, htb1::Htb1-linker-mCitrine-ADH1term-KlacURA3*	Haploid strain with mCitrine-tagged *HTB1* and *HTB2*	This study
DCY002-2	*Mat α; ADE2, ura3::CglaTRP1-HTB2prom-mCitrine-ADH11term-URA3,his3::ACT1prom-mKate2-ADH1term-HIS3*	Haploid strain with *HTB2* promoter expressing mCitrine and *ACT1* promoter expressing mKate2	This study
DCY003-6	*Mat α; ADE2, htb1::Htb1-linker-mCitrine-ADH1term-KlacURA3*	Haploid strain with mCitrine-tagged *HTB1*	This study

DCY006-1	*Mat α ; ADE2, ura3::CglaTRP1-HTB1prom (mutated UAS3/UAS4)-mCitrine-ADH1term-URA3,his3::ACT1pr-mKate2-ADH1term-HIS3*	Haploid strain expressing mCitrine under the *HTB1* promoter with mutated Spt10 binding sites in UAS3 and UAS4, and mKate2 under the A*CT1* promoter	This study
DCY008-8	*Mat α; ADE2, ura3::CglaTRP1-HTB1prom-mCitrine-ADH1term-URA3,his3::ACT1prom-mKate2-ADH1term-HIS3*	Haploid strain with *HTB1* promoter expressing mCitrine and *ACT1* promoter expressing mKate2	This study
DCY009-3	*Mat α; ADE2, htb1::Htb1-linker-mCitrine-HTB1term-CglaTRP1*	Haploid strain with mCitrine-tagged *HTB1* followed by the *HTB1* terminator sequence	This study
DCY011-1	*Mat α; ADE2, ura3::CglaTRP1-HTB1prom-MDN1 5'UTR-mCitrine-ADH1term-URA3*	Haploid strain with *HTB1* promoter and *MDN1* 5' UTR driving mCitrine	This study
DCY012-1	*Mat α; ADE2, ura3::CglaTRP1-HTB1prom-RPB4 5'UTR-mCitrine-ADH1term-URA3*	Haploid strain with *HTB1* promoter and *RPB4* 5' UTR driving mCitrine	This study
KCY002-3	*Mat α; ADE2, htb2::HTB2-linker-mCitrineADH1term-CglaTRP1*	Haploid strain with mCitrine-tagged *HTB2*	Kora-Lee Claude, Schmoller Lab
KCY005-1	*Mat α/a; ADE2/ADE2, whi5Δ::CglaTRP1/whi5Δ::kanMX6-LexAprom-WHI5-ADH1term-LEU2, his3/his3::LexA-ER-AD-TF-HIS3*	Whi5-inducible diploid strain	
KCY021-1	*Mat α; ADE2, ura3::CglaTRP1-300bpHTB1prom-mCitrine-ADH1term-URA3*	Haploid strain with truncated 300 bp *HTB1* promoter driving mCitrine	Kora-Lee Claude, Schmoller Lab
KCY022-1	*Mat α; ADE2, ura3::CglaTRP1-450bpHTB1prom-mCitrine-ADH1term-URA3*	Haploid strain with truncated 450 bp *HTB1* promoter driving mCitrine	Kora-Lee Claude, Schmoller Lab
KCY031-1	*Mat α/a; ADE2/ADE2, ura3::CglaTRP1-HTB1prom-mCitrine-ADH1term-URA3/ura3, WHI5/whi5Δ::kanMX6-LexAprom-WHI5-ADH1term-LEU2, his3/his3::LexA-ER-AD-TF-HIS3*	Whi5-inducible diploid strain with *HTB1* promoter driving mCitrine	Kora-Lee Claude, Schmoller Lab

KCY039-1	*Mat α/a; ADE2/ADE2, ura3::CglaTRP1-300bpHTB1prom-mCitrine-ADH1term-URA3/ura3, WHI5/whi5Δ::kanMX6-LexAprom-WHI5-ADH1term-LEU2, his3/his3::LexA-ER-AD-TF-HIS3*	Whi5-inducible diploid strain with truncated 300 bp *HTB1* promoter driving mCitrine	Kora-Lee Claude, Schmoller Lab
KCY041-1	*Mat α/a; ADE2/ADE2, ura3::CglaTRP1-450bpHTB1prom-mCitrine-ADH1term-URA3/ura3, WHI5/whi5Δ::kanMX6-LexAprom-WHI5-ADH1term-LEU2, his3/his3::LexA-ER-AD-TF-HIS3*	Whi5-inducible diploid strain with truncated 450 bp *HTB1* promoter driving mCitrine	Kora-Lee Claude, Schmoller Lab
KSY222-1	*Mat α; ADE2, ura3::CglaTRP1-HTB1prom-mCitrine-ADH1term-URA3, whi5Δ::kanMX6-LexAprom-WHI5-ADH1term-LEU2, his3::LexA-ER-AD-TF-HIS3*	Whi5-inducible haploid strain with *HTB1* promoter expressing mCitrine	Kurt Schmoller, Schmoller Lab
KSY229-1	*Mat α; ADE2, ura3::CglaTRP1-ACT1prom-mCitrine-ADH1term-URA3*	Haploid strain with *ACT1* promoter expressing mCitrine	Kurt Schmoller, Schmoller Lab
MMY116-2C	*Mat α; ADE2*	Haploid wildtype	Skotheim Lab

2.5 Plasmids

Table 5. Plasmids used in this work.

Plasmid	Description	Origin
DBE003-3	*full HTB1 promoter with mutated Spt10 binding sites in UAS3 and UAS4*	Daniela Bureik, Schmoller Lab
DCE001-1	*ACT1promotor-mKate2-ADH1term-HIS3*	This study
DCE003-3	*linker-mCitrine-HTB1term- CglaTRP1*	This study
KCE001-2	*linker-mCitrine-ADH1term-CglaTRP1*	Kora-Lee Claude, Schmoller Lab
KCE011-3	*linker-mCitrine-ADH1term- KlacURA3*	Kora-Lee Claude, Schmoller Lab
KSE166-4	*full HTB1 promoter*	Kurt Schmoller, Schmoller Lab

2.6 Oligonucleotides

Table 6. qPCR primers used in this work *(89)*. All primers were purchased from Sigma-Aldrich.

Gene	Primer direction	Primer sequence (5‘-3‘)
HTA1	forward	GTTGCCAAAGAAGTCTGCCA
	reverse	CAGTTTAGTTCCTTCCGCCTT
HTA2	forward	TCGCCCAAGGTGGTGTTTT
	reverse	TGATTTGCTTTGTTTCTTTTCAACT
HHF1	forward	TACACCGAACACGCCAAGAG
	reverse	TTGCTTGTTGTTACCGTTTTCTT
HHF2	forward	ACGAAGAAGTCAGAGCCGTC
	reverse	ACCGATTGTTTAACCACCGATTG
HHT1	forward	CAATCTTCTGCCATCGGTGC
	reverse	ACTGATGACAATCAACAAACTATGA
HHT2	forward	AGCAAACACTCCACAATGGC
	reverse	CAAGGCAACAGTACCTGGCT
HTB1	forward	TACACACATACAATGTCTGCTAAAG
	reverse	AGTGTCAGGGTGAGTTTGCTT
HTB2	forward	CCTCTGCCGCCGAAAAGAAA
	reverse	TCTTACCATCGACGGAGGTTG
ACT1	forward	AGTTGCCCCAGAAGAACACC
	reverse	GGACAAAACGGCTTGGATGG
mCitrine	forward	GAGCTGAAGGGCATCGACTT
	reverse	TTCTGCTTGTCGGCCATGAT
MDN1	forward	CATCAACAAACCTGACCAACTAATCC
	reverse	CATCAAGGTTTTCCAAAGTGGGC
RDN18	forward	AACTCACCAGGTCCAGACACAATAAGG
	reverse	AAGGTCTCGTTCGTTATCGCAATTAAGC

Table 7. qPCR primers used for the analysis of mRNA degradation shown in figure 14 (*137*).

Gene	Primer direction	Primer sequence (5‘-3‘)
ACT1	forward	TATGTGTAAAGCCGGTTTTGC
	reverse	GACAATACCGTGTTCAATTGGG
HTB1	forward	TGGCTGCGTATAACAAGAAGTCT
	reverse	CCAAAGGAAGTGATTTCATTATGC
HTB2	forward	TGCTCTATACTCAAACCAACAACA
	reverse	ATCTCTTCTTACCATCGACGGA

Table 8. Promoter, terminator and 5’ UTR sequences used in this study.

Gene feature	Position relative to ORF
HTB1 promoter (incl. HTB1 5’ UTR)	817 bp upstream of *HTB1* ORF
HTB2 promoter (incl. HTB2 5’ UTR)	699 bp upstream of *HTB2* ORF
ACT1 promoter (incl. ACT1 5’ UTR)	669 bp upstream of *ACT1* ORF
HTB1 5’ UTR	127 bp upstream of *HTB1* ORF
MDN1 5’ UTR	150 bp upstream of *MDN1* ORF
RPB4 5’ UTR	125 bp upstream of *RPB4* ORF
HTB1 terminator	310 bp downstream of *HTB1* ORF

2.7 Buffers and Growth Media

Table 9. Buffers used in this work.

Buffer	Composition
0.1 M TE/Lithium acetate	0.1 M Lithium acetate 10 mM Tris-HCl 1 mM EDTA
1 M TE/Lithium acetate	1 M Lithium acetate 10 mM Tris/HCl 1 mM EDTA

DNA extraction buffer	2 % (v/v) Triton X 100 1 % (w/v) SDS 100 mM NaCl 10mM Tris-HCl 1mM EDTA
Ponceau S staining solution	0.1 % (w/v) Ponceau S 5 % (v/v) Acetic acid
smFISH fixation buffer	1.2 M Sorbitol 0.1 M K_2HPO_4, (adjust to pH 7.5)
Tris-Buffered Saline Tween (TBST)	150 mM NaCl 50 mM Tris-HCl pH 8 0.2 % (v/v) Tween 20

Table 10. Liquid growth media used in this work. All growth media were stored at 4°C. Glucose, galactose, glycerol and ethanol stock solutions were sterilized by filtering. All the other media were autoclaved.

Growth Media	**Composition**
YPD	1 % (w/v) Yeast extract 2 % (w/v) Peptone 2 % (w/v) Glucose
SCD	0.139 % (w/v) Synthetic complete mix 0.17 % (w/v) Yeast nitrogen base 0.5 % (w/v) Ammonium sulfate 2 % (w/v) Glucose

SCGE	0.139 % (w/v) Synthetic complete mix 0.17 % (w/v) Yeast nitrogen base 0.5 % (w/v) Ammonium sulfate 2 % (v/v) Glycerol 1 % (v/v) Ethanol
SCGal	0.139 % (w/v) Synthetic complete mix 0.17 % (w/v) Yeast nitrogen base 0.5 % (w/v) Ammonium sulfate 2 % (w/v) Galactose
SDGE	0.17 % (w/v) Yeast nitrogen base 0.5 % (w/v) Ammonium sulfate 0.002 % (w/v) Methionine 0.012 % (w/v) Leucine 0.002 % (w/v) Uracil 0.008 % (w/v) Tryptophan 0.002 % (w/v) Histidine
YPGal	1 % (w/v) Yeast extract 2 % (w/v) Peptone 2 % (w/v) Galactose
YPGE	1 % (w/v) Yeast extract 2 % (w/v) Peptone 2 % (v/v) Glycerol 1 % (v/v) Ethanol
LB	2 % (w/v) LB broth
SOC	2 % (w/v) Tryptone 0.5 % (w/v) Yeast extract 0.05 % (w/v) NaCl 0.36 % (w/v) Glucose

Table 11. Solid growth media used in this work. All agar plates were stored at 4°C.

Agar plates	Composition
YPD	1 % (w/v) Yeast extract 2 % (w/v) Peptone 2.0 % (w/v) Agar 1 NaOH pellet per 1 L 2 % (w/v) Glucose
SCD	0.139 % (w/v) Synthetic complete mix 0.17 % (w/v) Yeast nitrogen base 0.5 % (w/v) Ammonium sulfate 2.0 % (w/v) Agar 1 NaOH pellet per 1 L 2 % (w/v) Glucose
LB	3.5 % (w/v) LB-Agar

Table 12. Synthetic complete mix used for growth media preparation.

Amino Acids	Composition
Adenine	0.004 % (w/v)
Arginine	0.002 % (w/v)
Aspartic acid	0.01 % (w/v)
Glutamic acid	0.01 % (w/v)
Histidine	0.002 % (w/v)
Isoleucine	0.003 % (w/v)
Leucine	0.012 % (w/v)
Lysine	0.003 % (w/v)
Methionine	0.002 % (w/v)
Phenylalanine	0.005 % (w/v)
Serine	0.0375 % (w/v)

Threonine	0.02 % (w/v)
Tryptophan	0.008 % (w/v)
Tyrosine	0.003 % (w/v)
Uracil	0.002 % (w/v)
Valine	0.015 % (w/v)

2.8 Cell culture conditions

All *S. cerevisiae* strains used in this work were stored long-term in 15% (v/v) glycerol, at -80°C. For pre-culture, the frozen yeast cells were first streaked onto an YPD agar plate and incubated for 2-3 days, at 30°C, until colonies were formed. Cells were then inoculated into 4 mL of liquid YPD medium and pre-cultured for 6-8 h, at 30°C and 250 rpm in a shaking incubator. After two washing steps, cells were transferred to a growth medium of choice *i.e.* yeast peptone, synthetic complete, or minimal medium containing glucose, galactose or glycerol and ethanol as carbon sources. Cell cultures were then grown in the selected nutrient for at least 18 h to reach steady state conditions. To monitor growth status, a spectrophotometer was used for optical density measurements and appropriate dilutions were made to ensure that the cultures grew exponentially. Eventually, cells were harvested by centrifugation at OD_{600}= 0.3-0.9 and were further processed according to the requirements of the experimental technique.

To increase the range of accessible cell volumes within a growth medium, a strain with β-estradiol-inducible *WHI5* was used. Cells were pre-cultured in YPD (30°C) for at least 6 h before being transferred to the growth medium of choice. After 12 h of growth, β-estradiol was added to the culture at a concentration of 5 nM. Cells were cultured in the presence of β-estradiol for at least 24 h to ensure a steady state.

2.9 Estimation of population doubling times from yeast growth curves

A growth curve represents the four well-established growth stages a yeast population typically undergoes (Fig. 6). When cells are first transferred to a fresh growth medium, they go through a lag phase, as they need to adapt to the new environment before they start dividing. During log-phase, cells enter exponential growth with a maximum, constant growth rate until they reach stationary phase, where division rate equals the death rate and cell numbers remain unchanged. While cells can survive in stationary phase over a prolonged period of time, if living conditions do not improve, cells will eventually enter death phase (*138*, *139*). To generate growth curves, cells were transferred to a selected liquid growth medium and optical densities OD at 600 nm were determined at fixed time points over the course of several hours. Natural logarithmic transformation of the OD values converts the exponential growth during log-phase to a linear growth pattern over time, and allows calculation of the growth rate (r) using the formula: r=[ln (OD2/OD1)] / (T2-T1), where OD1 and OD2, correspond to the time points T1 and T2 (Fig. 6). The population doubling time is then defined as t_D=ln (2)/r.

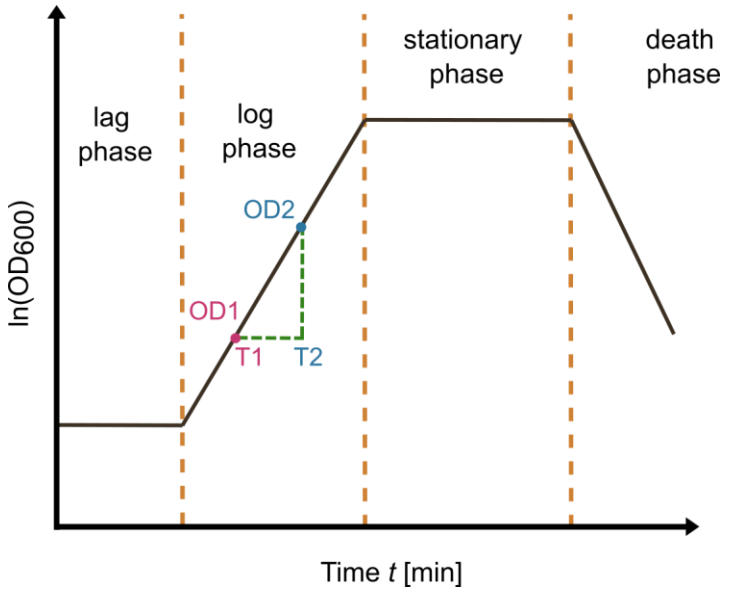

Figure 6. Schematic illustration of a growth curve representing the four stages a yeast population undergoes. On the semi-logarithmic plot, the growth rate (r) during log-phase can be calculated as the slope Δln (OD)/Δ*t*.

2.10 *S. cerevisiae* transformation

Efficient yeast transformation required the preparation of competent cells by incubation in a lithium acetate (LiOAc) solution. To this end, yeast cells were pre-cultured in 3 mL YPD overnight, before 1 mL of cell culture was added to 50 mL of fresh YPD medium. After 4-5 hours of growth at 30°C, cells were centrifuged (21°C, 4k rpm, 3 min) and washed with 20 mL double-distilled water. Next, cells were spun down and washed with 0.8 mL 0.1 M LiOAc, before being resuspended in 0.4 mL 0.1 M LiOAc. For transformation, 50 µL of competent cells were mixed with 240 µL 50% (w/v) PEG, 32 µL 1 M LiOAc, 25 µL 2 mg/mL salmon sperm carrier DNA and 13 µL of the DNA insert (PCR product or linearized plasmid). Prior to use, the carrier DNA was heated at 95°C for 3 min. In a next step, the mixture was incubated for 30 min at 30 °C and heated for 20 min at 42 °C. Cells were then pelleted by centrifugation (10k rpm, 3 min), resuspended in 400 µL double-distilled water and spread onto selective medium plates. After 2-3 days, single colonies were formed and yeast transformants were re-plated onto selective SCD dropout plates.

2.11 *Escherichia coli* transformation and plasmid DNA isolation

E. coli cells were made competent as previously described (*140*) and stored at – 80°C until use. For transformation, cells were mixed with plasmid DNA at a volume ratio of 1:20, followed by a 30 min incubation on ice. After a 90 s heat shock at 42 °C, the transformed cells were stored on ice for 2 min and then cultured in 800 µL SOC medium for 1-2 h (37 °C, 250 rpm). Following this recovery step, 100 µL of the cell suspension were spread onto a LB agar plate supplemented with 100 µg/mL ampicillin. After 24 h of incubation at RT, colonies were formed.

For plasmid isolation, *E. coli* cells were first grown in 5 mL LB medium with 100 µg/mL ampicillin for 12-16 h (37 °C, 250 rpm) before being harvested by centrifugation (11,000 x g, 1 min). Plasmid DNA was then isolated and purified using the NucleoSpin Plasmid Kit.

2.12 Genomic DNA extraction from yeast

Genomic DNA was isolated from yeast to verify transformants by PCR amplification and DNA sequencing. It also served as a template for PCR amplification prior to cloning. For DNA extraction, 300 µg of glass beads were added to a tube with yeast cells suspended in 200 µL of DNA extraction buffer and 200 µL of phenol:chloroform:isoamyl alcohol. The cell wall was then mechanically disrupted by vortexing. Following the addition of 200 µl of 1X TE buffer (pH 8.0), the mixture was centrifuged for 5 min at 17,000 x g. In a next step, the upper aqueous phase was transferred to a safe-lock tube filled with 1 mL of 100% ethanol. The tube was inverted to mix a few times, followed by another centrifugation step (17,000 x g, 5 min). After removing the supernatant, 1 mL of 70% ethanol were added to the tube before it was spun down again (17,000 x g, 5 min). Finally, the supernatant was carefully aspirated and the pellet was air dried until the residual ethanol evaporated. In a last step, the pellet was dissolved in 50 µL of nuclease-free water and DNA concentration and purity were determined using a spectrophotometer.

2.13 Western blot analysis

The nutrient-dependent protein levels of histone H2B and actin were quantified by western blotting. For the analysis, an equal number of wildtype cells in each nutrient condition was collected and total proteins were extracted as described in a previously published protocol (*141*). Briefly, cell cultures were grown at 30 °C in different nutrients, for at least 18 h before $5x10^7$ cells were harvested by centrifugation (4k rpm, 3 min). Measurements of average cell volumes and population densities (number of cells per mL) were performed using a Coulter Counter. Following centrifugation, the cells were washed with 1 mL of ice-cold double-distilled water, pelleted (10k rpm, 2 min) and then incubated in 400 µL of 0.1 M NaOH, for 10 min at room temperature (RT). After being spun down (10k rpm, 2 min), the cells were resuspended in 120 µL of reducing 1x LDS sample buffer and then heated for 3 min at 95 °C. The 1x LDS sample buffer was a mixture of 30 µL of 4X Bolt™ LDS sample buffer, 12 µL of 10X Bolt™ sample reducing agent and 78 µL of distilled water. After another centrifugation step (10k rpm, 2 min) the total protein extract (supernatant) was collected and 5-10 µL per lane were loaded into Bolt™ 12% Bis-Tris plus mini-gels. Following gel electrophoresis

(200V, 160 mA, 20-25 min) in 1X Bolt™ MES SDS running buffer, the proteins were transferred from the gel onto the surface of a nitrocellulose membrane using the Invitrogen's mini-blot-module. To assess the transfer efficiency and visualize the total protein bands in each lane, the membrane was stained with Ponceau S and imaged using the ChemiDocTM MP imaging system. For detection of the target proteins, the membrane was then blocked in 5% milk in TBST to prevent any non-specific antibody binding. Next, it was probed overnight at 4 °C with either a rabbit anti-histone H2B monoclonal antibody (1:2000) or a mouse anti-beta actin monoclonal antibody (1:10000). Subsequently, the membrane was washed in TBST and probed for 1.5 h at RT with HRP-conjugated goat anti-mouse (1:10000) or goat anti-rabbit (1:10000) secondary antibodies. Finally, the target proteins were visualized on the ChemiDocTM MP imaging system using the Clarity™ western ECL substrate, which was added to the membrane (5 min, RT) prior to imaging. The protein bands were quantified with the Image Lab 5.2.1 software.

2.14 RNA extraction and reverse transcription quantitative PCR (RT-qPCR)

Total RNA extracts from cells growing on different growth media were prepared using the YeaStar RNA Kit according to the manufacturer's instructions. Concentration and quality of the isolated RNA were assessed with a spectrophotometer, and by 1% agarose gel electrophoresis (100 V, 30 min). Complementary DNA (cDNA) was then synthesized from 800 ng of total RNA by reverse transcription using a high capacity cDNA reverse transcription kit. In a next step, a 10-fold (*HTB2*, *MDN1*, *mCitrine, ACT1*) or 100-fold (*HTB1, HTA1, HTA2, HHF1, HHF2, HHT1, HHT2*) dilution of the cDNA in double-distilled water was prepared as a template for the qPCR reaction. In each well of a LightCycler 480 Multiwell Plate 96, 2 µL of the dilution were mixed with SsoAdvanced Universal SYBR Green Supermix and gene-specific primers (0.5 µM) before qPCR was performed on a Light Cycler 96 instrument. The relative mRNA levels of the gene of interest were estimated using the formula: $\log_2$(relative concentration) = − (Cq^{Gene} – Cq^{RDN18}), where Cq^{Gene} and Cq^{RDN18} represent the mean Cq values of three technical replicates.

Table 13. Settings for qPCR reaction.

	Temperature (°C)	Time (s)	Cycles
Pre-incubation	95	30	1
Amplification	95	10	40
	60	30	
Melting	95	10	1
	65	60	
	97	1	

2.15 Measurement of mRNA decay following transcription inhibition by thiolutin

To measure the mRNA half-lives of *HTB1, HTB2* and *ACT1*, wildtype cells were cultured in 50 mL of YPD or SCGE to reach OD_{600} = 0.3 – 0.5, before being treated with the transcriptional inhibitor thiolutin (final concentration, 8 µg/mL (*142*)). Afterwards, 4 mL samples were collected at defined time points during a 60 min incubation period. Cells were spun down to remove supernatant (2500 x g, 3.5 min), washed with 1 mL of RNAse-free water and pelleted again (10k rpm, 2 min). Next, 80 µL of digestion buffer (YeaStar RNA Kit, Zymo Research) were added to the cells, which then were stored on ice until all samples were prepared for RNA extraction. Total RNA was extracted using the YeaStar RNA Kit according to the manufacturer's instructions. Traces of DNA contamination, were further removed from the RNA samples through DNAse I digestion. Finally, RT-qPCR was performed, as previously described, using target-specific primers to quantify the change in relative mRNA concentration over time (*137*). The respective mRNA half-lives were estimated by fitting the decay curves with a one-phase exponential function.

2.16 Flow cytometry analysis

Flow cytometry served as an experimental technique for quantitative protein analysis, allowing rapid generation of data from many samples across a wide range of nutritional conditions. Moreover, it was used to estimate the distribution of cells in the different cell cycle

phases, based on DNA content quantification. The flow cytometry measurements were carried out by Daniela Bureik (Kurt Schmoller Group, Helmholtz Zentrum München).
Cell cultures (2-5mL) were grown in different nutrients for 36 h at OD_{600} < 1 before flow cytometry was performed on a 577 CytoFlex S Flow Cytometer. The respective cell volume distributions of the exponentially growing populations were determined with a Coulter Counter. For protein analysis, mCitrine fluorescence was measured using a 488-nm laser paired with a 525/40-nm bandpass filter. Each sample was measured at flow rate of 10 µL/min and approximately 1000 events/s were acquired, resulting in an overall of 50000 events per experiment. Cell debris and doublets were excluded from the dataset via forward and side scatter gating using the FlowJo software (version 10.8.1). For all conditions, the fluorescence intensity of mCitrine was corrected for autofluorescence by measuring the wildtype strain that does not express mCitrine.

2.16.1 Cell cycle analysis by flow cytometry

For cell cycle analysis, wildtype cells were prepared according to a previously published procedure for cell fixation and DNA staining (*143*). Briefly, 1 mL of a cell culture growing for 36 h to OD_{600}=0.5 was slowly mixed with 9 mL of 80 % ethanol and kept at 4 °C overnight, before cells were collected by centrifugation (2.500 x g, 2 min, 4°C). After two wash steps in 50 mM Tris-HCl (pH = 8.0), cells were first incubated in 300 µL of 1 mg/mL RNase A (37°C, 40 min), washed again in 50 mM Tris-HCl (pH = 8.0) and then treated with 50 µL 20 mg/mL Proteinase K (37°C for 60 min). For DNA staining, cells were washed again in 50 mM Tris-HCl (pH = 8.0), followed by incubation in 200 µL of 10x SYBR Green I dye (22°C, 1 h). To quantify the DNA content, SYBR Green I fluorescence was detected using a 488-nm laser paired with a 525/40-nm bandpass filter. The FlowJo software (version 10.8.1) was used to generate DNA frequency histograms with distinct G1 and G2 peaks and to extract the distribution of cells in the different cell cycle phases by applying the Watson pragmatic algorithm.
SYBR Green I was not used to stain the DNA of cells expressing mCitrine as the emission profiles of the two fluorophores overlap. Yet, the cell cycle fractions of cells with mCitrine-labelled H2B could be determined because core histone synthesis occurs in parallel with DNA replication, resulting in defined G1 and G2 peaks in the mCitrine fluorescence profile.

Therefore, cells expressing H2B-mCitrine were analyzed as described above and cell cycle distributions were estimated based on the obtained fluorescent histograms.

2.17 Single-molecule fluorescence in situ hybridization (smFISH)

2.17.1 Experimental procedure

smFISH was performed to detect and quantify individual mRNAs in single cells growing on different nutrients. Custom Stellaris® oligonucleotide probes that bind along the mRNA target of interest were purchased from Biosearch Technologies and designed using the company's online Stellaris® RNA FISH Probe Designer. Specifically, the probe sets binding *MDN1* and *mCitrine* contained 27 to 48 different Quasar-670®-labeled 20-mer oligonucleotides and the probes against *ACT1* consisted of 41 20-mer oligonucleotides singly labeled with Quasar-570®. For smFISH analysis, cells were prepared following the Stellaris® RNA FISH protocol for *S. cerevisiae* (www.biosearchtech.com/stellarisprotocols). Briefly, cell cultures (45 mL) grown for at least 18 h to OD_{600} = 0.3-0.5 were fixed in 4% formaldehyde (45 min, RT) before being collected by centrifugation (1600 x g, 4 min). After two wash steps in 1 mL of ice-cold fixation buffer cells were treated with zymolyase (6.25 µg zymolyase in 1 mL of fixation buffer) at 30°C. Cell wall digestion was monitored by bright-field microscopy and stopped after 55 min, when most of the cells had turned dark. Next, cells were washed two times with fixation buffer, and kept overnight in 70% ethanol (4°C). Following the permeabilization step, 300 µL of cells were pelleted (500 x g, 5 min) and incubated overnight at 4°C in 100 µL of Stellaris® RNA FISH hybridization buffer with 10% v/v formamide and a probe concentration of 125 mM. Cells were spun down (500 x g, 5 min) and then resuspended in wash buffer A, before being treated with 1 mL of DAPI counterstain solution (5 ng/mL DAPI in wash buffer A) for 30 min at 30 °C. Finally, cells were washed with 1 mL of Stellaris® RNA FISH wash buffer B and directly mounted in Vectashield® mounting medium for image acquisition. To visualize individual mRNAs in the cell, wide-field fluorescence microscopy was carried out on a Zeiss LSM 800 microscope using an Axiocam 506 camera, a 63×/1.4 NA oil immersion objective and the Zen 2.3 software. DAPI was excited with a 385 nm LED, and Quasar-570® and Quasar-670®-labeled probes were imaged using a 530 nm and 630 nm LED. Z-stacks composed of 20 z-slices were acquired at RT with a z-interval of 240 nm.

2.17.2 Data analysis

For quantification of the detected mRNA signal, cells were first segmented with Cell-ACDC (*144*). Specifically, YeaZ (*145*) was applied to segment the cells based on the bright-field images, before mother-bud pairs were manually identified. The total cell volume was estimated by Cell-ACDC based on the 2D segmentation masks. Next, the number of individual mRNA spots per cell was analyzed in 3D with a Python routine, developed by Dr. Francesco Padovani (Kurt Schmoller Group, Helmholtz Zentrum München), consisting of the following steps :1) First, a 3D Gaussian filter with a small sigma (0.75 voxel) was used for the fluorescence spots in order to remove noise. 2) Instance segmentation of the fluorescent mRNA signal was then carried out using either the Li, triangle or Otsu threshold function from the Python library scikit-image (*146*). 3) Local peaks were detected in 3D within the mRNA signal after applying the peak_local_max function (Python library scikit-image). 4) In the next step, overlapping peaks within a resolution-limited volume were eliminated by removing the peak with the lowest intensity. 5) An iterative filtering process was used to filter the remaining peaks based on their effect size, which could not fall below the manually set threshold ranging from 0.2 to 1.0. The final number of peaks in each cell represented the fluorescent mRNA spots. mRNA concentrations were then defined as the number of fluorescent spots divided by the total cell volume. As a negative control for the analysis of *ACT1* and *MDN1,* cells were incubated without the respective smFISH probes (Fig 7A, B). Here, deletion strains were not constructed since both genes are essential for cell survival (*147*, *148*). For *mCitrine* analysis, wild-type cells not expressing the reporter were incubated with the corresponding Quasar-670®-labeled smFISH probes (Fig. 7C). Quantification of the fluorescent spots detected in all negative controls showed a drastically reduced mRNA signal.

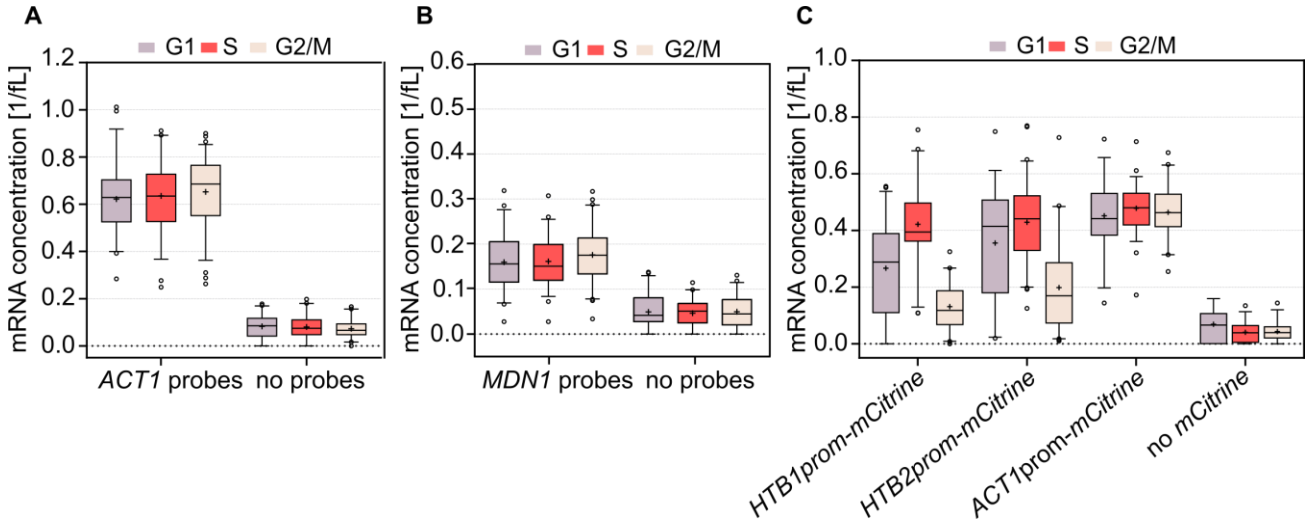

Figure 7. Target gene mRNA concentrations in G1-, S-, and G2/M-phase compared to negative controls. (**A-C**) Representative smFISH analysis of the cell cycle-dependent mRNA concentrations of *ACT1* (A) *MDN1* (B) and *mCitrine* (C) expressed from the *HTB1, HTB2* or *ACT1* promoter in YPD. As a negative control for the analysis of *ACT1* and *MDN1*, wildtype cells were incubated without smFISH probes. Moreover, cells expressing *HTB1-, HTB2-* or *ACT1prom-mCitrine*, as well as cells carrying no copy of the reporter gene were targeted with fluorescently labeled probes against *mCitrine*. Box plots show median values and 25th and 75th percentiles; whiskers represent the 2.5th and 97.5th percentiles; outliers are shown as individual symbols. $n_{G1}^{ACT1,MDN1}$=48, $n_{S}^{ACT1,MDN1}$=54, $n_{G2/M}^{ACT1,MDN1}$=74; $n_{G1}^{\text{no probes}}$=49, $n_{S}^{\text{no probes}}$=40, $n_{G2/M}^{\text{no probes}}$=43; $n_{G1}^{HTB1prom}$=58, $n_{S}^{HTB1prom}$=49, $n_{G2/M}^{HTB1prom}$=41; $n_{G1}^{HTB2prom}$=37, $n_{S}^{HTB2prom}$=64, $n_{G2/M}^{HTB2prom}$=59; $n_{G1}^{ACT1prom}$=35, $n_{S}^{ACT1prom}$=59, $n_{G2/M}^{ACT1prom}$=41; $n_{G1}^{no\ mCitrine}$=15, $n_{S}^{no\ mCitrine}$=28, $n_{G2/M}^{no\ mCitrine}$=37.

2.17.3 Cell cycle phase classification using smFISH

Cells were assigned to G1-, S-, or G2/M-phase based on two criteria: the bud-to-mother cell volume ratio and the number of detected nuclei in the cell. Specifically, cells with no bud were considered G1 cells, while cells with one DAPI-stained nucleus and a bud-to-mother cell volume ratio < 0.3 were assigned to S-phase (*89*). Finally, cells with one nucleus and a bud-to-mother cell volume ratio > 0.3, as well as cells containing two nuclei, were grouped into G2M-phase. To distinguish a G2M cell with two nuclei from two adjacent G1 cells, the bright-field images were used to examine the cell outlines.

2.18 Live-cell imaging by fluorescence microscopy

2.18.1 Experimental procedure

Cells (5 mL) were cultured in different nutrients for 18 h at 30° C. Live-cell experiments were then performed using the CellASIC® ONIX2 microfluidic system, which allows long-term tracking and imaging of single cells in a dynamic and controlled microenvironment. Briefly, 200 µL of sonicated cells were loaded into a CellASIC® ONIX2 Y04C microfluidic plate and were continuously supplied with fresh growth medium at 13.8 kPa via the ONIX2 microfluidic pump system. Imaging was carried out on a Zeiss LSM 800 microscope using the epifluorescence setup. The microscope was equipped with an environmental chamber, kept at 30°C throughout the course of the time-lapse experiment. Depending on the nutrient-specific growth rate, cells were imaged for 7 to 12 h with a 40×/1.3 NA oil immersion objective. To monitor histone synthesis during the cell cycle, fluorescence images of cells expressing mCitrine-labeled H2B were acquired every 3 min, using a 511 nm LED at 5% power, with an exposure time of 10 ms. For analysis of *HTB1, HTB2* or *ACT1* promoter-mediated mCitrine expression, the reporter was instead illuminated with a 511 nm LED at 12% power.

2.18.2 Data analysis

Microscopy data collected during the time-lapse experiments were analyzed according to the following steps: First, a custom Fiji script was utilized to align the images and define the region of interest (ROI) (*149*). Automated segmentation and tracking of individual cells were then performed using phase-contrast microscopy images (*150*). Pedigree and cell cycle information were generated by manually determining the time points of birth, bud emergence and cytokinesis of all newly born daughter cells *(150)*. For quantification of the mCitrine fluorescence, background signal, and cellular autofluorescence measured in unlabelled wildtype cells were subtracted (*151*). The mCitrine intensity per cell, obtained after the correction steps, was used as a proxy for total protein amount. The corresponding concentrations were defined as the amount of mCitrine divided by the cell volume, which was estimated from phase contrast images.

It should be noted that cells expressing H2B-mCitrine showed high fluorescence intensities in all growth media, so that the autofluorescence could be neglected. In this case, the cellular fluorescent signal was only background corrected (Fig. 8).

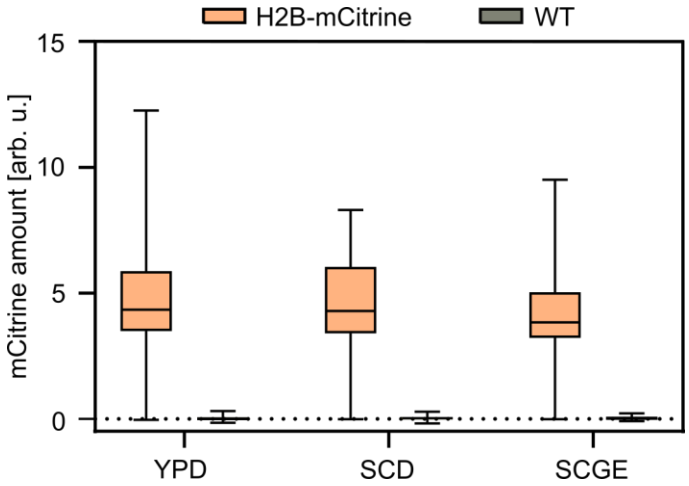

Figure 8. Autofluorescence can be neglected in cells with mCitrine-labeled histone H2B. Background-corrected fluorescence intensity detected in cells expressing H2B-mCitrine (n_{YPD} = 492, n_{SCD} = 392 n_{SCGE} = 275) and unlabeled wildtype cells (n_{YPD} = 227, n_{SCD} = 285 n_{SCGE} = 215). Here, Cell-ACDC was used for cell segmentation and analysis of the fluorescent signal (*144*). Box plots show median values and 25th and 75th percentiles; whiskers represent the 2.5th and 97.5th percentiles.

2.19 Statistical Analysis

Statistical significance was estimated using the software GraphPad Prism (version 9.4.1). First, the Shapiro–Wilk test at a confidence level of α = 0.05 was performed to assess whether or not the data sets fit to a Gaussian distribution. Statistical significance was then estimated by an unpaired, two-tailed t-test for normally distributed datasets. Alternatively, a Mann-Whitney test was used for datasets that did not follow a Gaussian distribution (* $p<0.05$, ** $p<0.01$, *** $p<0.001$, **** $p<0.0001$).

3 Results

3.1 Characterization of cell growth in different nutrient environments

Histones are strongly coupled to the genomic content, and their biosynthesis is highly coordinated with DNA replication during S-phase (*88*, *89*, *123*). To understand the regulation of histone homeostasis across changing environments I asked how cells produce the right amount of histones even when cell growth and cell cycle progression are drastically modulated by nutrients. To this end, I selected three different types of growth media as well as various carbon sources in order to obtain a wide range of nutrient-specific cell growth phenotypes. More specifically, I used yeast peptone (YP), synthetic complete (SC), and minimal medium (SD) containing glucose (D), galactose (Gal) or glycerol and ethanol (GE) as carbon sources. To characterize the different growth phenotypes, I measured mean cell volumes and estimated the population doubling times of asynchronous haploid wildtype cells growing exponentially in the different growth media. As expected, cells showed shorter doubling times in nutrient-rich conditions, especially in the presence of glucose, but divided more slowly on glycerol and ethanol (Fig. 9A). At the same time, the mean cell volumes were increased in glucose-containing media (Fig. 9B). Overall, doubling times varied between 1.3 h to 6.6 h, while mean cell volumes ranged from 46 fL to 62 fL. I also used flow cytometry to determine the cell cycle-phase distributions in each nutrient condition by quantifying the SYBR Green I-stained cellular DNA content (Fig 9C). The analysis of the DNA content distribution throughout the cell cycle revealed that the fraction of cells in G1-phase increased in growth media containing glycerol and ethanol. At the same time, the percentage of cells in S- and G2/M-phase, became relatively smaller. Based on the nutrient-dependent cell cycle phase distributions, I then estimated the absolute duration of S-phase by taking into account the population doubling times in each growth condition (Fig. 9D). The greatest change in absolute S-phase duration compared to YPD was observed in SDGE, with the S-phase increasing approximately threefold.

Given that histones are highly cell cycle regulated proteins, which are thought to be expressed in proportion to the DNA content, the question arises as to how the described nutrient-specific changes in cell growth and cell cycle progression affect the cellular histone protein levels.

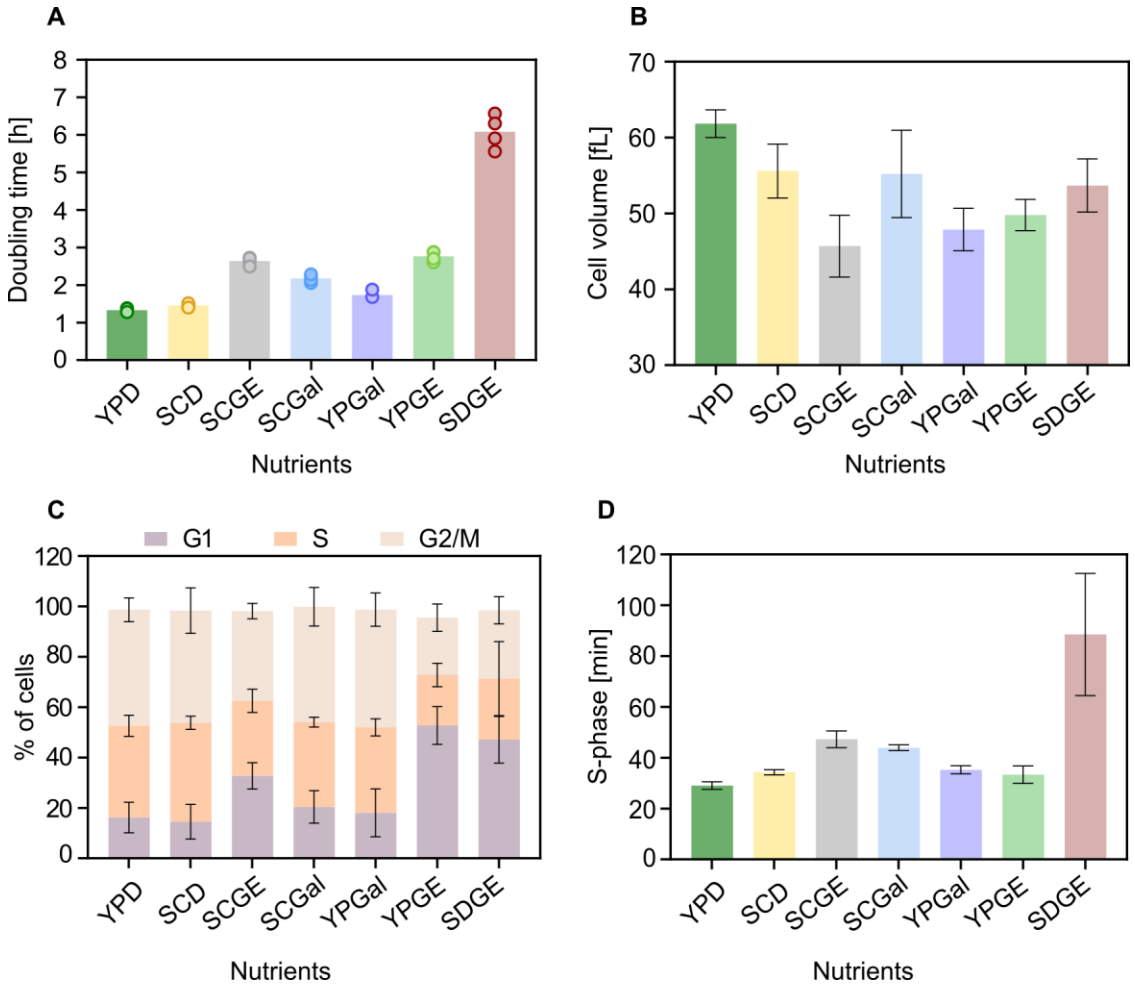

Figure 9. Nutrient-specific changes in cell growth and cell cycle. (**A**) Haploid wildtype cells were cultured in yeast peptone (YP), synthetic complete (SC), and minimal medium (SD) containing glucose (D), galactose (Gal) or glycerol and ethanol (GE) as carbon sources. Doubling times were estimated from the growth curves of asynchronous cell populations, growing exponentially in the different nutrients. Bar graphs show the mean of n=4 replicate measurements, each displayed as an individual dot. (**B**) Corresponding mean volumes of the exponentially growing cell populations in the different nutrients. Measurements of cell volume were carried out with a Coulter counter. Bar graphs and error bars show mean and standard deviation of n=6 biological replicates. (**C**) Nutrient-specific distributions of cells in G1, S and G2/M phase were determined by DNA content measurement using flow cytometry. Error bars show the standard deviation of n=5 independent measurements. (**D**) Absolute durations of S-phase were estimated from the cell cycle phase distributions shown in (C) by

taking into account the corresponding mean population doubling times in (A). Bar graphs and error bars represent mean and standard error of n=5 independent measurements.

3.2 Concentration of histone proteins decreases with increasing cell volume in different nutritional environments

To determine the effect of different nutrient environments on the histone protein regulation, I measured the relative protein concentrations of the core histone H2B by western blot. As a control, I additionally quantified the nutrient-dependent protein levels of actin, a constitutively expressed housekeeping protein that scales proportionally with cell size (*89*, *90*, *152*). For western blot analysis, I harvested an equal number of wildtype cells in each nutrient condition and quantified the extracted total proteins by Ponceau S staining (Fig. 10A). Nutrient availability strongly dictates cellular biosynthetic capacity, leading to decreased protein biosynthesis in nutrient-poor environments (*153*, *154*). Overall, I observed less total protein content in the growth media containing glycerol and ethanol (Fig. 10B). In fact, I found that changes in total protein abundance between the media were highly correlated with the nutrient-induced changes in cell volume (Fig. 9B). This is consistent with existing literature showing that cellular protein content scales with cell volume (*155*).

For quantitative analysis of the relative protein concentrations, I normalized the detected H2B and actin amounts to total protein in the different growth media (Fig. 10C-D). As shown in figure 10C, the protein concentration of H2B decreases with increasing cell volume across changing environments, while actin concentration remains constant over cell volume (Fig. 10D). These results suggest that the expression of histone proteins is coupled to DNA content rather than cell volume. On the other hand, actin synthesis is tightly coordinated with cell volume, keeping protein concentrations constant as cells grow in the different nutrients.

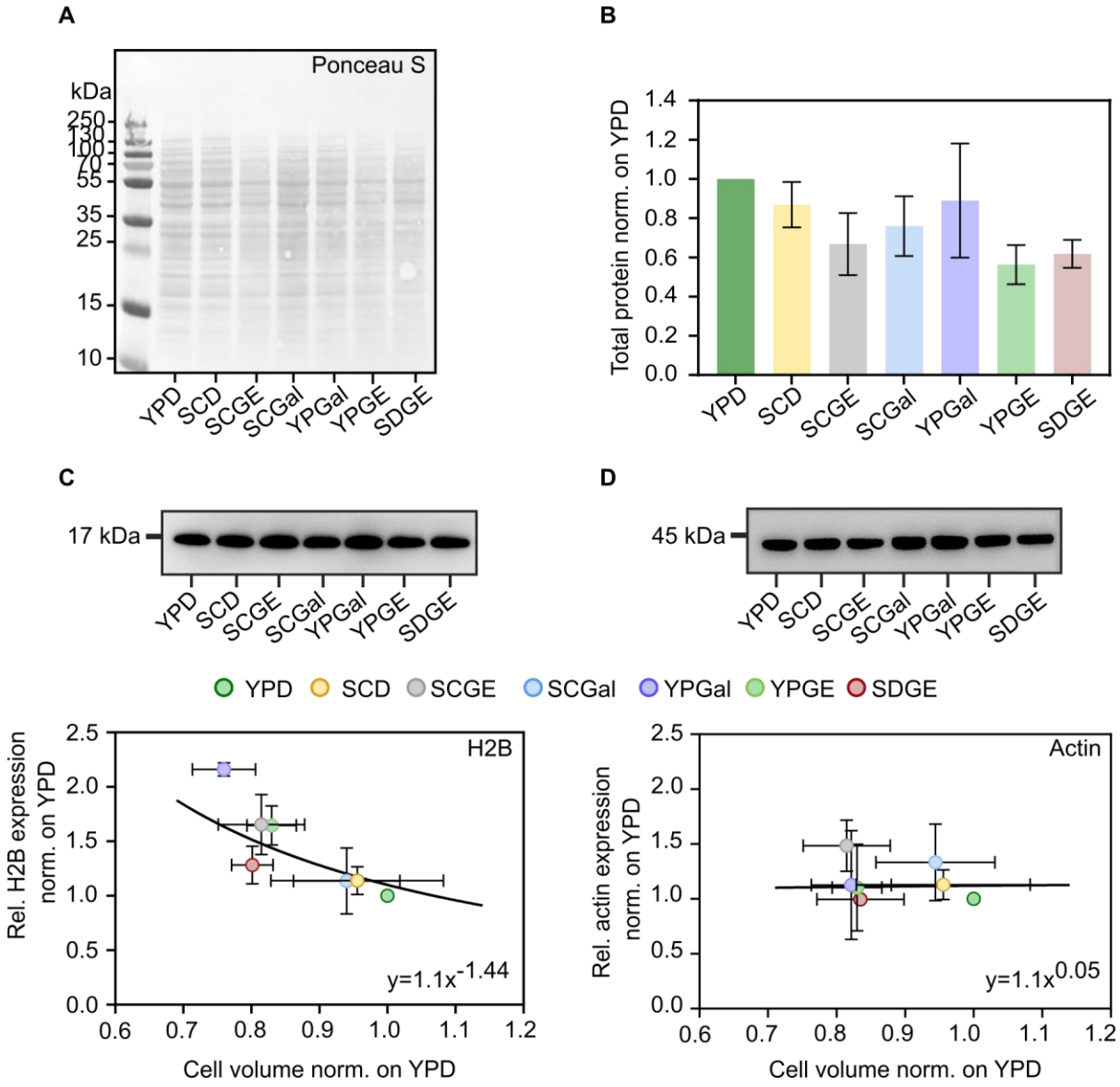

Figure 10. Histone protein concentrations decrease in inverse proportion to the cell volume in different nutrient environments. (**A**) Ponceau S staining of a representative western blot membrane used for the measurement of total proteins extracted from the same number of cells in different nutrient conditions. (**B**) Total protein content in each nutrient condition was normalized to YPD. Bar graphs and error bars show mean and standard deviation (n_{YPD}=7, n_{SCD}=5, n_{SCGE} =5, n_{SCGal} =7, n_{YPGal} =7, n_{YPGE} =7, n_{SDGE} =4). (**C-D**) The protein amounts of H2B (C) and actin (D) were normalized to total protein in the different growth media and are plotted as a function of the nutrient-dependent cell volume, relative to YPD. Means and standard deviations are shown (n_{YPD}=5, n_{SCD} =4, n_{SCGE} =4, n_{SCGal} =5, n_{YPGal} =3, n_{YPGE}=4, n_{SDGE} =3). The black lines represent fits whose coefficients were extracted from linear regression on the double-logarithmic raw data.

3.3 Single-cell histone protein amounts are constant across nutrient conditions

So far, I have shown that the nutrient-dependent H2B protein concentrations measured in asynchronous cell populations decrease with increasing cell volume. These results suggest that cells grown on different growth media maintain constant histone amounts, independently of cell volume, and despite the nutrient-related changes in cell growth and cell cycle. Using microfluidics-based fluorescence microscopy, I next performed dynamic live-cell studies and quantified the protein amounts of fluorescently tagged H2B at the single-cell level. The utilized microfluidic plates provided a dynamic and controlled microenvironment for monitoring cell growth and histone production over several hours. To detect and quantify the amounts of histone H2B in single cells, I tagged *HTB1* and *HTB2* endogenously with the fluorescent reporter *mCitrine* ($\lambda_{excitation}$=516 nm, $\lambda_{emission}$=529 nm) (*156*) (Fig. 11A-B). mCitrine is an improved variant of the yellow fluorescent protein (YFP), as it exhibits a reduced environmental sensitivity and higher photostability compared to YFP (*156*, *157*). In addition, it provides a bright fluorescent signal relative to background and autofluorescence (*157*) and shows fast maturation with a half-time of 10.4 min, at 30 °C in glucose-containing growth medium (*158*). For my analysis, I tested a set of three growth media: YPD, SCD and SCGE. To avoid possible phototoxicity and bleaching effects caused by the frequent light exposure during very long time-lapse experiments, I refrained from selecting very poor growth media, on which cells would grow extremely slow. In all three conditions, I monitored cell growth and measured the cellular H2B-mCitrine fluorescence during the cell cycle. The mCitrine intensity per cell, obtained after background correction was used to estimate total protein amount (see Materials and Methods). For each newborn cell, G1-phase was considered as the time from cell birth to bud emergence and S/G2/M-phase as the time between bud emergence and cytokinesis. Since histone synthesis is initiated in late G1 and continues during S-phase, the expression profile of H2B-mCitrine shows a plateau during early G1, suggesting constant histone amounts (Fig. 11C). Around the time of bud emergence, histone amounts start to increase and approximately double before reaching a second plateau. The fluorescence intensity traces shown in figure 11C represent the average amounts of mCitrine-labeled H2B during the first cell cycle of daughter cells growing on YPD, SCD and SCGE. It can be seen that the cell cycle length is highly dependent on the nutrient environment and notably

increases in SCGE. Still, I find that in all growth media the H2B-mCitrine concentration at birth *i.e.* the amount of protein per cell volume, decreases with increasing cell volume (Fig. 11D). This is because constant amounts of H2B-mCitrine are produced independently of the nutrient condition (Fig. 11E). To verify these results I also performed flow cytometry measurements and quantified the H2B-mCitrine amounts in G1 cells growing on different growth media (Fig. 11F). I find that in addition to the three media tested with microscopy, histone amounts are maintained constant across all selected nutrient conditions.

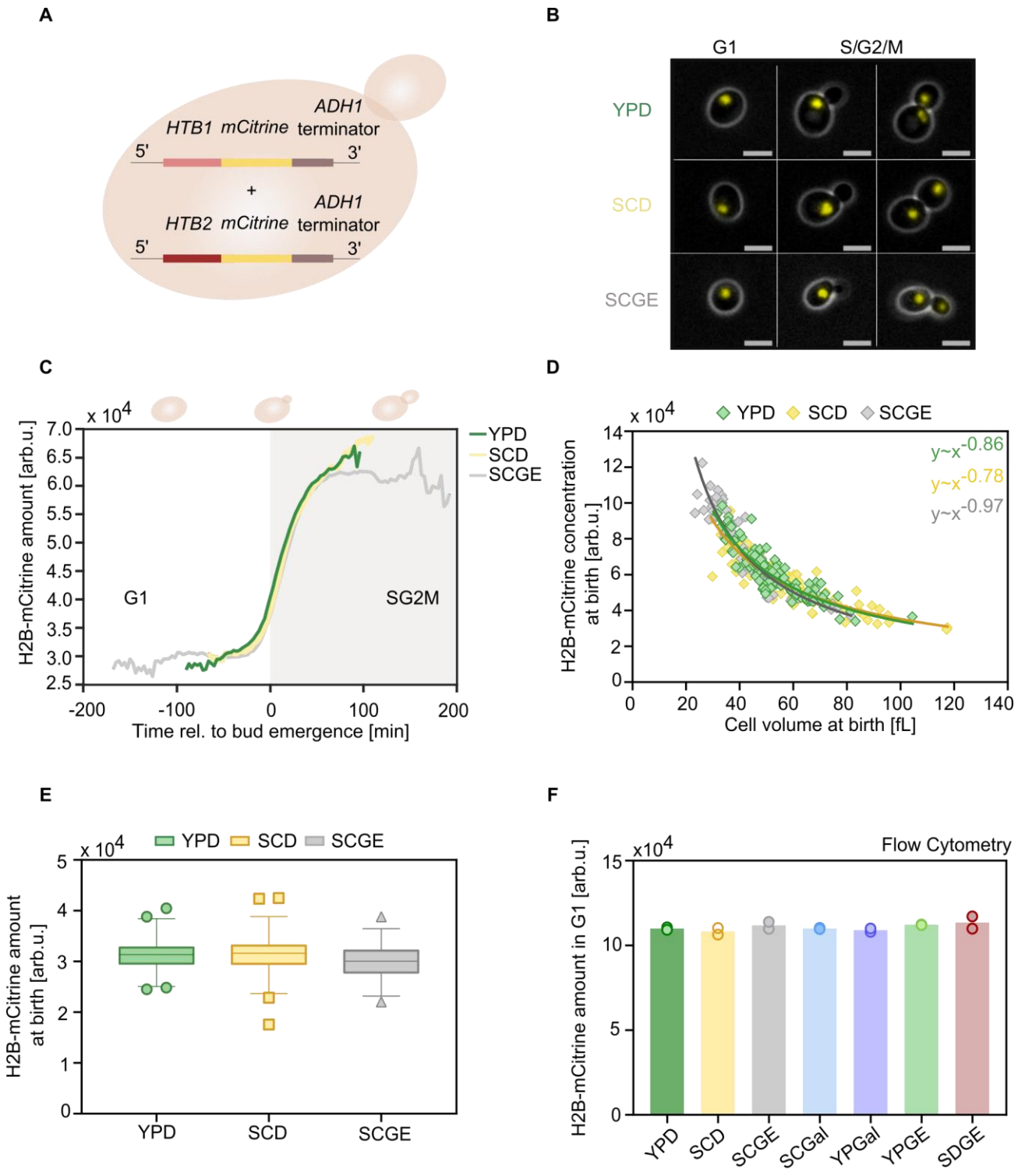

Figure 11. Single-cell histone protein amounts are constant across changing nutrient environments. (**A**) Live-cell fluorescence microscopy was used to track the fluorescent amounts of labeled H2B throughout the cell cycle of haploid cells growing on different growth media. To this end, *HTB1* and *HTB2* were endogenously tagged with *mCitrine*, which was followed by an *ADH1* terminator. (**B**) Representative phase-contrast and live-cell fluorescent images of individual cells with mCitrine-tagged H2B in G1- and S/G2/M-phase, growing on YPD, SCD and SCGE, respectively.

Scale bar: 5 µm (**C**) Mean expression profile of mCitrine-labeled H2B during the first cell cycle of daughter cells in different nutrients (n_{YPD}=87), SCD (n_{SCD}=83) and SCGE (n_{SCGE}=55). Fluorescent intensity traces were aligned at t=0. (**D**) H2B-mCitrine concentration at birth *i.e*. the amount of protein per cell volume decreases with cell volume across different growth media. Line represents fit with coefficients extracted from linear regression on the double-logarithmic raw data. (**E**) Distribution of nutrient-dependent H2B-mCitrine amounts at birth. Box plots show median values and 25th and 75th percentiles; whiskers represent the 2.5th and 97.5th percentiles; outliers are shown as individual symbols (n_{YPD}=87), SCD (n_{SCD}=83) and SCGE (n_{SCGE}=55). (**F**) Total H2B-mCitrine amounts in G1 cells growing on different growth media as determined by flow cytometry. Bar graphs show the mean of n=2 replicates, each displayed as an individual dot.

3.3.1 Fluorescent labeling influences histone mRNA expression

To test whether the fluorescent tagging of *HTB1* and *HTB2* induces an unwanted cell growth phenotype, I determined the nutrient-specific population doubling times, mean cell volumes and cell cycle fractions (Fig. 12A-C). I found that while cells expressing H2B-mCitrine had similar doubling times (Fig.12A) and cell cycle distributions (Fig. 12B) to the wild type, they showed slightly larger mean cell volumes (Fig. 12C). To further investigate the effect of the fluorescent tag on *HTB1* and *HTB2* mRNA expression under different nutrient conditions, I performed reverse-transcription quantitative PCR (RT-qPCR) (Fig. 12D). For the analysis, I included the untagged housekeeping gene *ACT1* as a control. My data revealed that tagging both histone genes with *mCitrine* results in elevated mRNA concentrations, especially for *HTB2-mCitrine*. I also examined histone mRNA levels in strains expressing either *HTB1-mCitrine* or *HTB2-mCitrine*, and in both cases detected increased concentrations of the tagged histone gene (Fig. 12E-F). Interestingly, the tagging of *HTB1* had a stronger impact on the *HTB1* mRNA concentration in cells with only *HTB1-mCitrine*.

As *mCitrine* is followed by an *ADH1* terminator, and also given the importance of the 3' untranslated region (UTR) in regulating mRNA stability (*159*, *160*) I next sought to examine the influence of the terminator sequence on the observed increase in histone mRNA levels. To this end, I replaced the *ADH1* terminator with the endogenous *HTB1* terminator sequence (Fig. 12E) and compared the mRNA concentrations of *HTB1-mCitrine-HTB1term* with *HTB1-mCitrine-ADH1term* in YPD (Fig. 12F). However, despite the exchanged terminator sequence, the mRNA levels of the tagged *HTB1* remained elevated. Overall, these results indicate that the C-terminal *mCitrine* tag most likely affects histone mRNA abundance by

modulating mRNA stability. Therefore, the regulation of mCitrine-tagged histones in these strains requires careful interpretation.

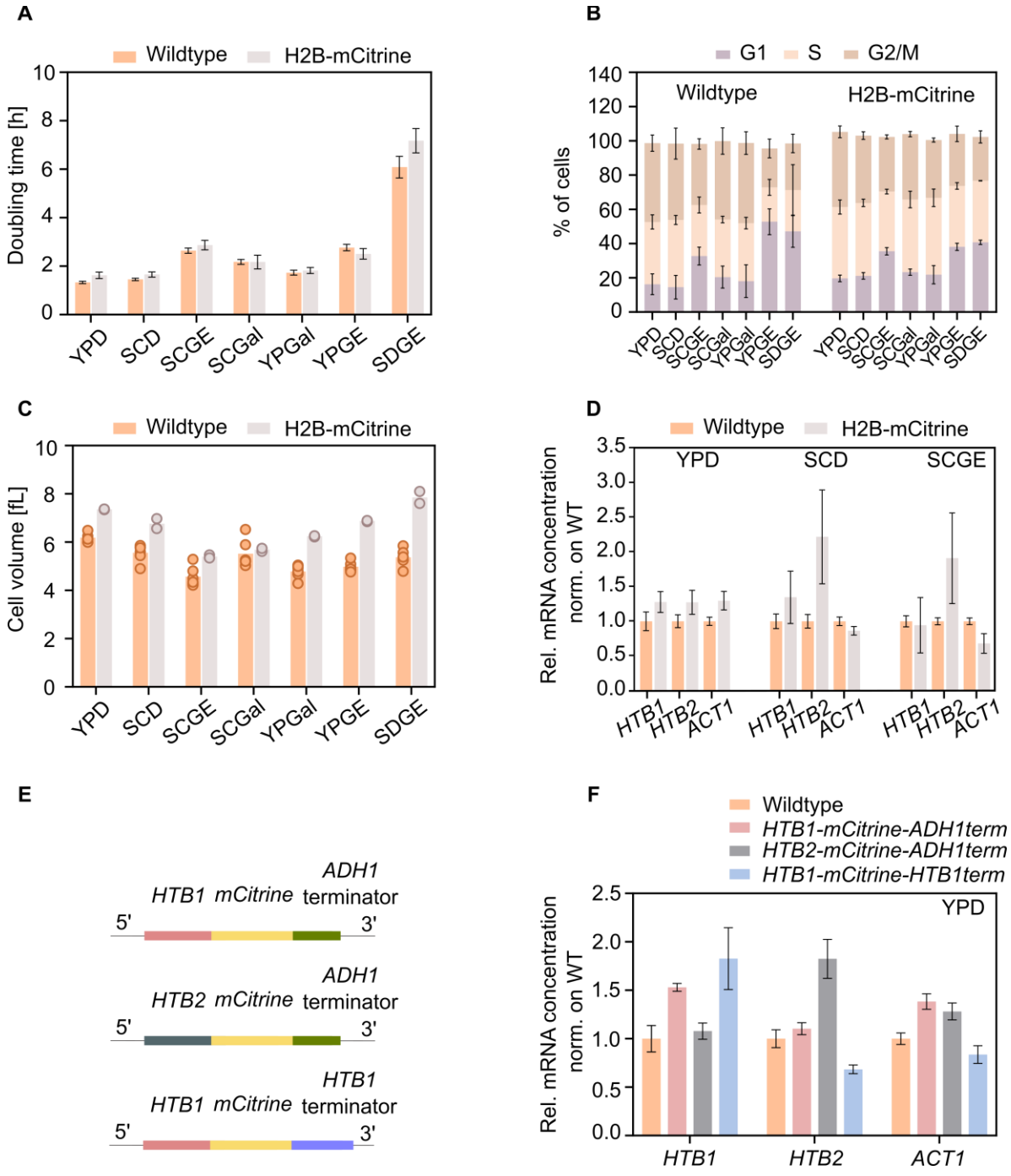

Figure 12. Characterization of strain with mCitrine-tagged H2B, in different nutrient conditions. (**A**) Doubling times estimated from the growth curves of asynchronous cell populations, growing exponentially on different growth media. Bar graphs and error bars show mean and standard deviation ($n_{Wildtype}$ =4, $n_{H2B\text{-}mCitrine}$ =3). (**B**) Cell cycle phase distributions were determined by flow cytometry based on the H2B-mCitrine fluorescence and compared to wildtype. Error bars indicate the

standard deviation of $n_{Wildtype}$ =5 or $n_{H2B\text{-}mCitrine}$ =2 independent measurements. (**C**) Mean volumes of cell populations growing exponentially on the different growth media. Cell volume measurements were carried out with a Coulter counter. Bar graphs represent the mean of $n_{Wildtype}$=6 and $n_{H2B\text{-}mCitrine}$=2 replicates, each displayed as a single dot. (**D**) RT-qPCR measurements of the relative *HTB1*, *HTB2* and *ACT1* mRNA concentrations in wildtype cells and cells with mCitrine-tagged H2B. mRNA concentrations (normalized on *RDN18)* are shown as fold changes relative to the wildtype. The bar graphs and error bars represent mean and standard errors of n=3-6 independent biological replicates. (**E**) Schematic illustration of mCitrine-tagged *HTB1* and *HTB2*, followed by the *ADH1* or the endogenous *HTB1* terminator. (**F**) RT-qPCR was performed in YPD to measure the relative mRNA concentrations of *HTB1*, *HTB2* and *ACT1* in untagged cells (wildtype), and cells expressing mCitrine-tagged *HTB1* or *HTB2*, followed by the *ADH1* or *HTB1* terminator. The concentrations were normalized on the reference gene *RDN18* and are presented with respect to the untagged wildtype. The bar graphs and error bars represent mean and standard errors of n=3-4 independent biological replicates.

3.4 Concentration of histone transcripts decreases in poor nutrient environments

While biosynthesis of most proteins and transcripts increases in proportion to cell volume, cells couple histone protein and transcript amounts to the DNA content (*89*, *90*). Consequently, histone expression scales with ploidy rather than cell volume *(89)*. So far, I have shown that histone proteins are maintained at constant amounts across different nutrient conditions, regardless of changes in cell growth and cell cycle distributions. However, it is still unclear whether this nutrient-dependent regulation of histones is established at the mRNA level. Assuming that equal amounts of histone transcripts are produced in the different growth media, one would expect higher transcript concentrations in nutrient-poor conditions, because of the smaller cell volumes. Surprisingly, RT-qPCR measurements revealed that all core histones showed significantly lower transcript concentrations in poor compared to rich nutrient conditions (Fig. 13). Yet, the control genes *ACT1* and *MDN1* were maintained at constant levels across nutrients. The latter can be explained by the fact that *ACT1* and *MDN1* are housekeeping genes, whose mRNA amounts scale with increasing cell volume, resulting in constant concentrations during growth (*89*, *90*). These results suggest that histone mRNA expression strongly depends on the nutritional environment. At the same time, histone proteins are kept at a constant protein-to-DNA ratio across different nutrient conditions. This decoupling of transcript and protein levels highlights the need of regulated translation or

protein degradation in order to achieve histone protein homeostasis in different growth media.

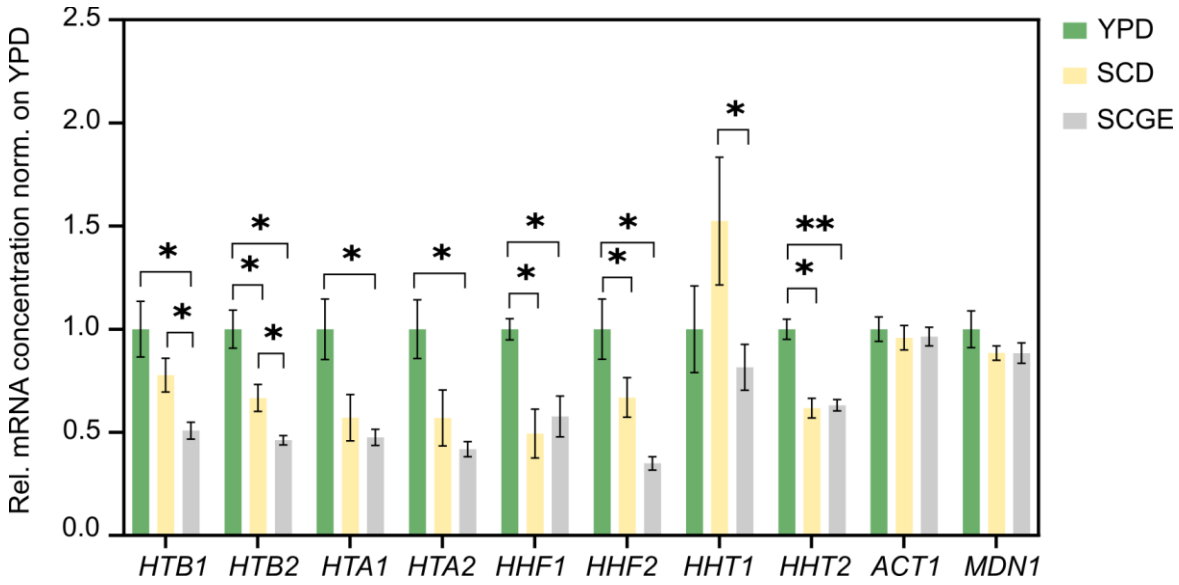

Figure 13. Histone mRNA concentrations decrease in poor nutrient conditions. Nutrient-specific mRNA concentrations of core histone genes, as well as *ACT1* and *MDN1* were analyzed by RT-qPCR and normalized on the rRNA *RDN18*. mRNA concentrations are presented as fold changes relative to YPD. The bar graphs and error bars show mean and standard errors of n=4-6 independent biological replicates. Statistical significance was estimated by an unpaired, two-tailed t-test for datasets following a Gaussian distribution. Alternatively, a Mann-Whitney test was used for not normally distributed datasets (* $p<0.05$, ** $p<0.01$).

3.4.1 Nutrient-dependent transcription explains downregulation of histone mRNA expression in poor nutrient environments

Cellular mRNA concentrations are determined by both, RNA pol II-dependent transcription and subsequent mRNA degradation. In response to changing environments, cells can regulate gene expression by modifying mRNA synthesis and/or decay rates to adjust mRNA concentrations (*161*, *162*). For most genes, transcription and mRNA degradation correlate positively with growth rate, keeping mRNA concentrations constant (*116*, *117*). However, certain gene groups uncouple mRNA synthesis from degradation, leading to increased or decreased mRNA concentrations in different growth conditions. For example, the mRNA levels of ribosome-associated genes are upregulated in fast growth conditions as a result of

increased transcription rates. On the other hand, mitochondria-related genes tend to downregulate their mRNA levels with faster growth, by decreasing the mRNA stability at constant transcription (*116*, *117*).

As I have shown in section 3.4, histone mRNA concentrations are significantly reduced in poor compared to rich nutrient environments. This may reflect relatively lower histone transcription rates in poor nutrients, reduced mRNA stability or a combination of both. To better understand how the mRNA levels are regulated in the different growth media I quantified the contribution of mRNA degradation to the nutrient-dependent changes in histone mRNA expression. To this end, I estimated the mRNA half-lives of the histone genes *HTB1* and *HTB2*, as well as the control gene *ACT1* from mRNA decay curves that were measured after transcriptional inhibition by thiolutin (Fig. 14). Thiolutin is a sulphur-containing antibiotic that inhibits RNA polymerases in yeast and causes a global transcriptional shut-off (*163*). Following the addition of thiolutin, I quantified the histone and *ACT1* mRNA levels over time by RT-qPCR. I then calculated the respective mRNA half-lives by fitting the decay curves with a one-phase exponential function. In agreement with previous literature, in YPD histone mRNAs degrade more rapidly than *ACT1,* which has a longer mRNA half-life (Fig. 14A) (*137*, *164*). Furthermore, the results suggest that both, histone and *ACT1* mRNA stabilities increase in SCGE compared to YPD (Fig. 14B). I noticed however, that the one-phase or single exponential decay model did not always provide a good fit, especially to the decay curves measured in SCGE. The actual half-lives may therefore deviate from the estimated values.

As the relative *ACT1* mRNA concentrations remained constant in the different growth media, the destabilisation of *ACT1* mRNA in YPD is likely compensated by an increased transcription rate. This would be consistent with prior studies suggesting that transcription and mRNA decay of most genes increase with faster growth to maintain constant mRNA levels across changing environments (*116*, *117*). By contrast, histone mRNA concentrations depend on the nutrient environment and significantly decrease in SCGE compared to YPD. Since histone mRNA stability increases in SCGE, I conclude that the downregulation of histone transcripts in poor nutrients must be due to a decrease in histone transcription.

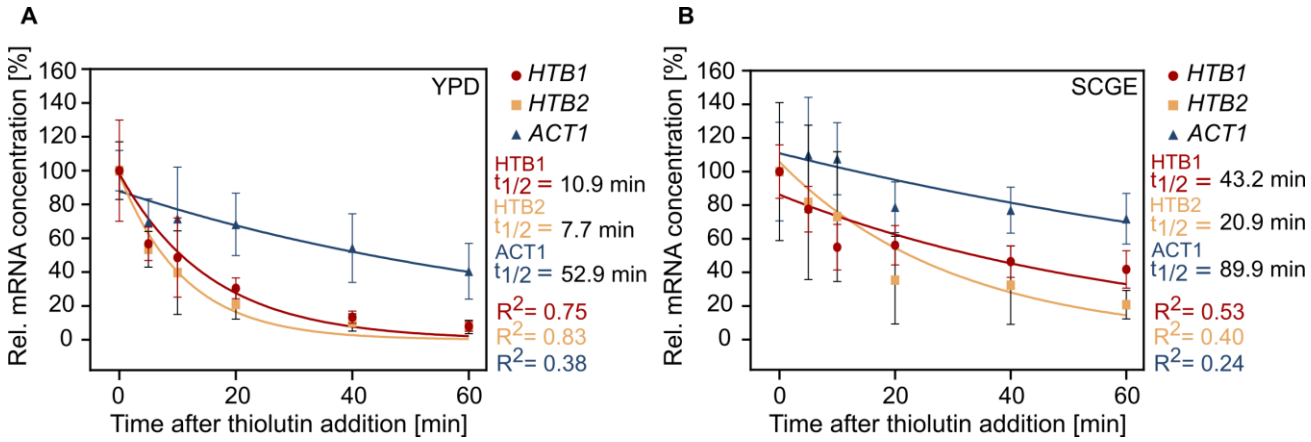

Figure 14. Histone mRNA stability increases in poor growth medium. (**A-B**) RT-qPCR analysis of the *HTB1*, *HTB2* and *ACT1* mRNA degradation, following transcription inhibition by thiolutin. Time course experiments were performed in YPD (A) and SCGE (B). Relative mRNA concentrations were normalized on the reference gene *RDN18* and plotted relative to the initial concentration at t=0 min. Mean and standard deviation of n=4-9 independent replicates are shown for the time points between t=0 and t=60 min. The mRNA half-lives were estimated by fitting the data from all replicate measurements with a one-phase exponential decay model (line).

3.5 Histone promoters mediate nutrient-dependent mRNA expression

After establishing that nutrient-dependent transcription likely accounts for the changes in histone mRNA concentration, I asked whether the promoter can mediate the distinct regulation of histone transcripts across different nutrients. For this, I inserted an extra copy of the *HTB1*, *HTB2* or *ACT1* promoter driving *mCitrine* into the *URA3* locus of the wildtype strain (Fig. 15A). The promoter sequences also included the 5' UTRs of *HTB1*, *HTB2* and *ACT1*, respectively. Using RT-qPCR I quantified the relative mRNA concentrations of *mCitrine* in three growth media and found that *mCitrine* transcripts expressed from the histone promoters are downregulated in SCGE, compared to YPD and SCD (Fig. 15B). At the same time, the mRNA concentrations of *ACT1prom-mCitrine* remain constant between the conditions. This is consistent with my findings on the endogenous histone and *ACT1* mRNA concentrations (Fig. 15C). Interestingly, I find that in SCD the mRNA concentrations of *mCitrine* driven by the histone promoters are more elevated compared to the endogenous *HTB1* and *HTB2* mRNA concentrations. Thus, these results suggest that the nutrient-dependence of histone mRNA levels is at least partly promoter-mediated.

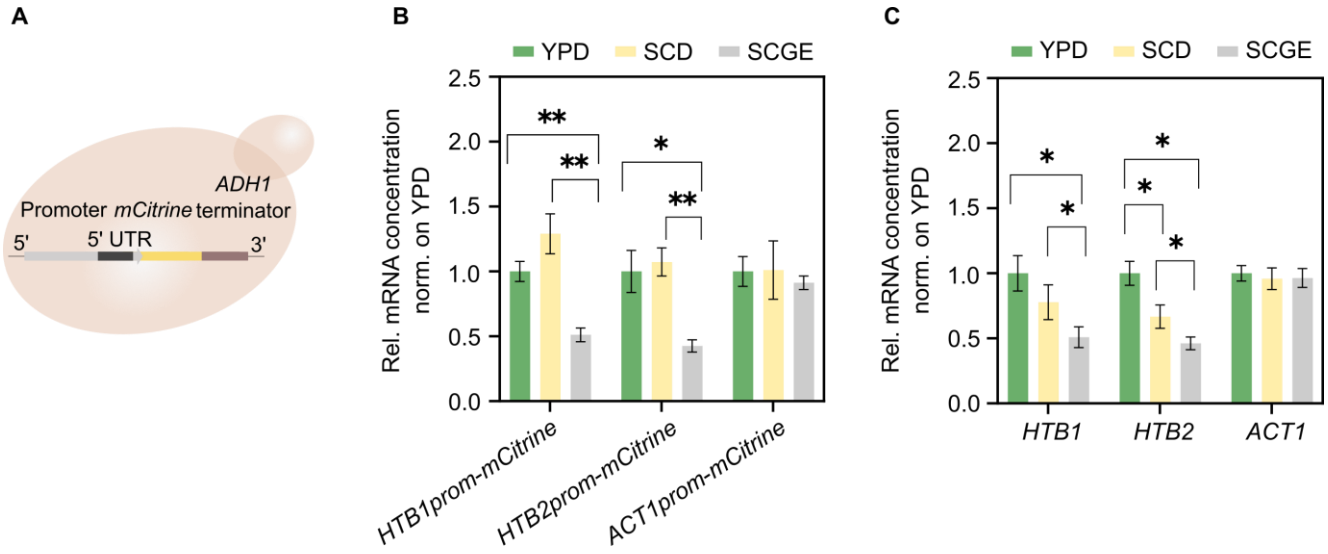

Figure 15. Reporter transcripts expressed from histone promoters are downregulated in poor growth medium. (**A**) A copy of the *mCitrine* reporter ORF driven by the promoter of choice and followed by the *ADH1* terminator was inserted into the *URA3* locus of the wildtype. All promoters included the respective 5' UTRs. (**B**) Relative mRNA concentrations of *mCitrine* driven by the *HTB1*, *HTB2* and *ACT1* promoter. The concentrations were normalized on the rRNA *RDN18* and are presented as fold changes relative to YPD. Mean and standard deviations of n=4-5 independent biological replicates are shown. (**C**) Relative mRNA concentrations of *HTB1*, *HTB2* and *ACT1* were quantified by RT-qPCR in different growth media. The concentrations were normalized on the rRNA *RDN18* and are presented as fold changes relative to YPD. The bar graphs and error bars show mean and standard deviations of n=4-6 independent biological replicates. Statistical significance was estimated using an unpaired, two-tailed t-test (* $p<0.05$, ** $p<0.01$).

3.6 Characterization of the cell cycle- and cell-volume-dependent histone gene expression in different nutrients

Histone promoters can match histone mRNA expression to the genome content, in a cell-volume-independent manner (*89*). However, here I show that histone mRNA concentrations are differentially regulated across changing environments, and decrease significantly in poor nutrients. As shown in section 3.5, the promoter can mediate this nutrient-dependence of histone transcripts. However, it is not known whether histone mRNA levels are uncoupled from cell volume for each nutrient condition. To answer this question, I performed single-molecule fluorescence in situ hybridisation (smFISH) to detect and quantify individual mRNAs in single cells grown in different media. I used fluorescently labelled oligonucleotide

probes that bind along the mRNA target of interest and visualised the fluorescent mRNA molecules by epifluorescence microscopy (Fig. 16A). Based on the bright-field images, I then estimated the cell volume and classified each cell into G1-, S- or G2/M-phase according to the bud-to-mother cell volume ratio and the number and shape of its nuclei. This allowed me to study the cell-volume-dependent mRNA expression during the cell cycle, in different nutrient conditions. Here it should be noted that I measured the number of individual mRNA spots in the cell and did not include the amount of potentially multiple nascent transcripts present at the transcription start site.

3.6.1 *ACT1* and *MDN1* mRNA amounts increase with cell volume, independently of the nutrient environment

I first analyzed the mRNA levels of *ACT1* and *MDN1*, two housekeeping genes, whose expression is known to scale with cell volume (*89*, *90*). *MDN1* is also the largest yeast gene (*148*, *165*), which is advantageous for detection of the fluorescent signal as more probes can bind to the mRNA. This was very helpful in successfully establishing the smFISH technique in the laboratory. For the mRNA analysis, the *ACT1* and *MDN1* transcripts were targeted with Quazar-570- and Quazar-670-labeled smFISH probes, respectively. Moreover, I stained the cell nuclei with the fluorescent dye DAPI (Fig. 16B).

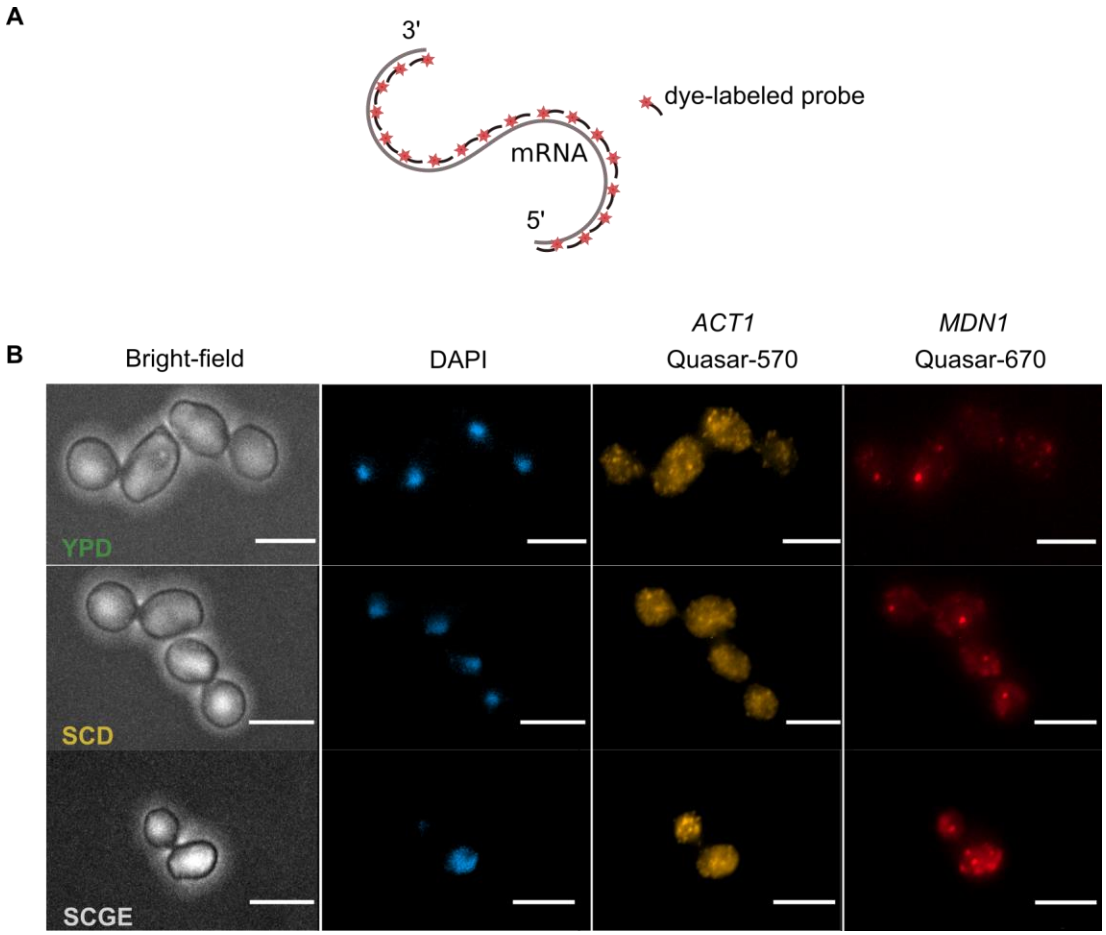

Figure 16. smFISH analysis of nutrient-dependent *ACT1* and *MDN1* mRNA expression. (**A**) Fluorescently-labeled oligonucleotide probes hybridizing to the mRNA target of interest enabled the visualization and quantification of individual mRNAs in single cells using bright-field fluorescence microscopy. (**B**) To analyze the mRNA levels of *ACT1* and *MDN1* across the different nutrients, I used a set of Quasar-570-(yellow) and Quasar-670-labeled (red) probes, respectively. Nuclei were counterstained using DAPI. Representative bright-field and fluorescence images of individual cells grown in YPD, SCD and SCGE. All scale bars indicate 5 µm.

Consistent with the literature, *ACT1* showed overall higher expression levels than *MDN1* (*165*, *166*). Moreover, our results demonstrate that both genes were constitutively transcribed during the cell cycle yielding constant mRNA concentrations (number of mRNA spots divided by cell volume) independent of the respective bud-to-mother cell volume ratio, which is a proxy for cell cycle progression (Fig. 17A-B). This is because the mRNA copy numbers increased with increasing cell volume in all nutrient conditions (Fig. 17C-D). In fact, I observed a stronger dependence on cell volume than on the nutrients, as similar mRNA amounts were detected at a given cell volume, independently of the nutrient environment.

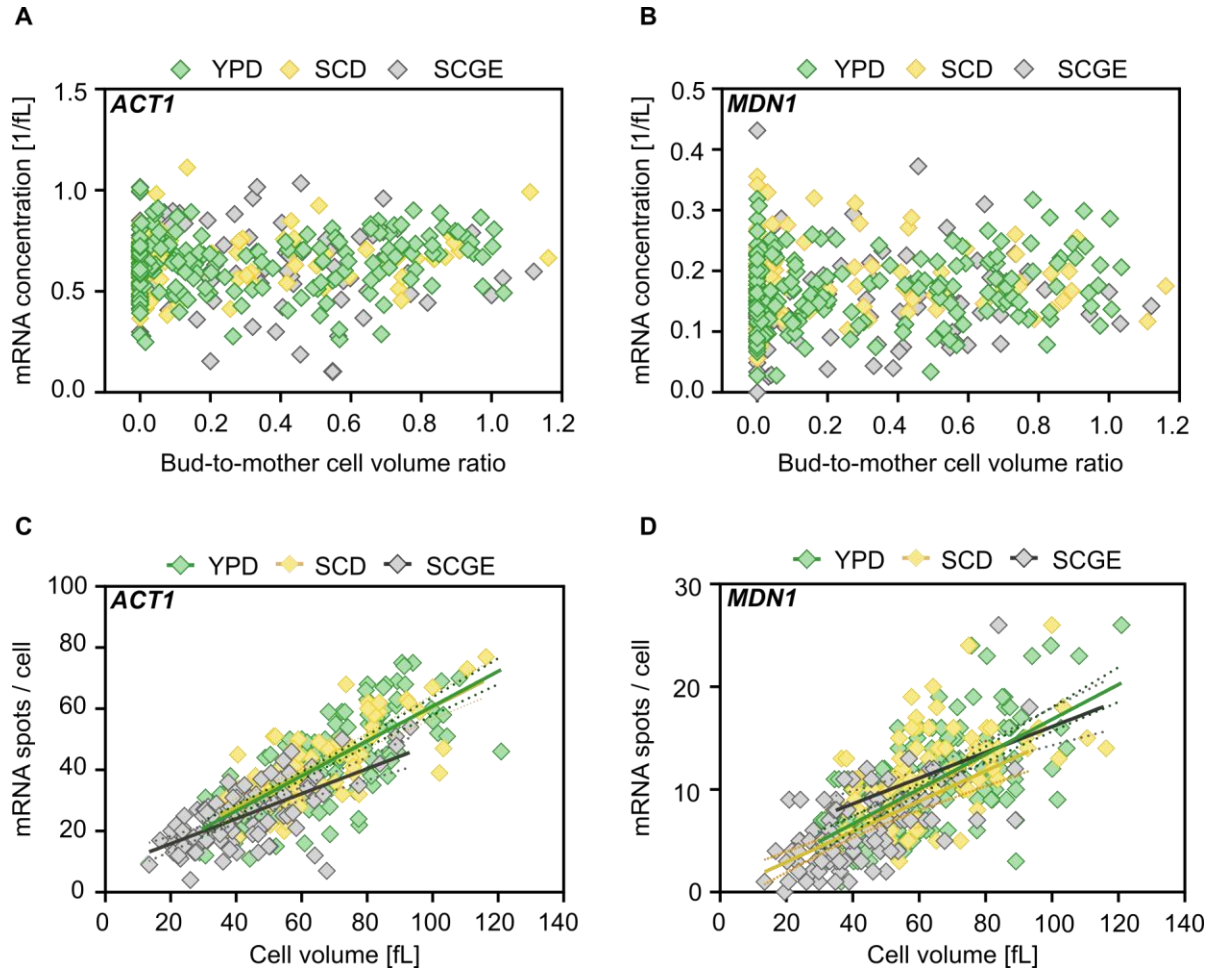

Figure 17. mRNA expression of *ACT1* and *MDN1*, as determined by smFISH, scales with cell volume, independently of the nutrient conditions. (**A-B**) *ACT1* (A) and *MDN1* (B) mRNA concentration *i.e.* number of mRNA spots divided by cell volume as a function of the bud-to-mother cell volume ratio in different nutrient conditions (n_{YPD}=176, n_{SCD}=87, n_{SCGE} =98). (**C-D**) mRNA spots of *ACT1* (C) and *MDN1* (D) per cell plotted against the cell volume in different nutrient conditions (n_{YPD}=176, n_{SCD}=87, n_{SCGE}=98). Solid lines indicate linear fits and dashed lines show the 95% confidence intervals.

3.6.2 mRNA expression driven by histone promoters is independent of cell volume in different nutrients

I next used smFISH to quantify the nutrient-dependent mRNA levels expressed from histone promoters in single cells. More precisely, I targeted *mCitrine* reporter transcripts expressed

from the *HTB1* or *HTB2* promoter with Quasar-670-labeled probes and determined the mRNA concentrations per cell during the cell cycle (Fig. 18A-B).

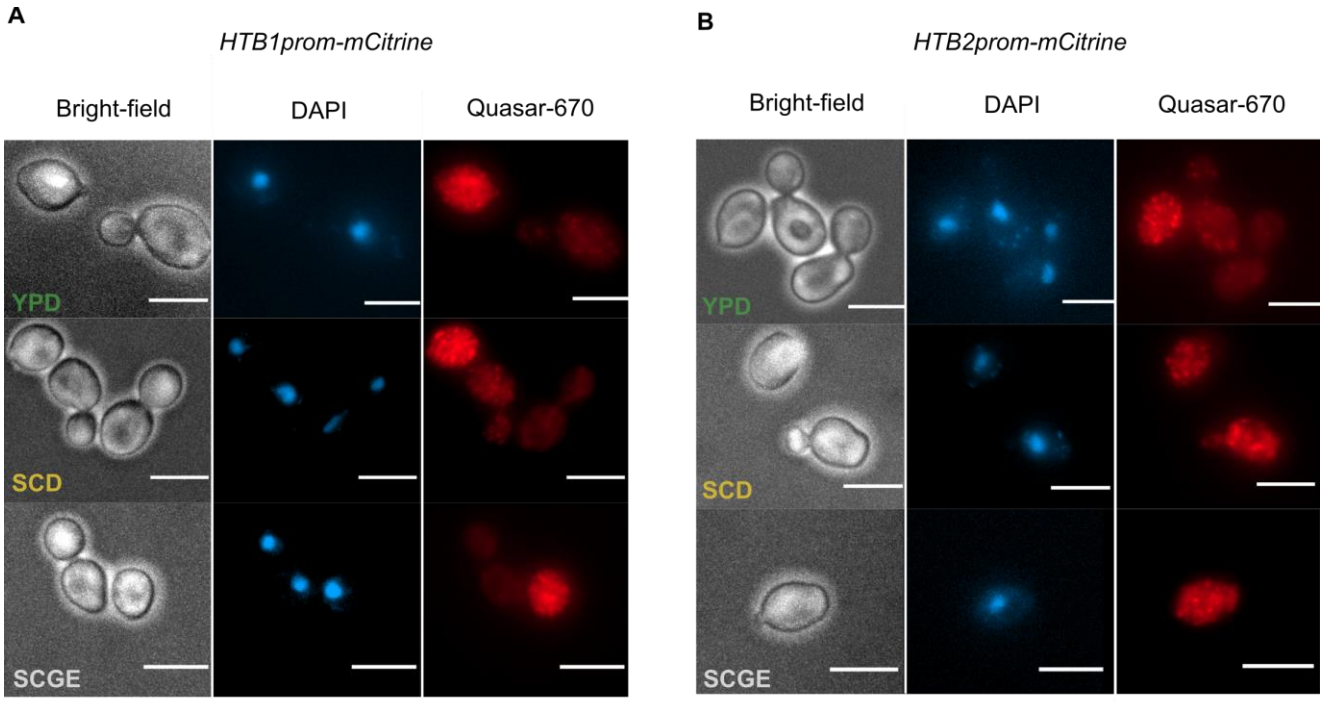

Figure 18. smFISH analysis of nutrient-dependent *mCitrine* expression driven by histone promoters. (**A-B**) smFISH combined with bright-field fluorescence microscopy was performed to quantify the nutrient-dependent mRNA expression of *mCitrine* from the *HTB1* (A) and *HTB2* promoter (B). *mCitrine* mRNAs were targeted with Quasar-670-labeled oligonucleotide probes. Nuclei were counterstained using DAPI. Representative bright-field and fluorescence images of cells grown in YPD, SCD and SCGE. Scale bars indicate 5 µm.

While *ACT1* and *MDN1* are transcribed continuously throughout the cell cycle, the transcription of histone genes is only activated in late G1 and continues during S-phase (*88*, *124*). Since histone promoters can confer cell cycle-regulated transcription (*128*, *167*), I found that the mRNA concentrations of *HTB1prom-mCitrine* and *HTB2prom-mCitrine* peaked during S-phase and dropped as cells progressed through G2/M phase (Fig. 19A-B). The wide distribution of mRNA concentrations in G1 (at a bud-to-mother-cell volume ratio of 0) most likely resulted from inactivated and activated gene transcription in early and late G1 cells, respectively. However, here I did not use cell cycle progression markers to distinguish between early and late G1-phase. One common approach to this would be to monitor the subcellular localization of fluorescently labeled Whi5 in unbudded cells. Whi5 is a cell cycle

inhibitor that resides in the nucleus between late M- and early G1-phase before it is exported to the cytoplasm in late G1, at the START checkpoint (*168*, *169*).

To determine whether the nutrient-dependent mRNA expression driven by the histone promoters is uncoupled from cell volume, I analysed the *mCitrine* peak-expression during S-phase (Fig. 19C-D). My results showed constant, volume-independent mRNA amounts for each condition. At the same time, the mRNA copies at a given cell volume were downregulated in poor growth medium.

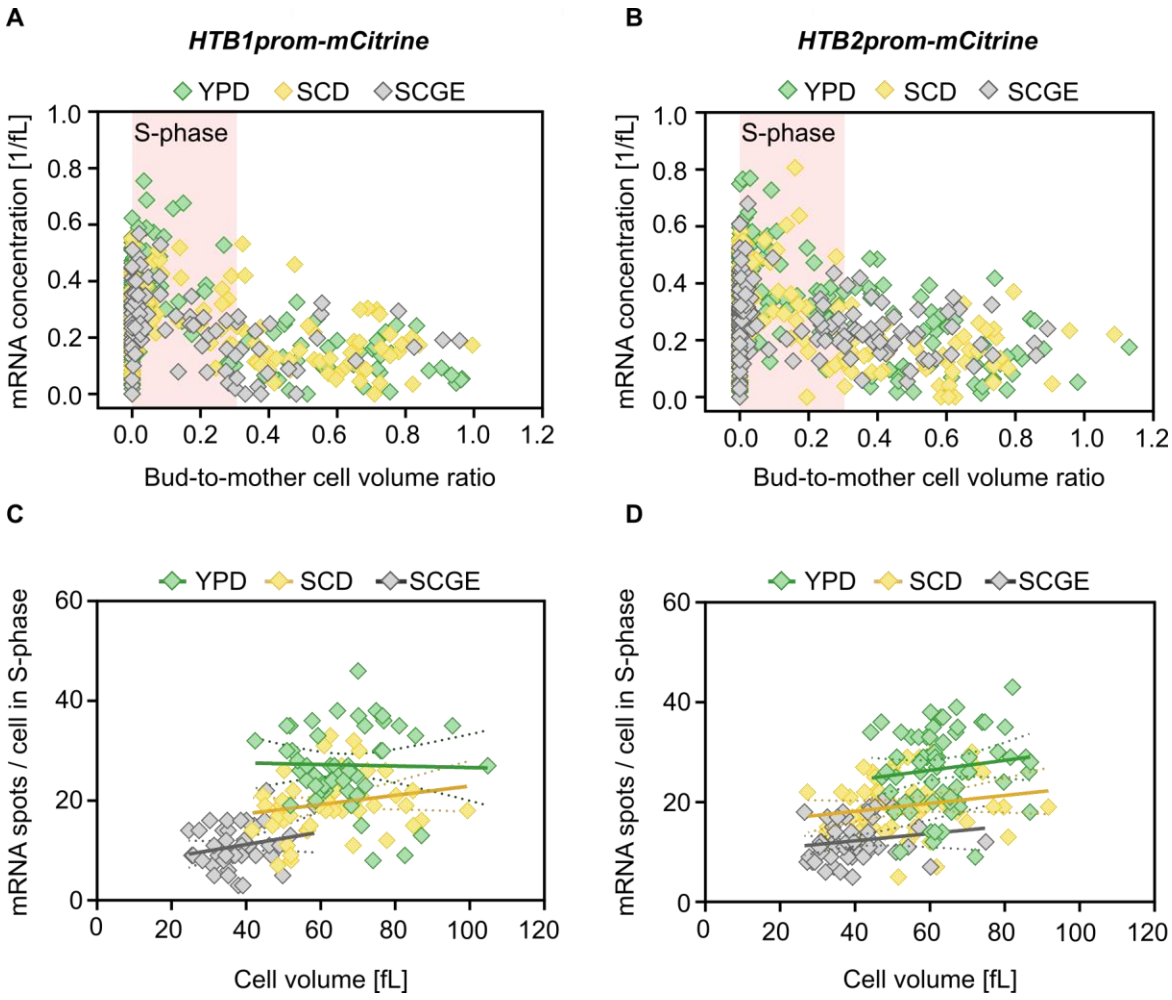

Figure 19. In different nutrients, mRNA expression driven by histone promoters is independent of cell volume. (**A-B**) Cellular mRNA concentrations of *HTB1prom-mCitrine* (n_{YPD}=149, n_{SCD}=158, n_{SCGE}=95) (A) and *HTB2prom-mCitrine* (n_{YPD}=161, n_{SCD}=194, n_{SCGE}=170) (B), determined by smFISH, are shown as a function of the bud-to-mother cell volume ratio in different nutrient conditions. (**C-D**) *mCitrine* mRNA copy number per cell expressed from the *HTB1* (n_{YPD}=49, n_{SCD}=51, n_{SCGE}=39*)* (C) *and HTB2* promoter (n_{YPD}=64, n_{SCD}=59, n_{SCGE}=50) (D) is plotted against the corresponding cell volume in different nutrient conditions. Solid lines indicate linear fits and dashed lines show the 95%

confidence intervals. Here, budded cells with a bud-to-mother cell volume ratio < 0.30 that contained one nucleus were classified as S-phase cells.

To further disentangle the effect of cell volume and nutrient quality on the *HTB1prom-mCitrine* mRNA abundance, I increased the range of cell volumes in poor medium and determine any potential changes in the mRNA expression. I used a haploid strain with a β-estradiol-inducible allele of Whi5, carrying an extra copy of the *HTB1* promoter driving *mCitrine* (*89*, *170*) (Fig. 20A). Whi5 is a cell size regulator that inhibits the G1/S transition in cells by repressing the transcription factor SBF (*171*, *172*). As cells grow during G1, Whi5 is diluted, allowing them to progress through the cell cycle (*171*). Overexpression of Whi5 therefore causes cells to grow larger before entering S phase (*170*, *171*). Using a β-estradiol concentration of 5 nM, I increased the range of cell volumes in SCGE and measured the *mCitrine* mRNA amounts per cell during S-phase (Fig. 20B). Yet, I found no significant change in the coordination of *mCitrine* transcripts with cell volume between hormone-induced and wildtype cells. Similar to the wildtype in SCGE, the mRNA copy numbers in the induced cells were lower than in YPD and SCD, but remained constant over cell volume. Overall, the single-cell results highlight the nutrient-dependent transcript regulation mediated by histone promoters and support the RT-qPCR analysis in asynchronous cell populations. At the same time, they suggest that for each nutrient condition the produced transcript amounts are uncoupled from cell volume.

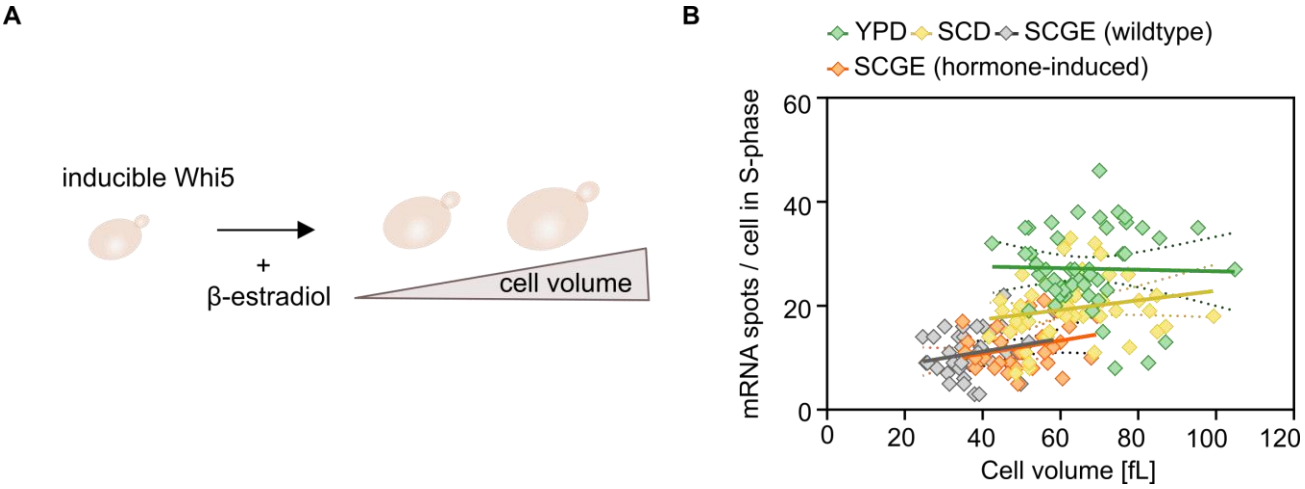

Figure 20. Hormone-induced cell volume changes in SCGE do not alter the nutrient-independence of *HTB1prom-mCitrine* mRNA amounts. (**A**) The range of observable cell volumes in SCGE was extended by adding β-estradiol to cells with hormone-inducible Whi5, expressing *HTB1prom-mCitrine*. (**B**) *mCitrine* mRNA amounts from wildtype or hormone-induced cells as a function of cell volume in different nutrient conditions (n_{YPD}=49, n_{SCD}=51, n_{SCGE}=39, $n_{SCGE,\ induced}$ =30). Solid lines indicate linear fits and dashed lines show the 95% confidence intervals. Here, budded cells with a bud-to-mother cell volume ratio < 0.30 that contained one nucleus were classified as S-phase cells.

For comparison, I also studied the cell-volume-dependent *mCitrine* expression driven by the *ACT1* promoter. Cellular mRNA concentrations during the cell cycle were determined using Quasar-670-labeled probes (Fig. 21A). Similar to the endogenous *ACT1*, *ACT1prom-mCitrine* was continuously expressed at constant mRNA concentrations in rich and poor conditions (Fig. 21B). Moreover, the *mCitrine* copy numbers per cell increased with cell volume, independent of the nutrients, suggesting that the *ACT1* promoter can confer cell-volume-dependent transcript regulation across changing environments (Fig. 21C). These results further emphasize the distinct regulation mediated by histone promoters, which is strongly dependent on the nutrient environment.

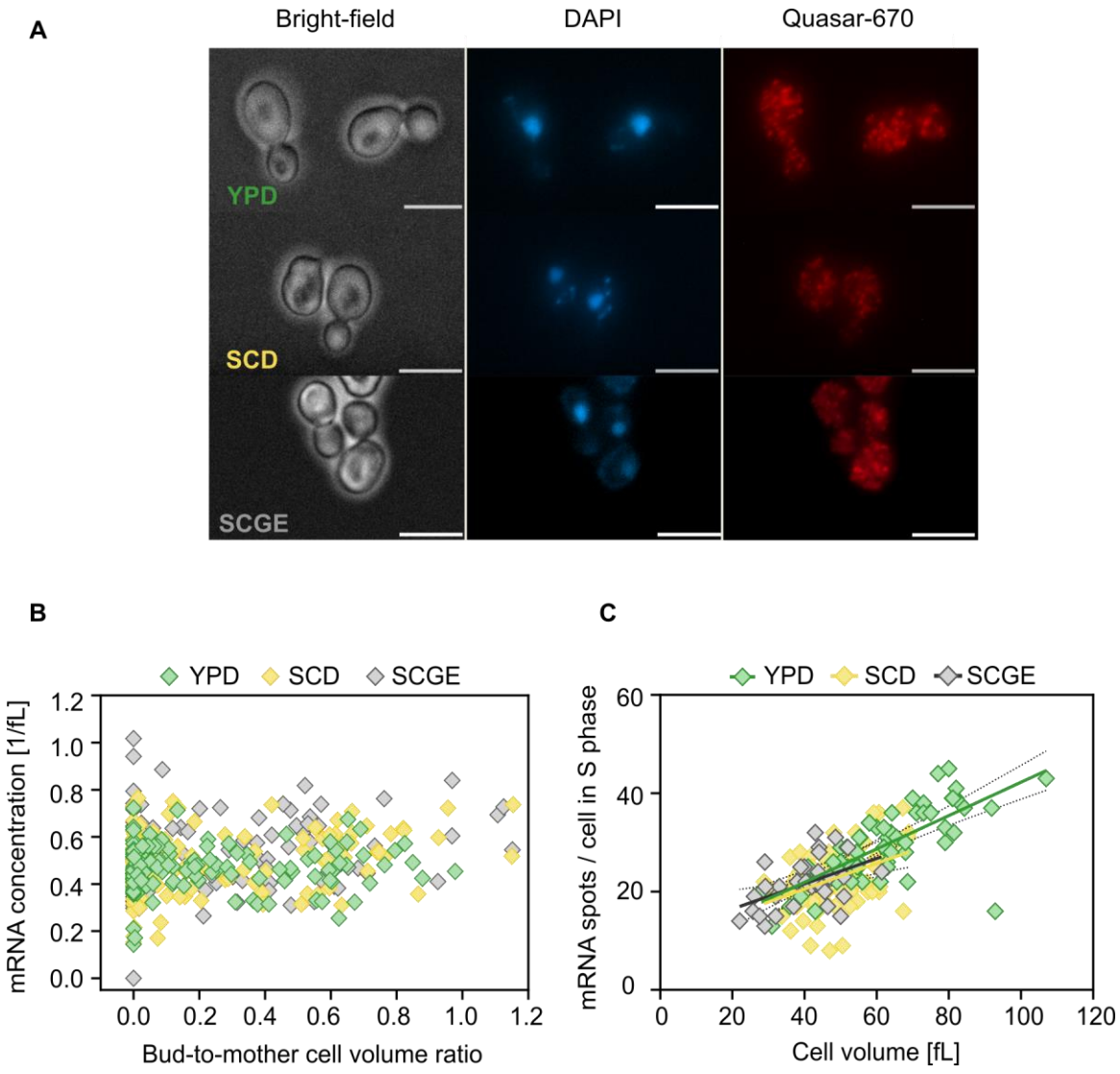

Figure 21. *mCitrine* mRNA expression driven by the *ACT1* promoter scales with cell volume, independently of the nutrient conditions. (**A**) smFISH combined with epifluorescence microscopy was used to detect *ACT1prom-mCitrine* mRNAs, targeted with Quasar-670-labeled oligonucleotide probes. Nuclei were counterstained using DAPI. Representative bright-field and fluorescence images of cells grown in YPD, SCD and SCGE. Scale bars indicate 5 µm. (**B**) *mCitrine* mRNA concentration as a function of the bud-to-mother cell volume ratio in different nutrient conditions (n_{YPD} =135, n_{SCD} = 155, n_{SCGE}=124). (**C**) Number of *ACT1prom-mCitrine* copies per cell plotted against the corresponding cell volume in different nutrient conditions (n_{YPD} =59, n_{SCD} =75, n_{SCGE} =33). Solid lines indicate linear fits and dashed lines show the 95% confidence intervals. Here, budded cells with a bud-to-mother cell volume ratio < 0.30 that contained one nucleus were classified as S-phase cells.

3.7 Truncated histone promoters alter nutrient and cell size dependence of reporter gene expression

In budding yeast, core histone promoters contain positive and negative cis-acting regulatory elements that couple gene expression to DNA replication in S-phase (*87*). Specifically, the cell cycle-dependent activation of core histone genes requires the 16 bp upstream activating sequences (UASs), which are recognized by the transcription factors Spt10 and SBF. While SBF promotes a small initial expression peak of histone transcripts, Spt10 acts as a master transcription activator (*87*, *128*). In contrast, negative transcriptional regulation of histone genes is mediated by the histone regulatory (HIR) complex, which is recruited to the NEG element to repress histone transcription outside of S-phase. The NEG element is located in three of the four core histone promoters, with the exception of the *HTA2–HTB2* promoter (*87*, *88*).

We previously showed that a truncated 300 bp *HTB1* promoter, missing two of the four UASs and the NEG element, is no longer sufficient to strictly uncouple transcription from cell volume (*89*). Instead, population level analysis of haploid and diploid cultures growing on SCGE indicated that the promoter truncation alters the volume-dependence of the *mCitrine* transcripts, leading to a stronger coordination with cell size. To investigate if this change in promoter behavior is due to a disrupted cell cycle dependence, I worked with Kora-Lee Claude (Kurt Schmoller Group, Helmholtz Zentrum München) and performed smFISH experiments to analyze the *mCitrine* concentrations expressed from different *HTB1* promoter truncations. Specifically, we used diploid strains with an integrated copy of a 300 bp or 450 bp *HTB1* promoter, shortened from the 5' end, and driving the expression of *mCitrine* (Fig. 22A). The 450 bp truncation comprised all four UASs and the NEG element, whilst the 300 bp truncation only contained two of the four UASs (UAS3/4), and was missing the NEG element. As a control, we included a diploid strain carrying a copy of the full *HTB1* promoter driving *mCitrine*. For all promoters, we found cell cycle-dependent *mCitrine* mRNA concentrations that peaked during S-phase (Fig. 22B). Moreover, the 300 bp *HTB1* promoter caused a significant decrease in *mCitrine* expression, which is likely attributed to the partial loss of the UAS elements. In the study by Claude et al., bulk analysis of the mCitrine transcript and protein levels revealed that the 300 bp promoter truncation resulted in a weaker decrease in *mCitrine* mRNA concentration with cell volume, compared to the 450 bp truncation (*89*).

Here, the smFISH analysis showed a similar, but less pronounced trend (Fig. 22C-E). Overall, our results indicate that by removing the 150 bp fragment between the 450 bp and 300 bp *HTB1* promoter constructs, the initial cell volume-dependent gene expression of the reporter transcripts is affected. However, this is not caused by the loss or disruption of their cell cycle dependence.

It should be noted, that the data from figure 22 were published by Claude et al. (*89*). The smFISH experiments were conducted by me, and Kora-Lee Claude performed the data analysis using FISH-quant v3 (*173*). In this work, I re-analysed the raw data using a Python routine, developed by Dr. Francesco Padovani (Kurt Schmoller Group, Helmholtz Zentrum München) (see Materials and Methods). For mRNA spot detection and quantification, I used a global intensity threshold applied to all cells imaged within a biological replicate, whereas Kora-Lee Claude chose an individual threshold for each cell. The use of a global intensity threshold resulted in a broader distribution of measured mRNA concentrations.

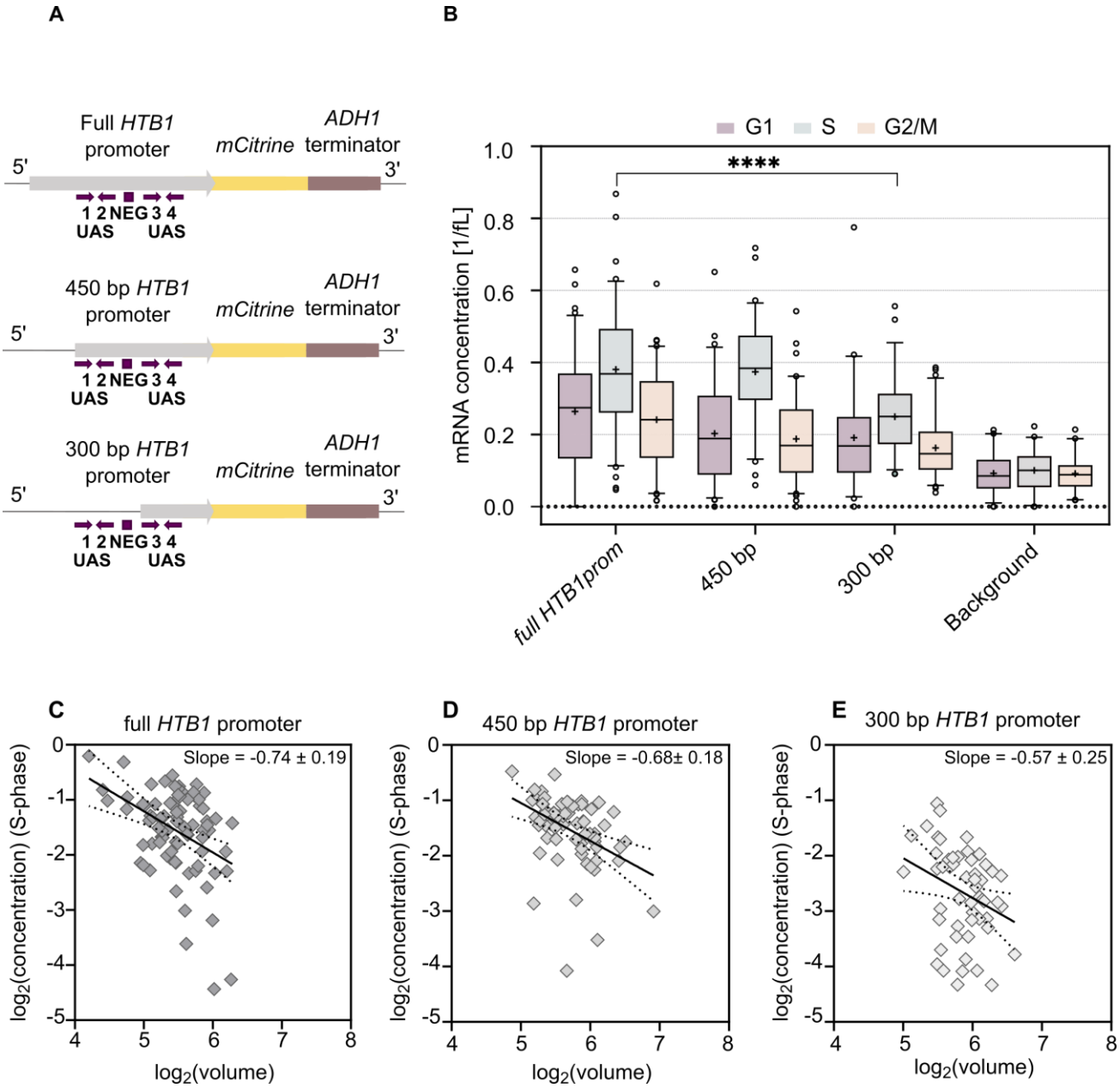

Figure 22. smFISH analysis of the cell cycle-dependent *mCitrine* expression driven by *HTB1* promoter truncations. (**A**) Schematic illustration of full-length and serially truncated *HTB1* promoter constructs driving the expression of *mCitrine*. The *HTB1* promoter was shortened from the 5' end to 450 bp and 300 bp. All constructs included the *HTB1* 5' UTR. Arrows display the position and orientation of the UASs within the promoter, and the boxes indicate the NEG elements. (**B**) Cell cycle phase distributions of the *mCitrine* mRNA concentrations (number of mRNA spots per cell) measured in diploid cells grown on SCGE and carrying a copy of the full-length or serially truncated *HTB1* promoter driving the reporter gene. As a negative control, diploid wildtype cells expressing no *mCitrine* were targeted with fluorescently labeled probes against the reporter gene. Box plots show median values and 25th and 75th percentiles; whiskers represent the 2.5th and 97.5th percentiles. $n_{G1}^{full HTB1prom}$=90, $n_{S}^{full HTB1prom}$=84, $n_{G2/M}^{full HTB1prom}$=80, n_{G1}^{450bp}=75, n_{S}^{450bp}=70, $n_{G2/M}^{450bp}$=80, n_{G1}^{300bp}=58, n_{S}^{300bp}=56, $n_{G2/M}^{300bp}$=70, $n_{G1}^{background}$=48, $n_{S}^{background}$=41, $n_{G2/M}^{background}$=40. Statistical significance was measured

using a Mann-Whitney test (**** p<0.0001). (**C-E**) Double-logarithmic plot showing the *mCitrine* mRNA concentration in S-phase expressed from the full-length (C), 450 bp (D) and 300 bp *HTB1* promoter (E) as a function of cell volume ($n_{full\,HTB1prom}$ =84, n_{450bp} =70, n_{300bp}=56). The black lines represent linear fits and the dashed lines show the 95% confidence intervals. The slopes of the linear fits (± standard errors) are shown.

Having established that histone promoter elements can confer cell volume-independent transcript regulation, I next sought to identify whether they are also required for the nutrient-dependence of histone transcripts. For this purpose, I followed the strategy of Claude et al. described above, and used haploid strains expressing *mCitrine* driven by a series of truncated *HTB1* promoters with increasingly shorter sequences (*89*). Here, I analyzed the *mCitrine* concentrations expressed from either a 300 bp or a 450 bp truncated *HTB1* promoter in rich and poor medium, to identify potential changes in the nutrient-dependence of the reporter transcripts. In addition to removing whole portions of the promoter, I also used a strain in which the binding of Spt10 to UAS3 and UAS4 is inhibited by mutation of the specific recognition sites (*128*). This would provide information on whether Spt10 plays a role in the regulation of histone transcripts across different nutrients. A strain expressing *mCitrine* under the full-length *HTB1* promoter was used as a control. The RT-qPCR analysis showed that the truncated 450 bp promoter drives nutrient-dependent mRNA expression similar to that of the full-length promoter, with *mCitrine* concentrations being reduced in poor growth medium (Fig. 23A). However, shortening the *HTB1* promoter to 300 bp notably altered the nutrient dependence of the reporter transcripts, resulting in lower levels of *mCitrine* in rich compared to poor nutrients. Moreover, in both, rich and poor media, I detected a pronounced decrease in the mRNA concentration of *mCitrine* when expressed from the truncated 300 bp promoter instead of the full-length promoter (Fig. 23B). Interestingly, in rich medium this decrease was more significant than in poor medium. Similarly, mutation of UAS3 and UAS4 significantly reduced the *mCitrine* levels in rich medium, ultimately leading to comparable mRNA concentrations between rich and poor conditions.

These findings indicate that removing the 150 bp fragment between the 450 bp and 300 bp *HTB1* promoter constructs disrupts the initial nutrient-dependence of the reporter transcripts. Hence, I propose that regulatory elements located within these 150 bp, *i.e.* UAS1, UAS2 and/or the NEG element, may be involved in the regulation of histone transcripts across different nutrients. Moreover, the results provide first evidence that Spt10 may contribute to such regulation.

Next, I asked how the observed changes in the nutrient-dependent transcript regulation affect the mCitrine protein levels expressed from the truncated promoters. To this end, I performed flow cytometry measurements and quantified the fluorescence intensity of mCitrine in cell populations growing in rich and poor nutrients (Fig. 23C). The results demonstrate that the protein amounts of mCitrine driven by the full-length *HTB1* promoter are constant between the growth media, despite the downregulated *mCitrine* mRNA levels in poor medium (Fig. 15B). This is consistent with my previous findings on the endogenous histone proteins, and suggests that the nutrient-dependent protein regulation is promoter-mediated. While protein amounts expressed from the 450 bp promoter were more comparable in rich and poor nutrients, I found that mCitrine protein levels driven by the 300 bp truncation were notably increased in poor medium (Fig. 23C), consistent with the higher mRNA concentrations determined by RT-qPCR (Fig. 23A). Finally, cells carrying the mutated *HTB1* promoter expressed very low levels of mCitrine, close to the background fluorescence, and therefore did not allow for accurate and reliable data interpretation (Fig. 23C).

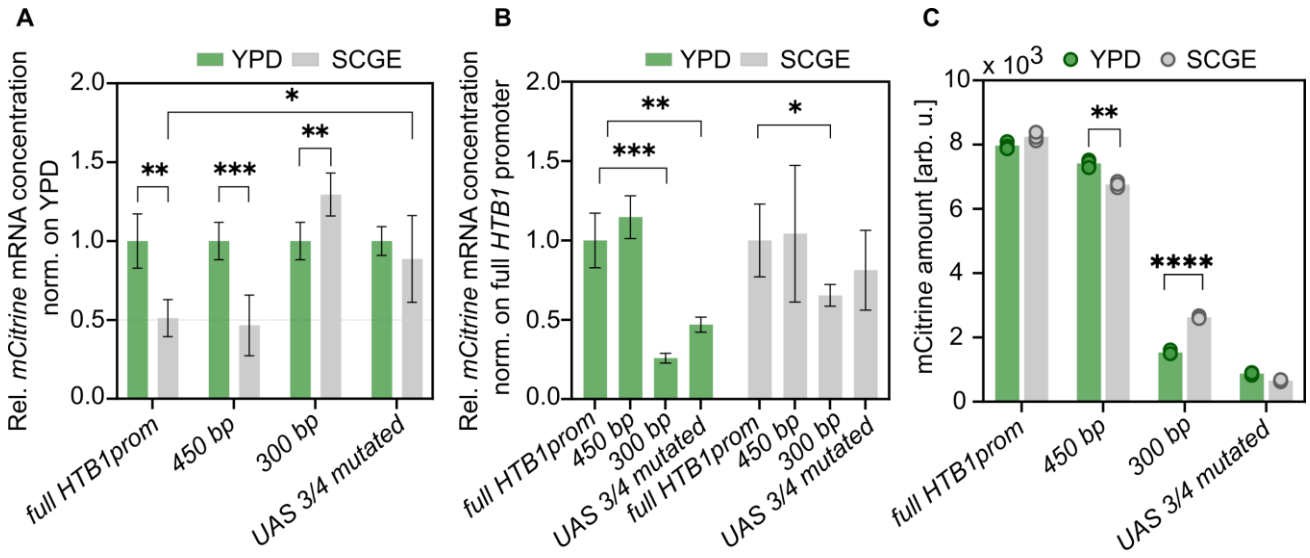

Figure 23. Removal or mutation of regulatory elements within the *HTB1* promoter alters nutrient-dependent reporter gene expression. (**A**) mRNA concentrations of *mCitrine* driven by different *HTB1* promoter constructs were quantified by RT-qPCR in rich and poor growth medium. The mRNA concentrations were normalized on the rRNA *RDN18* and are shown as fold changes relative to YPD. The bar graphs and error bars represent mean and standard deviations of n=5-8 independent biological replicates. (**B**) For each nutrient condition, the *mCitrine* mRNA concentrations were normalized on the reference gene *RDN18* and plotted relative to the full-length *HTB1prom-mCitrine*. Mean and standard deviations of n=5-8 independent biological replicates are shown. (**C**) Flow cytometry measurements of the protein levels of mCitrine driven by the different *HTB1* promoter

constructs in rich and poor growth medium. Bar graphs show the mean of n=3 independent replicates, each displayed as an individual dot. Statistical significance was estimated by an unpaired, two-tailed t-test (* p<0.05, ** p<0.01, *** p<0.001, **** p<0.0001).

3.8 Histone promoter can decouple reporter protein expression from the cellular mRNA levels in different nutrients

So far, I have shown that while histone proteins are maintained at constant amounts across different growth media, histone mRNA levels strongly depend on the nutrient environment. The flow cytometry analysis in figure 23C further revealed that decoupled protein and mRNA expression is also observed for the reporter gene *mCitrine* when driven by the *HTB1* promoter. Motivated by these findings, I sought to investigate histone promoter-mediated protein regulation in rich and poor medium at the single cell level. To this end, I performed microfluidics-based live-cell fluorescence microscopy and quantified the mCitrine protein amounts driven by the *HTB1* or *HTB2* promoter throughout the cell cycle. Similar to the endogenous histones, the promoter-mediated expression profile of mCitrine shows an increase in fluorescence intensity upon bud emergence, followed by a plateau prior to cytokinesis, suggesting that the histone promoter can confer cell cycle-dependent protein regulation (Fig. 24A). However, unlike endogenous H2B proteins, which are imported into the nucleus and distributed equally to mother and daughter cells during cytokinesis, mCitrine diffuses freely in the cytoplasm and is partitioned according to the cell volume (*90*). As budding yeast divides asymmetrically, the amount of inherited mCitrine therefore depends on the size of the daughter cell at the time of cell division. Thus, for the analysis, I did not compare the protein amounts at birth, but rather quantified the amounts of mCitrine produced during the cell cycle. My data show that the protein amount of mCitrine expressed from the histone promoters is more similar between the media (Fig. 24B-C), than the previously determined mRNA levels, which are reduced by approximately twofold in poor nutrients (Fig.15B, 19C-D). This is consistent with our population-level flow cytometry analysis (Fig. 23C) and suggests that the promoter is sufficient to decouple reporter mRNA and protein expression across changing environments. Based on these findings, I propose that cells compensate for reduced histone mRNA levels in poor nutrient conditions through regulated nutrient-dependent translation.

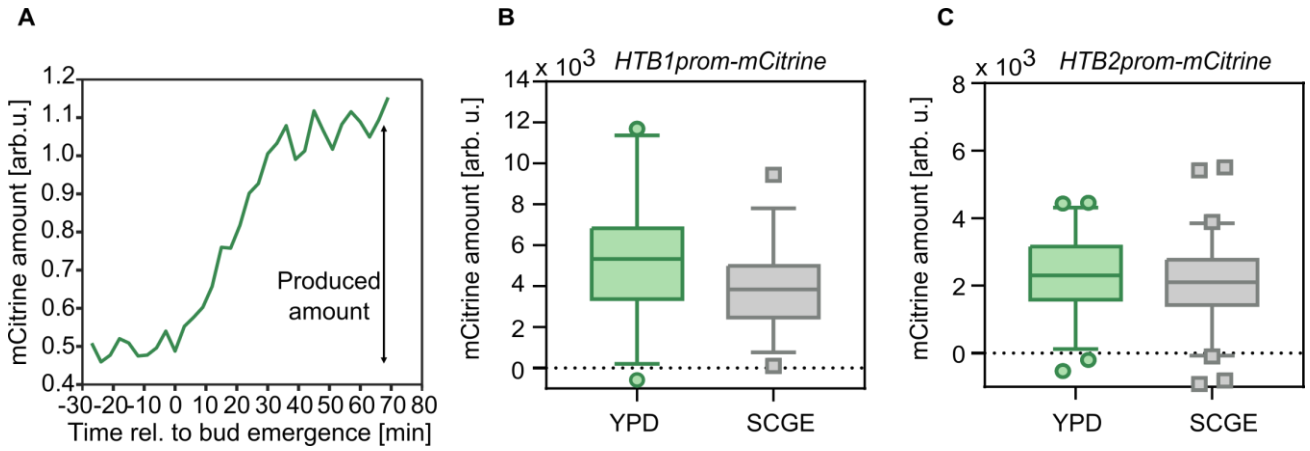

Figure 24. Live-cell fluorescence microscopy analysis reveals that histone promoters can regulate protein expression to compensate for nutrient-dependent mRNA levels. (**A**) Representative intensity profile of mCitrine expressed from the *HTB1* promoter in a haploid cell growing on YPD. Total mCitrine protein amounts synthesized during the cell cycle were estimated by calculating the difference between the median of the first and last four time points, respectively. (**B-C**) Total protein amounts of *HTB1prom-mCitrine* ($p_{YPD\text{-}SCGE}$ =0.0004) (B) and *HTB2prom-mCitrine* ($p_{YPD\text{-}SCGE}$ = 0.04) (C) in rich and poor growth medium ($n_{YPD}^{HTB1prom}$=70, $n_{SCGE}^{HTB1prom}$=76, $n_{YPD}^{HTB2prom}$=106, $n_{SCGE}^{HTB2prom}$= 157). Box plots show median values and 25th and 75th percentiles; whiskers represent the 2.5th and 97.5th percentiles; outliers are shown as individual symbols.

In addition to the H2B promoters, I also examined the expression levels of mCitrine driven by the *ACT1* promoter. As previously mentioned, *ACT1* is constitutively expressed throughout the cell cycle in a cell-volume-dependent manner (*89*, *90*, *152*). This is also reflected in the *ACT1prom-mCitrine* fluorescence intensity traces, which increase continuously throughout the cell cycle as the cells grow in size (Fig. 25A). Furthermore, I find that in both rich and poor media, the amount of mCitrine produced between cell birth and cytokinesis is proportional to the amount of cell growth during this period (Fig. 25B). In contrast, the total mCitrine amounts expressed from the histone promoter are more constant over cell growth (Fig. 25C).

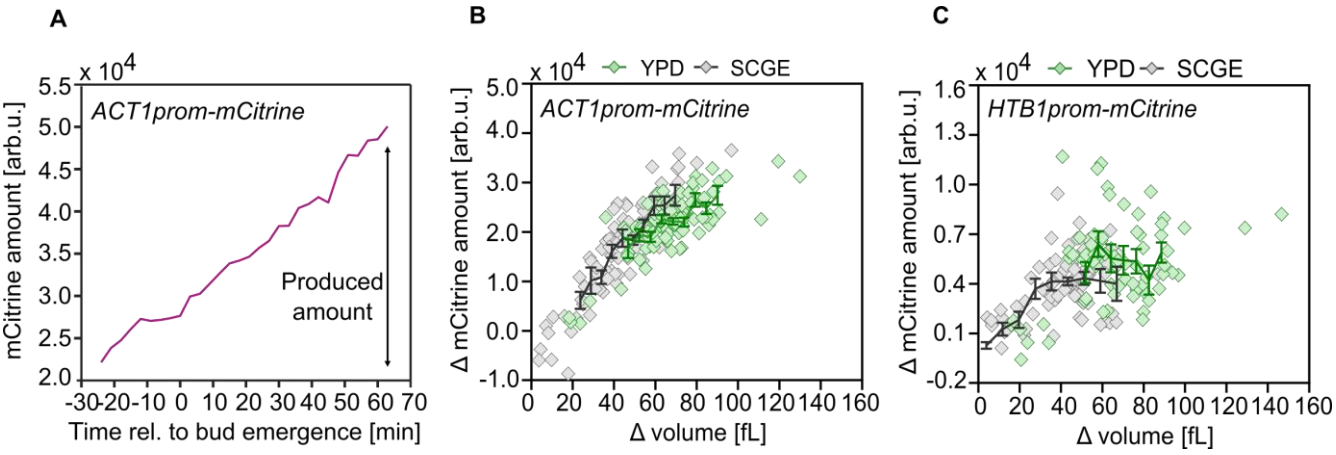

Figure 25. *ACT1* promoter drives cell-volume-dependent reporter expression in different nutrient conditions. (**A**) Representative expression profile of mCitrine driven by the *ACT1* promoter in a haploid cell growing on YPD. The overall amounts of mCitrine produced during the cell cycle were estimated by calculating the difference between the median of the first and last four time points, respectively. (**B-C**) Nutrient-specific total protein amounts of *ACT1prom-mCitrine* (**B**) and *HTB1-prom-mCitrine* (**C**) plotted as a function of cell growth during the cell cycle ($n_{YPD}^{ACT1prom}$=95, $n_{SCGE}^{ACT1prom}$= 87, $n_{YPD}^{HTB1prom}$=70, $n_{SCGE}^{HTB1prom}$=76). The individual data points were binned according to Δvolume; mean and standard error of each bin are shown.

3.9 5’ UTR is not required for promoter-mediated homeostasis of histone proteins across nutrient environments

The 5' untranslated regions (UTRs) are involved in the post-transcriptional regulation of gene expression as they contain cis-regulatory elements that control the fate of transcripts in terms of stability, ribosome interactions and translation efficiency, ultimately determining protein abundance (*174–178*). The length of 5′ UTRs ranges from ~100 to ~220 nucleotides on average across different eukaryotes, extending from the 5’ cap structure to the start codon (*176*, *179*). Features of 5’ UTRs include among others, upstream AUGs and upstream ORFs, secondary structures, binding sites for RNA binding proteins and internal ribosome entry sites (*174–177*). In previous studies, translation efficiency and protein abundance have been modulated by using perturbed 5′-UTR sequences (*174*, *180–184*). Here, I sought to determine the effects of the *HTB1* 5’ UTR on the nutrient-dependent protein levels of *HTB1prom-mCitrine*, by replacing it with the 5’ UTR sequences of *MDN1* and *RPB4*, respectively (Fig. 26A). *RPB4* encodes a subunit of the RNA polymerase II, and unlike *HTB1*, its expression is coordinated with cell size (*185*). For all strains tested, I measured similar

doubling times and mean cell volumes (Fig. 26B-C). To investigate whether substitution of the 5’ UTR alters *mCitrine* gene expression in the different nutrients, I first quantified the relative mRNA concentrations by RT-qPCR. Independent of the 5’ UTR I found that the mRNA concentrations of *mCitrine* were reduced in poor compared to rich medium (Fig. 26D). Moreover, for each nutrient condition, mRNA concentrations normalised to the wildtype (*HTB1* 5' UTR) decreased when regulated by the promoter and the *RPB4* 5' UTR (Fig. 26E). Interestingly, the *MDN1* 5' UTR did not alter *mCitrine* mRNA expression with respect to the wildtype. As a next step, I performed flow cytometry measurements to determine the nutrient-dependent protein amounts of mCitrine. In spite of the overall decrease in protein abundance, induced by the 5' UTR replacements, the expressed protein amounts were constant between the media (Fig. 26F). Therefore, I propose that the histone 5'-UTR does not contribute to the homeostasis of histone proteins across nutrients. Still, in each nutrient condition, it can affect the regulation of mRNA and protein abundance.

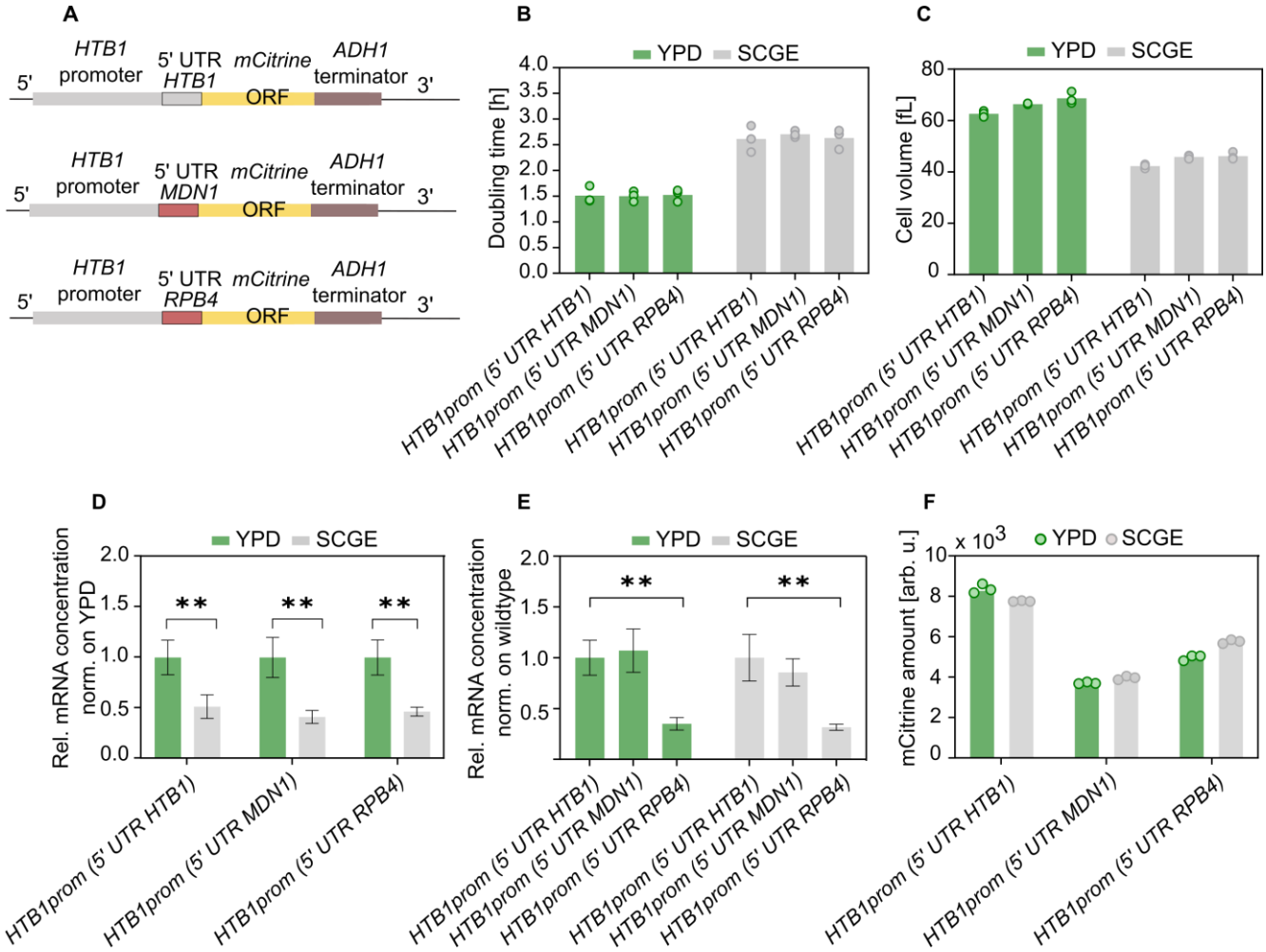

Figure 26. Substitution of the 5' UTR results in constant protein amounts of mCitrine between nutrient-rich and nutrient-poor conditions. (**A**) Illustration of the *HTB1* promoter constructs driving the expression of *mCitrine* with the 5' UTR of *HTB1*, *MDN1* or *RPB4*, respectively. (**B-C**) Doubling times (B) and mean cell volumes (C) of the different strains growing on rich and poor growth medium. Measurements of cell volume were carried out with a Coulter counter. Bar graphs represent the mean of n=3 replicates, each displayed as an individual dot. (**D-E**) Relative mRNA concentrations of *mCitrine* were quantified by RT-qPCR in the different growth media. The mRNA concentrations were normalized on the rRNA *RDN18* and are presented as fold changes relative to YPD (D) or the wildtype (*HTB1* promoter + *HTB1* 5' UTR) (E). The bar graphs and error bars show mean and standard deviations of n=4-5 biological replicates. Statistical significance was estimated by an unpaired, two-tailed t-test for datasets following a Gaussian distribution. Alternatively, a Mann-Whitney test was used for not normally distributed datasets (* $p<0.05$, ** $p<0.01$). (**F**) Flow cytometry measurements of the nutrient-dependent mCitrine protein amounts. Bar graphs show the mean of n=3 independent replicates, each displayed as an individual dot.

3.10 Cells on non-fermentable carbon sources are more sensitive to increased histone accumulation

So far, I have shown that to ensure histone protein homeostasis in different growth media cells decouple histone transcript and protein levels by downregulating the transcriptional output in nutrient-poor conditions. In addition to identifying potential regulators required for this nutrient-dependent decrease in histone transcripts, I also sought to understand why this was necessary, given that histone proteins remained constant across nutrients. According to a previous study by Bruhn et al., cells grown under low-glucose conditions are more sensitive to excess histone accumulation than in glucose-rich media, resulting in impaired cell growth *(132)*. This is partly due to the preferential acetylation of excess histones, which under glucose-restriction has a greater impact on the already limited availability of acetyl-CoA in cells (*132*). Motivated by these results, I asked whether cells growing on poor, non-fermentable carbon sources have a lower tolerance to aberrant histone levels than cells on fermentable carbon sources, thus maintaining lower transcript levels to avoid histone overexpression. To test this hypothesis, I used a *sml1Δrad53Δ* mutant provided by Christopher Bruhn (Foiani Lab, IFOM), which accumulates elevated histone levels, as Rad53 is involved in the control of histone gene expression. More specifically, Rad53 mediates the degradation of excess histones that are not incorporated into chromatin, and additionally inhibits histone transcription by phosphorylating the transcriptional activator Spt21 (*132*, *133*, *186*) (Fig. 27A). However, since Rad53 is essential for cell growth, the *rad53Δ* mutant cannot

survive unless the gene *SML1*, which encodes an inhibitor of ribonucleotide reductase, is also deleted (*132*, *187*). Thus, I used *sml1Δ* as the reference strain and compared it to the wildtype used in this study so far. Specifically, I measured the respective population doubling times and cell volumes in the different nutrients (Fig. 27B-C). The data show no major differences in cell growth between the two strains.

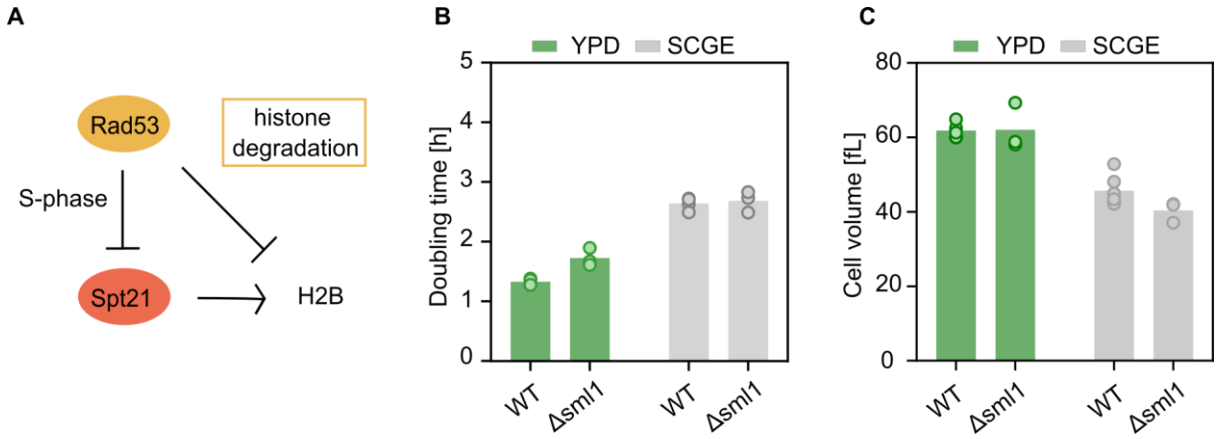

Figure 27. Characterization of *sml1Δ* cells on fermentable and non-fermentable carbon sources. (**A**) Rad53 regulates cellular histone levels by mediating the degradation of excess histones and inhibiting the transcription activator Spt21. (**B-C**) Nutrient-specific doubling times (B) and mean cell volumes (C) of the wildtype and *sml1Δ* mutant strain. Cell volume measurements were carried out with a Coulter counter. Bar graphs represent the mean of n=3-6 replicates, displayed as individual dots.

To determine whether cells on fermentable and non-fermentable carbon source respond differently to excess histone accumulation, I then calculated the doubling times of *sml1Δ* and *sml1Δrad53Δ* cells in YPD and SCGE, respectively (Fig. 28A). Indeed, I found that while both strains had similar doubling times in YPD, *sml1Δrad53Δ* cells grew considerably slower than the reference strain in SCGE. To analyze the effects of the RAD53 deletion on histone expression, I quantified the nutrient-dependent histone levels in *sml1Δ* and *sml1Δrad53Δ* cells by RT-qPCR and western blot analysis (Fig. 28B-D). While the *HTB1* mRNA levels remained fairly constant in both growth media, I detected elevated mRNA concentrations of *HTB2* and *HHT2* in *sml1Δrad53Δ* cells compared to the reference (Fig. 28B-C). *HHT2* was previously reported to show increased mRNA expression in *sml1Δrad53Δ* cells and was therefore used as a control (*132*). Furthermore, the western blot analysis showed an over-accumulation of H2B protein in the double deletion mutant (Fig. 28D). However, given that Rad53 is a DNA damage response kinase and is also involved in DNA replication, I sought

to investigate to what extent the induced histone overexpression contributes to the nutrient-dependent growth phenotype of *sml1Δrad53Δ*. Therefore, I considerably reduced histone gene expression in *sml1Δrad53Δspt21Δ* cells, by additionally deleting the gene *SPT21*, encoding the transcriptional activator. In both growth media, the triple deletion mutant showed decreased *HTB2* and *HHT2* transcript concentrations compared to the reference strain (Fig. 28B-C). Interestingly, *HTB1* concentrations were not significantly altered. Yet, the western blot data reveal that H2B protein expression was drastically reduced (Fig. 28D). Finally, by measuring the nutrient-specific population doubling times of *sml1Δrad53Δspt21Δ* cells, I found that lowering the histone levels partly rescued the growth phenotype in SCGE, promoting faster growth (Fig. 28A). However, in YPD, the doubling time remained unchanged.

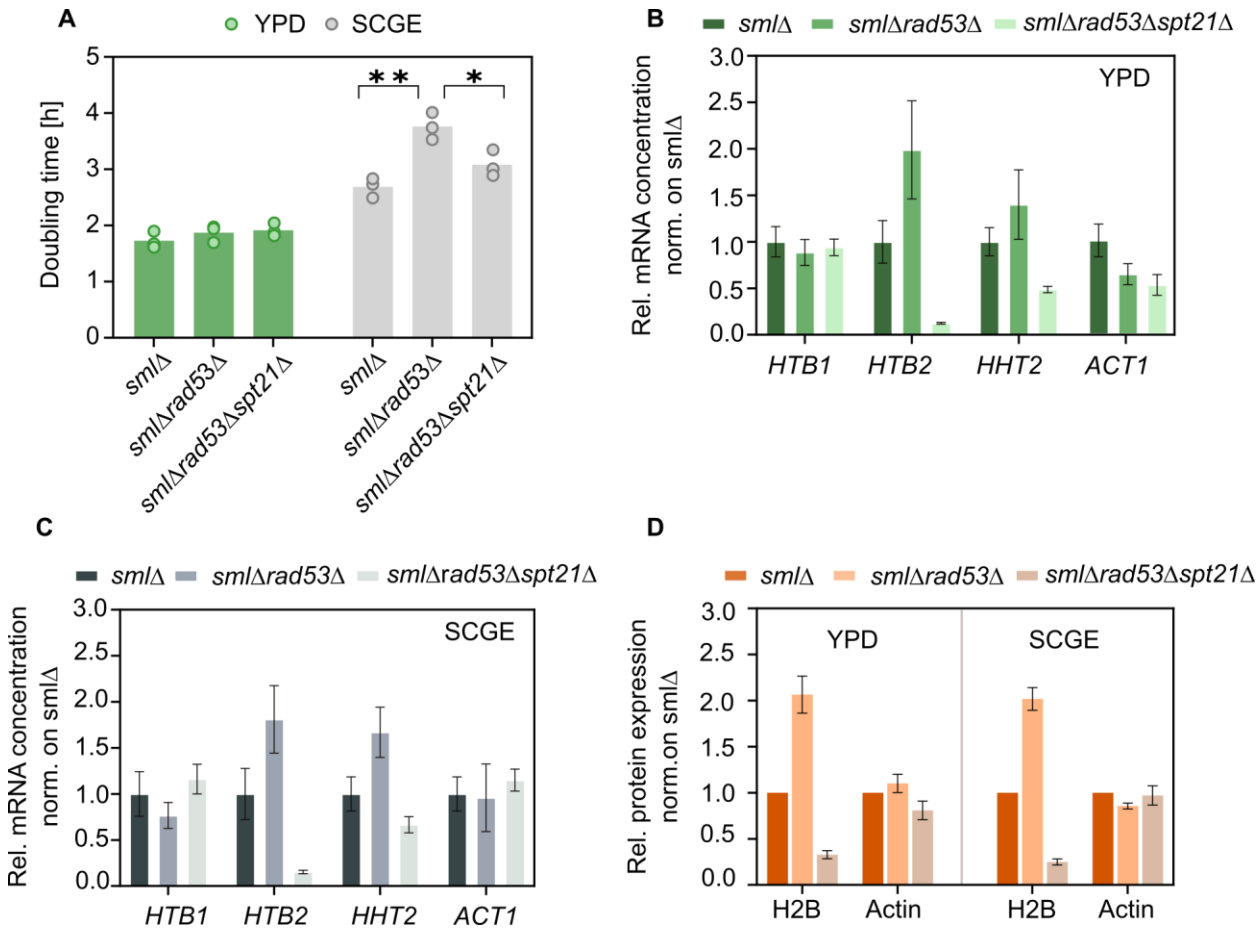

Figure 28. Cells growing on poor carbon source have a lower tolerance to increased histone levels than on rich carbon source. (**A**) Doubling times estimated from the growth curves of *sml1Δ, sml1Δrad53* and *sml1Δrad53Δspt21Δ* cells in the different growth media. Bar graphs show the mean of n=3 biological replicates, displayed as individual dots. Statistical significance was estimated by an

unpaired, two-tailed t-test (* p<0.05, ** p<0.01). (**B-C**) Relative *HTB1*, *HTB2, HHT2* and *ACT1* mRNA concentrations in YPD (B) and SCGE (C) were measured for *sml1Δ, sml1Δrad53* and *sml1Δrad53Δspt21Δ* cells using RT-qPCR. The concentrations were normalized on the reference gene *RDN18* and are shown as fold changes relative to the reference strain *sml1Δ*. Bar graphs and error bars represent mean and standard errors of n=3-5 independent biological replicates. (**D**) Western blot analysis of the nutrient-dependent H2B and actin protein expression in *sml1Δ, sml1Δrad53* and *sml1Δrad53Δspt21Δ* cells. The bar graphs and error bars indicate mean and standard errors of n=4-7 independent biological replicates.

My results suggest that cells in poor nutritional environment are indeed more sensitive to abnormally high histone levels, but can restore cell fitness upon histone depletion. I speculate that keeping histone transcript levels low allows cells to tightly regulate histone expression in nutrient-poor conditions. In contrast, under rich, *i.e*. fast growth conditions, the higher transcript levels may facilitate the rapid production of histone proteins. To further confirm this, I followed a different strategy using a diploid strain in which the endogenous alleles of *HTB1* and *HTB2* were serially deleted, in order to examine how the reduced histone expression affects cell growth on rich and poor carbon source (Fig. 29A). While the single and double hemizygous deletion strains, *HTB1/Δhtb1 and HTB1/Δhtb1HTB2/Δhtb2*, exhibited similar population doubling times as the wild type in YPD, further deletion of the second *HTB2* allele in *HTB1/Δhtb1Δhtb2Δhtb2* resulted in slower cell growth (Fig. 29B). In contrast, cells in SCGE either showed no change in doubling time or even grew slightly faster. It should be noted that a more in-depth analysis of the histone transcript and protein levels in these strains is required. In summary, I have shown that increased histone accumulation is more toxic for cells growing on poor as opposed to rich carbon sources. Thus, decoupling of histone transcript and protein expression might allow cells to fine-tune histone protein levels across nutrients, while preventing histone overexpression in poor growth media.

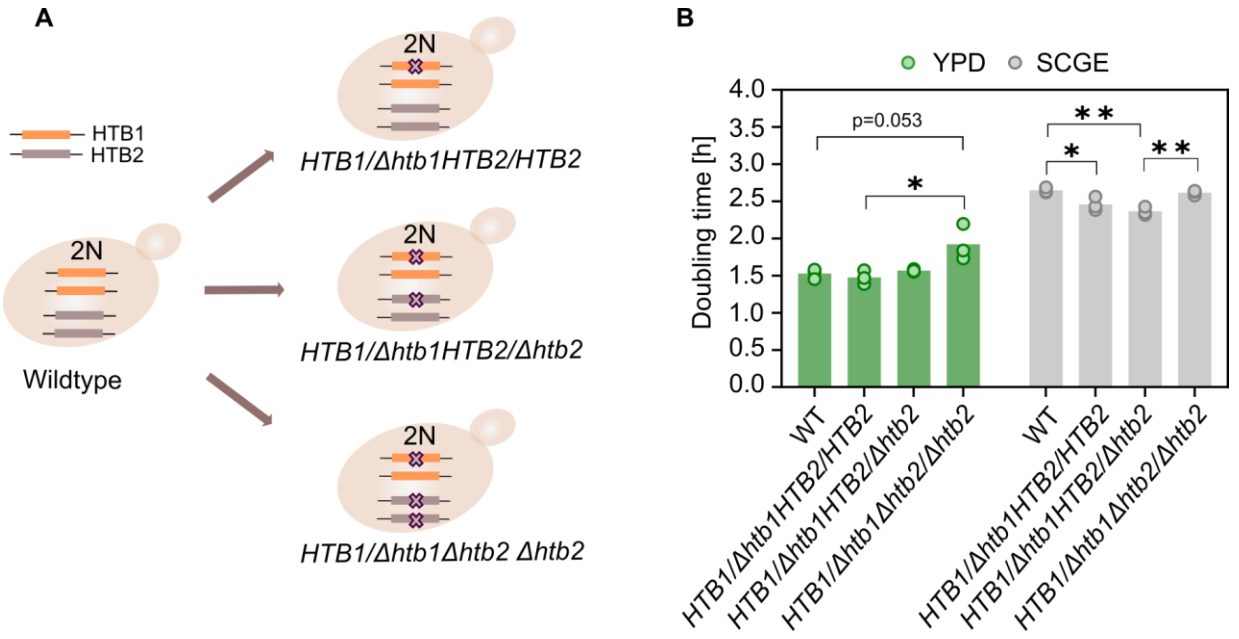

Figure 29. Cells growing on rich and poor carbon sources respond differently to decreased histone expression. (**A**) The endogenous *HTB1* and *HTB2* alleles were serially deleted in diploid wildtype cells to reduce histone expression levels. (**B**) Population doubling times of wildtype and deletion strains, growing exponentially on rich and poor carbon source. Bar graphs show the mean of n=3 biological replicates, displayed as individual dots. Statistical significance was estimated by an unpaired, two-tailed t-test (* p<0.05, ** p<0.01).

4 Discussion

Maintaining accurate protein homeostasis during growth is essential for proper cell function and requires cells to precisely control RNA and protein levels, even in situations where growth and cell cycle progression are drastically modulated by external conditions (*26*, *54*, *55*, *188*). In this work, I focused on histone biogenesis across different nutrient environments, and asked how cells produce the right amount of histones despite the nutrient-related changes in growth rate, cell volume and cell cycle progression. As histones are highly cell cycle regulated proteins (*87*, *189*, *190*) that are synthesized in proportion to the genome content (*89–91*), they constitute an ideal model to understand differential regulation of cell cycle-genes in changing nutrient conditions.

4.1 Gene-limited transcription cannot explain nutrient-dependent histone homeostasis

After selecting a variety of growth media, I performed population-level and single-cell protein analysis to quantify the histone H2B levels in rich and poor nutrients. My results show that cells maintain constant amounts of H2B in different environments, independent of cell volume or other nutrient-related changes in cell growth and cell cycle. Consequently, H2B concentrations increase in poor growth media, due to the smaller cell volumes. In contrast, actin synthesis is tightly coordinated with cell volume, resulting in constant, nutrient-independent concentrations. Unlike histones whose expression is tied to genome content, most proteins scale with cell volume (*135*, *89*, *90*). This is because the biosynthesis of these proteins is limited by the transcriptional and translational machinery, which increases with increasing cell size or growth rate (*64*, *134*, *136*, *154*, *191*). For example, in nutrient-rich, fast-growth conditions, cells are typically larger and have more limiting machinery, which allows for higher biosynthetic capacity and ensures constant protein concentrations (*55*, *134*, *136*, *64*, *56*, *65*). However, such a limiting mechanism cannot explain the coordination of histones with DNA content. Instead, Claude et al. proposed that the distinct regulation of histones is established at the mRNA level through gene-limited transcription mediated by the promoter (*89*). The idea is that the transcription of histones is limited by the gene itself, rather

than the transcriptional machinery, thereby coupling the transcriptional output to genome content instead of cell volume (*89*). Assuming that the gene-limited transcription hypothesis is true across changing environments, one might expect the nutrient-dependent histone homeostasis to be already established at the mRNA level. This would indicate that constant, nutrient-independent transcript amounts were produced in all growth media, leading to increased concentrations in the smaller cells growing on poor nutrients. Here, I combined population-level with single-cell approaches to analyze the histone transcript levels in different nutrient conditions. Contrary to my expectations, I found that histone transcript levels are downregulated in poor growth media. However, the nutrient-dependent mRNA expression, mediated by the histone promoter, was independent of cell volume. On the other hand, *ACT1*, *MDN1* and *ACT1prom-mCitrine* transcripts increase with increasing cell volume, regardless of the nutrient environment. These results demonstrate that gene-limited transcription alone cannot account for the nutrient-dependent histone transcript levels, but nor would actin-like regulation decouple histone transcripts from cell volume in different growth media. This suggests that histones are subject to a differential nutrient-dependent regulation.

4.2 Nutrient-specific relative S-phase duration does not account for differential histone mRNA expression

Given that histone gene expression occurs during S-phase, it could be argued that histone transcript levels change across different growth media according to the nutrient-specific relative S-phase duration. Cell cycle-phase distributions as determined by flow cytometry revealed that the percentage of cells in G1-phase increase in poor nutrients, leading to smaller fractions of cells in S- and G2/M-phase. Is a shortening of the relative S-phase responsible for the decrease in histone transcript concentrations in poor growth media? My data on the nutrient-dependent cell cycle fractions showed that the relative duration of S-phase only changes from 36.4 % in YPD to 29.8% in SCGE. However, qPCR analysis revealed that histone transcript concentrations are twice as high in YPD as in SCGE, indicating that the change in relative S-phase duration alone cannot account for the nutrient-dependent histone mRNA expression levels. This was further supported by smFISH analysis of histone promoter-mediated *mCitrine* expression during S-phase.

Here, it should be noted that the period of histone expression must not necessarily coincide with the whole S-phase duration. In fact, it has been reported that histone synthesis peaks in mid S-phase, followed by a decline in the expression levels before cells exit S-phase (*88*). Nevertheless, the relative histone production phase could be still considered proportional to the relative S-phase.

4.3 Regulation of histone transcripts across changing nutrients

As transcript concentrations are determined by transcription and mRNA degradation, the reduced histone mRNA levels in poor nutrients may result from lower transcription rates, reduced mRNA stability, or a combination of both. In this work, I examined the contribution of mRNA degradation to the nutrient-dependent changes in histone mRNA expression and found that histone mRNA stability increases in poor compared to rich growth medium. This suggests that a decrease in histone transcription is most likely responsible for the downregulation of histone transcript concentrations in poor nutrients. For *ACT1*, I also observed mRNA stabilisation in poor medium, but this is most likely compensated by decreased transcription rates, resulting in constant *ACT1* mRNA concentrations across the nutrients. I speculate that alongside the global nutrient-dependent shift in mRNA expression, histone transcript levels are differentially regulated and might be increased in nutrient-rich conditions to facilitate rapid protein synthesis in fast growing cells, containing higher ribosome concentrations (*64*, *65*, *192*). The fact that histones are not produced constitutively during the cell cycle, but only in S- phase, further underlines the need for fast biosynthesis under nutrient-rich conditions. At the same time, lower ribosome concentrations in cells growing on poor carbon sources may limit rapid histone production, causing cells to keep the relative concentration of histone transcripts low. Another reason why cells downregulate histone transcripts in poor growth media could be their reduced tolerance against excess histone accumulation. Bruhn et al. previously showed that cells experiencing glucose-limitation were more impaired in their cell fitness by histone overexpression than cells growing on glucose. This is in part due to the preferential acetylation of excess histones, which under glucose-restriction influences the already limited availability of acetyl-CoA, and hence acetyl-CoA-dependent carbon metabolism in cells (*132*). As part of this work, I tested whether cells on non-fermentable carbon source are also more sensitive to aberrant histone

levels. Indeed, cells in SCGE grow significantly slower in response to histone overexpression, compared to YPD. I therefore propose that cells tightly regulate histone expression in nutrient-poor conditions, keeping histone transcript levels low to minimize the risk of high histone accumulation.

4.4 Specific regulation of histone mRNA translation ensures histone protein homeostasis under different nutrient conditions

I have shown that in spite of the nutrient-specific regulation of histone transcripts, cells ultimately produce the same amounts of histone proteins across different nutrient environments. Protein abundance is determined by the mRNA abundance, translation efficiency and protein stability (*9*, *193*, *194*). Thus, measurements of both, transcript and protein levels, were complementary and equally important for gaining a better understanding of the regulatory mechanisms underlying nutrient-dependent histone homeostasis. In general, the degree of correlation between protein and mRNA levels in yeast can vary between different functional gene categories, and across nutrient conditions (*193*–*196*). In fact, it has been reported that the protein levels of some genes with similar mRNA levels can differ by more than 20-fold. At the same time, different mRNA levels can lead to invariant protein levels (*195*). My results show a clear decoupling of histone mRNA and protein abundance, with transcript levels being reduced in poor compared to rich growth medium, and protein levels remaining constant across all nutrient conditions. This suggests that cells compensate for the lower histone transcript concentrations by increasing the relative histone translation efficiency, or protein stability under poor nutrient conditions.

In this work, I have demonstrated that the histone promoter can decouple reporter mRNA and protein expression across changing nutrients, leading to constant protein amounts in rich and poor growth media. The fact that the promoter can compensate for the nutrient-dependent transcript levels, suggests that histone proteostasis is achieved through additional nutrient-specific regulation of translation. As the 5’ UTR is known to influence translation efficiency and protein abundance, I investigated the effect of the histone 5’ UTR on the protein levels of mCitrine when expressed from a histone promoter. However, I found that

mCitrine protein levels remained constant between growth media even after replacing the histone 5' UTR with that of other genes. So, how do cells adjust histone mRNA translation in the different media to achieve histone proteostasis?

4.5 Nutrient-dependent histone translation might be modulated through an mRNA imprinting mechanism

One possibility could be that histone translation is controlled through an mRNA imprinting mechanism. In recent years, various studies have challenged the notion that transcription, mRNA decay and translation machineries operate independently in the different cellular compartments (*197–199*). Instead, different factors have been identified that mark or 'imprint' newly synthesized mRNAs in the nucleus, often through co-transcriptional association, regulating post-transcriptional and translational processes *(197)*. Such factors may include RNAs, ribonucleoproteins, various proteins or protein complexes that are loaded onto the mRNAs and remain associated with them, controlling processes such as mRNA export, stability, localization or translation (*197*, *198*, *200*). A prominent example is the imprinting of Pol II transcripts by the heterodimer Rpb4/7. Pol II has been reported to remotely regulate mRNA decay and translation by recruiting Rpb4/7, which co-transcriptionally binds the nascent transcript and remains attached to it throughout its lifetime. Rpb4/7 later controls post-transcriptional processes by physically interacting with key regulators, such as components of the translation initiation factor 3 or the decay complex (*199*, *201–203*). Another study reports that translation of ribosomal genes is regulated through imprinting of the mRNAs with Not1, the scaffold of the Ccr4–Not complex *(204)*. Co-transcriptional association of Not1 with emerging transcripts is promoted by Not5, which is also a subunit of the Ccr4–Not complex. Not5-mediated Not1 imprinting controls the translatability of mRNAs encoding ribosomal proteins, which in turn defines the translational capacity of the cell (*204*). Several studies have sought to elucidate how mRNA imprinting is achieved. However, the underlying mechanisms and the nature of imprinting vary, and are not always clear (*198*). Similar to the Pol II-dependent imprinting, it is possible that the transcriptional machinery itself recruits the imprinting factor, facilitating its association with the nascent transcript during transcription. Moreover, it has been indicated that promoter elements can regulate cytoplasmic processes such as mRNA degradation through promoter-mediated mRNA

imprinting (*164*, *198*, *200*, *205*). For example, Bregman et al. proposed that binding of Rap1 to the Rap1p-binding sites located within the UAS of *RPL30*, promotes the co-transcriptional imprinting of *RPL30* transcripts, and determines mRNA stability (*200*). Overall, these collective studies have described potential crosstalk between the different stages of gene expression, suggesting that mRNA decay and translation in the cytoplasm can be regulated from the nucleus through an imprinting mechanism. Thus, I propose that histone core promoter elements may modulate translation efficiency according to the nutrient environment through mRNA imprinting. However, further studies will be needed to identify specific translational regulators required for the nutrient-dependent histone protein homeostasis.

4.6 Model of budding yeast histone homeostasis across different nutrient environments

In summary, I have investigated nutrient-dependent histone homeostasis in *S. cerevisiae* using a combination of population-level and single-cell approaches and demonstrated that cells maintain histone proteins in proportion to the DNA content, independent of nutrient-related changes in cell growth and cell cycle (Fig. 30A). However, I found that histone protein levels are uncoupled from mRNA levels in rich and poor growth media. I propose that histone transcripts are differentially regulated according to the nutrient environment, so cells can minimise the risk of high histone accumulation in poor nutrient conditions, but also facilitate rapid protein synthesis under fast growth conditions. By separating the regulation of histone transcripts and their translation, cells can finely tune histone expression across different nutrient conditions, by shifting the balance between the speed and accuracy of protein production (Fig. 30B-C).

The described decoupling of mRNA and protein expression may be a more general form of differential regulation of cell cycle-regulated genes across changing nutrient environments. Maintaining precise protein levels despite the changes in cell growth and cell cycle phases poses a challenge, especially for genes with expression profiles that peak during short periods of the cell cycle. However, it remains to be determined whether this specific nutrient-dependent regulation of histones also occurs for other genes.

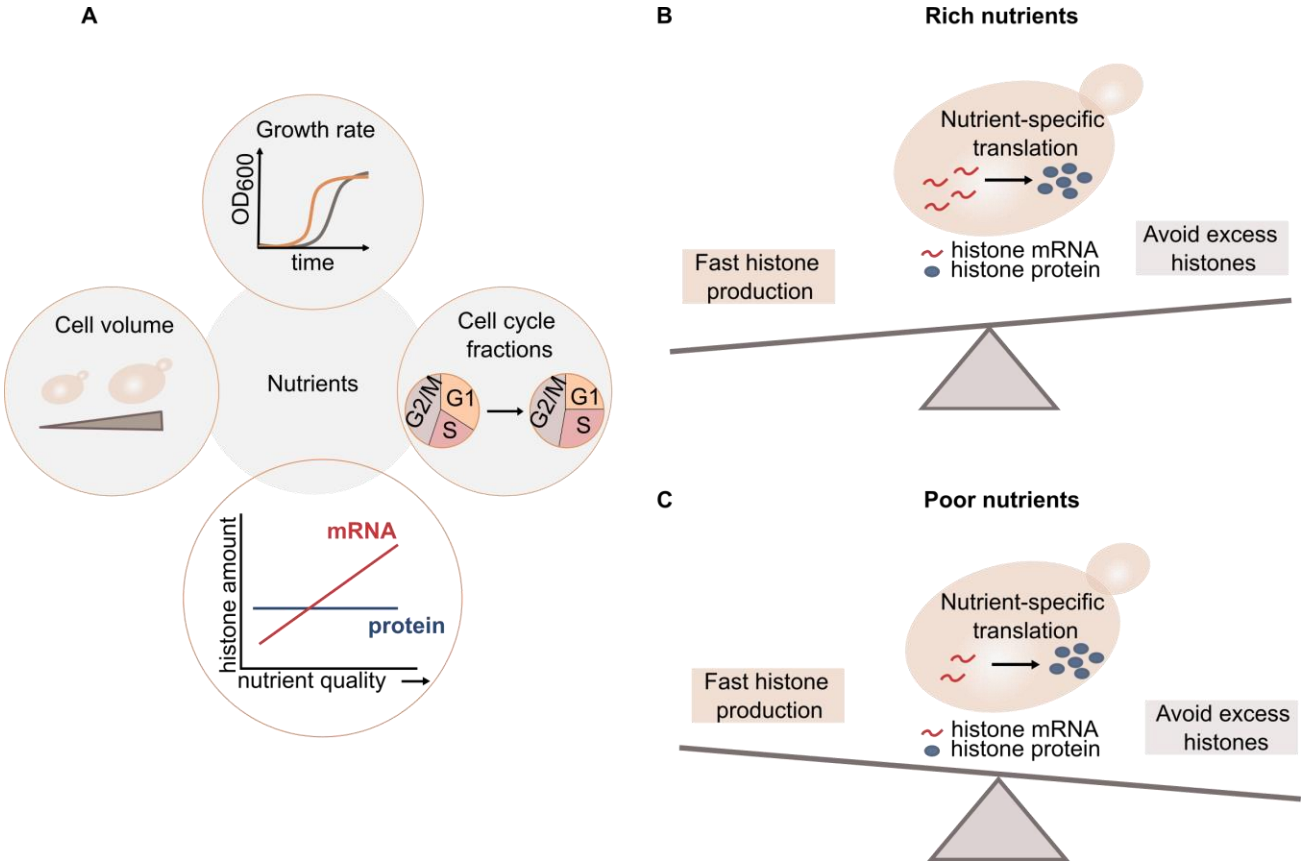

Figure 30. Model of nutrient-dependent budding yeast histone homeostasis. (**A**) Regardless of the nutrient-related changes in cell growth and cell cycle, histone proteins are produced at constant amounts in rich and poor growth media. By contrast, histone transcript amounts depend on the nutrient environment, and are upregulated in rich conditions. (**B-C**) Cells compensate for the differentially regulated transcript levels through nutrient-specific translation, finding the optimal balance between the speed and accuracy of protein production. This allows cells to facilitate fast histone biosynthesis in rich nutrients (B), but also avoid histone overproduction in poor nutrients (C).

5 Outlook

To gain a deeper understanding of the regulation of histone homeostasis in changing nutrients, further investigations are required. In this work, I have shown that regardless of the nutrient-related changes in cell volume, growth rate or cell cycle progression, cells produce equal amounts of H2B, ensuring a constant ratio between histone proteins and genome content. Although it has been previously reported that cell growth on different carbon sources does not drastically alter nucleosome occupancy (*206*), it would be interesting to map and compare nucleosome occupancy levels in the growth media used in this study. Such measurements most often involve chromatin digestion with micrococcal nuclease (MNase), and high throughput sequencing of the nucleosome-protected DNA fragments (*207*).

The histone mRNA analysis revealed a differential regulation of histone transcript concentrations across different nutrients. After measuring the nutrient-dependent mRNA stability in cells treated with the transcriptional inhibitor thiolutin, I draw the conclusion that transcription most likely accounts for the decreased histone transcripts in poor growth conditions. As a next step, it would be important to actually quantify the nutrient-dependent transcription rates of histone transcripts, for example by metabolic labelling with the uracil analog 4-thiouracil (4tU). This approach allows a direct measurement of mRNA synthesis and decay kinetics in unperturbed cells, and in combination with RNA sequencing, can be further extended to a genome-wide analysis of nutrient-dependent transcription and degradation rates (*208*, *209*).

In this study, I also performed smFISH to investigate the cell cycle-regulated mRNA expression of *mCitrine* driven by histone promoters in different nutrient conditions. To quantify individual mRNAs in single cells I used fluorescently labelled oligonucleotide probes that bind along the mRNA target of interest. While these probes were perfectly suited to detect *mCitrine* transcripts, they could not be applied for the detection of the endogenous histone genes *HTB1* and *HTB2* as their short gene length did not allow for sufficient probe binding. If not enough probes bind to the mRNA target, the quality of the fluorescent spots is too poor for proper quantification. Here, an alternative approach would be the use of branched probes that amplify the fluorescence signal by providing docking sites for additional oligonucleotide probes to bind sequentially (*210*). This would allow for the study of histone

mRNA expression at a single cell level, thereby providing insight into the cell cycle regulation of histone transcripts across different nutrients.

To determine which regulatory promoter elements confer the nutrient-dependence of histone transcripts I analysed the transcript levels of *mCitrine* driven by a serially truncated or mutated *HTB1* promoter. My results indicate that promoter motifs such as the UAS1, UAS2 and/or the NEG element may be required for the regulation of histone transcripts across different nutrients. To disentangle the contribution of the NEG element to the nutrient-dependence of histone concentrations, one could delete the 54-bp NEG region between UAS2 and UAS3 and quantify any potential changes to the initial trend.

Moreover, this study provided first evidence that the major transcriptional activator Spt10 may be involved in the differential regulation of histone transcripts. It would be interesting to test whether the concentration of Spt10 in the cell changes according to the nutrient environment, possibly decreasing in poor growth medium. This in turn could affect the binding of Spt10 to the promoter, thereby reducing histone transcription. The interaction of Spt10 with histone promoters in the different nutrients can be further investigated by chromatin immunoprecipitation (Chip).

In this work, I also found that increased histone levels were more toxic to cells on SCGE compared to YPD. Part of the reason for this may be the preferential acetylation of excess histones, which has a greater effect on the already limited availability of acetyl-CoA in cells growing on non-fermentable carbon sources *(132)*. To further test this hypothesis, one could increase the levels of acetyl-CoA in cells on SCGE by supplying acetate as a source for the synthesis of additional acetyl-CoA (*132*, *211*). Subsequent measurements of the population doubling times will then reveal whether the increased availability of acetyl-CoA can rescue the cell growth phenotype in SCGE.

The characterization of histone biogenesis at the mRNA and protein level revealed a decoupling of transcript and protein abundance across different nutrients. Based on my results I therefore proposed that nutrient-specific regulation of translation is necessary to ensure histone protein homeostasis in different growth media. More specifically, cells compensate for the lower histone transcript concentrations by increasing the relative translation efficiency under nutrient-poor conditions. To further validate this conclusion, a comprehensive analysis of the nutrient-dependent synthesis rates of histone proteins is required. Here, ribosome profiling, which relies on deep sequencing of mRNA fragments protected by the ribosome, provides a quantitative measurement of protein specific and

global translation (*212*). To complement these data, histone protein degradation in rich and poor nutrients can be analyzed by translation inhibition experiments *i.e*. cycloheximide chase followed by western blot (*213*). As I ruled out the contribution of the histone 5'UTR to the nutrient-specific translation efficiency of histones, it would be interesting to investigate the potential role of mRNA imprinting in the regulation of translation efficiency. This would shed light on how promoter elements can remotely coordinate histone translation in the cytoplasm. It is possible that following transcription, imprinting factors bind to the histone transcript in a promoter-dependent manner and accompany it throughout its life cycle, controlling cytoplasmic processes. To elucidate a potential mechanism of promoter-dependent mRNA imprinting, protein-RNA complexes can be extracted and histone RNA-associated proteins can be identified in the different nutrients by mass spectrometry. To determine the histone-specific coordinators, one can use strains with an integrated copy of *mCitrine* driven by a histone or a housekeeping gene promoter, *i.e.* an *ACT1* or *MDN1* promoter. Factors associated only with transcripts expressed from histone promoters can be examined to assess their role in regulating protein abundance and synthesis rate. Candidates found to significantly influence the nutrient-dependent translation efficiency of histones can be further tested for possible interactions with the promoter itself or components of the translational machinery. These extensive studies will provide a more comprehensive picture of the regulatory processes required to maintain histone protein homeostasis in different nutrients. Finally, I propose that histone homeostasis could also lay the foundation for a deeper understanding of the differential regulation of other cell cycle-regulated genes across changing nutrient environments. Therefore, it would be interesting to extend the analysis genome-wide using RNA-seq and mass spectrometry to identify further cell cycle-regulated or even DNA-binding proteins that show similar nutrient-dependent regulation.

6 References

1. A. Noormohammadi, G. Calculli, R. Gutierrez-Garcia, A. Khodakarami, S. Koyuncu, D. Vilchez, Mechanisms of protein homeostasis (proteostasis) maintain stem cell identity in mammalian pluripotent stem cells. *Cell. Mol. Life Sci.* **75**, 275–290 (2018).

2. E. T. Powers, R. I. Morimoto, A. Dillin, J. W. Kelly, W. E. Balch, Biological and Chemical Approaches to Diseases of Proteostasis Deficiency. *Annu. Rev. Biochem.* **78**, 959–991 (2009).

3. F. U. Hartl, Cellular Homeostasis and Aging. *Annu. Rev. Biochem.* **85**, 1–4 (2016).

4. W. E. Balch, R. I. Morimoto, A. Dillin, J. W. Kelly, Adapting Proteostasis for Disease Intervention. *Science* **319**, 916–919 (2008).

5. C. L. Klaips, G. G. Jayaraj, F. U. Hartl, Pathways of cellular proteostasis in aging and disease. *Journal of Cell Biology* **217**, 51–63 (2018).

6. G. G. Jayaraj, M. S. Hipp, F. U. Hartl, Functional Modules of the Proteostasis Network. *Cold Spring Harb Perspect Biol* **12**, a033951 (2020).

7. A. J. Sala, L. C. Bott, R. I. Morimoto, Shaping proteostasis at the cellular, tissue, and organismal level. *Journal of Cell Biology* **216**, 1231–1241 (2017).

8. T. D. Williams, A. Rousseau, Actin dynamics in protein homeostasis. *Bioscience Reports* **42**, BSR20210848 (2022).

9. Y. Liu, A. Beyer, R. Aebersold, On the Dependency of Cellular Protein Levels on mRNA Abundance. *Cell* **165**, 535–550 (2016).

10. T. I. Lee, R. A. Young, Transcriptional Regulation and Its Misregulation in Disease. *Cell* **152**, 1237–1251 (2013).

11. R. I. Morimoto, A. M. Cuervo, Protein Homeostasis and Aging: Taking Care of Proteins From the Cradle to the Grave. *The Journals of Gerontology Series A: Biological Sciences and Medical Sciences* **64A**, 167–170 (2009).

12. B. Sampaio-Marques, P. Ludovico, Linking cellular proteostasis to yeast longevity. *FEMS Yeast Research* **18** (2018).

13. C. López-Otín, M. A. Blasco, L. Partridge, M. Serrano, G. Kroemer, The Hallmarks of Aging. *Cell* **153**, 1194–1217 (2013).

14. D. C. David, N. Ollikainen, J. C. Trinidad, M. P. Cary, A. L. Burlingame, C. Kenyon, Widespread Protein Aggregation as an Inherent Part of Aging in C. elegans. *PLoS Biol* **8**, e1000450 (2010).

15. D. F. Moreno, K. Jenkins, S. Morlot, G. Charvin, A. Csikasz-Nagy, M. Aldea, Proteostasis collapse, a hallmark of aging, hinders the chaperone-Start network and arrests cells in G1. *eLife* **8**, e48240 (2019).

References

16. G. E. Neurohr, R. L. Terry, J. Lengefeld, M. Bonney, G. P. Brittingham, F. Moretto, T. P. Miettinen, L. P. Vaites, L. M. Soares, J. A. Paulo, J. W. Harper, S. Buratowski, S. Manalis, F. J. Van Werven, L. J. Holt, A. Amon, Excessive Cell Growth Causes Cytoplasm Dilution And Contributes to Senescence. *Cell* **176**, 1083-1097.e18 (2019).

17. H. J. Lee, R. Gutierrez-Garcia, D. Vilchez, Embryonic stem cells: a novel paradigm to study proteostasis? *FEBS J* **284**, 391–398 (2017).

18. T. Koyama, M. J. Texada, K. A. Halberg, K. Rewitz, Metabolism and growth adaptation to environmental conditions in Drosophila. *Cell. Mol. Life Sci.* **77**, 4523–4551 (2020).

19. L. R. Alagar Boopathy, S. Jacob-Tomas, C. Alecki, M. Vera, Mechanisms tailoring the expression of heat shock proteins to proteostasis challenges. *Journal of Biological Chemistry* **298**, 101796 (2022).

20. P. N. Rao, J. Engelberg, HeLa Cells: Effects of Temperature on the Life Cycle. *Science* **148**, 1092–1094 (1965).

21. K. L. Vakkayil, T. Hoppe, Temperature-Dependent Regulation of Proteostasis and Longevity. *Front. Aging* **3**, 853588 (2022).

22. C. G. Mackenzie, J. B. Mackenzie, P. Beck, THE EFFECT OF pH ON GROWTH, PROTEIN SYNTHESIS, AND LIPID-RICH PARTICLES OF CULTURED MAMMALIAN CELLS. *The Journal of Biophysical and Biochemical Cytology* **9**, 141–156 (1961).

23. H. M. Taïeb, D. S. Garske, J. Contzen, M. Gossen, L. Bertinetti, T. Robinson, A. Cipitria, Osmotic pressure modulates single cell cycle dynamics inducing reversible growth arrest and reactivation of human metastatic cells. *Sci Rep* **11**, 13455 (2021).

24. B. Ortmann, J. Druker, S. Rocha, Cell cycle progression in response to oxygen levels. *Cell. Mol. Life Sci.* **71**, 3569–3582 (2014).

25. A. Gutteridge, P. Pir, J. I. Castrillo, P. D. Charles, K. S. Lilley, S. G. Oliver, Nutrient control of eukaryote cell growth: a systems biology study in yeast. *BMC Biol* **8**, 68 (2010).

26. B. L. Bohnsack, K. K. Hirschi, NUTRIENT REGULATION OF CELL CYCLE PROGRESSION. *Annu. Rev. Nutr.* **24**, 433–453 (2004).

27. D. A. Ratkowsky, J. Olley, T. A. McMeekin, A. Ball, Relationship between temperature and growth rate of bacterial cultures. *J Bacteriol* **149**, 1–5 (1982).

28. E. Spedden, D. L. Kaplan, C. Staii, Temperature response of the neuronal cytoskeleton mapped via atomic force and fluorescence microscopy. *Phys. Biol.* **10**, 056002 (2013).

29. L. Pavlovsky, R. A. Sturtevant, J. G. Younger, M. J. Solomon, Effects of Temperature on the Morphological, Polymeric, and Mechanical Properties of *Staphylococcus epidermidis* Bacterial Biofilms. *Langmuir* **31**, 2036–2042 (2015).

30. J. R. Lepock, How do cells respond to their thermal environment? *International Journal of Hyperthermia* **21**, 681–687 (2005).

31. I. Watanabe, S. Okada, EFFECTS OF TEMPERATURE ON GROWTH RATE OF CULTURED MAMMALIAN CELLS (L5178Y). *Journal of Cell Biology* **32**, 309–323 (1967).

32. J. C. Senez, Some considerations on the energetics of bacterial growth. *Bacteriol Rev* **26**, 95–107 (1962).

33. M. Vanoni, M. Vai, G. Frascotti, Effects of temperature on the yeast cell cycle analyzed by flow cytometry. *Cytometry* **5**, 530–533 (1984).

34. M. Benet, A. Miguel, F. Carrasco, T. Li, J. Planells, P. Alepuz, V. Tordera, J. E. Pérez-Ortín, Modulation of protein synthesis and degradation maintains proteostasis during yeast growth at different temperatures. *Biochimica et Biophysica Acta (BBA) - Gene Regulatory Mechanisms* **1860**, 794–802 (2017).

35. R. I. Morimoto, Regulation of the heat shock transcriptional response: cross talk between a family of heat shock factors, molecular chaperones, and negative regulators. *Genes Dev.* **12**, 3788–3796 (1998).

36. X.-D. Liu, Conservation of a stress response: human heat shock transcription factors functionally substitute for yeast HSF. *The EMBO Journal* **16**, 6466–6477 (1997).

37. J. Anckar, L. Sistonen, Regulation of H SF 1 Function in the Heat Stress Response: Implications in Aging and Disease. *Annu. Rev. Biochem.* **80**, 1089–1115 (2011).

38. Z. Ivanovic, Hypoxia or in situ normoxia: The stem cell paradigm. *J. Cell. Physiol.* **219**, 271–275 (2009).

39. R. H. Wenger, Mammalian oxygen sensing, signalling and gene regulation. *Journal of Experimental Biology* **203**, 1253–1263 (2000).

40. E. Meilhoc, K. D. Wittrup, J. E. Bailey, Influence of dissolved oxygen concentration on growth, mitochondrial function and antibody production of hybridoma cells in batch culture. *Bioprocess Eng.* **5**, 263–274 (1990).

41. O. Couvert, M.-L. Divanac'h, A. Lochardet, D. Thuault, V. Huchet, Modelling the effect of oxygen concentration on bacterial growth rates. *Food Microbiology* **77**, 21–25 (2019).

42. P. J. Lee, A. M. K. Choi, Pathways of cell signaling in hyperoxia. *Free Radical Biology and Medicine* **35**, 341–350 (2003).

43. A. Al-Ani, D. Toms, D. Kondro, J. Thundathil, Y. Yu, M. Ungrin, Oxygenation in cell culture: Critical parameters for reproducibility are routinely not reported. *PLoS ONE* **13**, e0204269 (2018).

44. W. G. E. J. Scoonen, A. H. Wanamarta, J. M. van der Kle-van Moorsel, C. Jakobs, H. Joejne, Hyperoxia-induced clonogenic killing of HeLa cells associated with respiratory failure and selective inactivation of Krebs cycle enzymes. *Mutation Research/DNAging* **237**, 173–181 (1990).

45. F. Hakim, T. Kaitsuka, J. Mohd. Raeed, F.-Y. Wei, N. Shiraki, T. Akagi, T. Yokota, S. Kume, K. Tomizawa, High Oxygen Condition Facilitates the Differentiation of Mouse and Human Pluripotent Stem Cells into Pancreatic Progenitors and Insulin-producing Cells. *Journal of Biological Chemistry* **289**, 9623–9638 (2014).

46. T. Iida, S. Mine, H. Fujimoto, K. Suzuki, Y. Minami, Y. Tanaka, Hypoxia-inducible factor-1α induces cell cycle arrest of endothelial cells: HIF-1-induced apoptosis of endothelial cells. *Genes to Cells* **7**, 143–149 (2002).

47. M. Dubois, D. Inzé, Plant growth under suboptimal water conditions: early responses and methods to study them. *Journal of Experimental Botany* **71**, 1706–1722 (2020).

48. A. H. Undeen, E. Frixione, The Role of Osmotic Pressure in the Germination of *Nosema algerae* Spores [1]. *The Journal of Protozoology* **37**, 561–567 (1990).

49. G. Bellí, E. Garí, M. Aldea, E. Herrero, Osmotic stress causes a G1 cell cycle delay and downregulation of Cln3/Cdc28 activity in *Saccharomyces cerevisiae*: Stress and G 1 cell cycle regulation in yeast. *Molecular Microbiology* **39**, 1022–1035 (2001).

50. L. Schwartz, J. da Veiga Moreira, M. Jolicoeur, Physical forces modulate cell differentiation and proliferation processes. *J. Cell. Mol. Med.*, doi: 10.1111/jcmm.13417 (2017).

51. G. Yaakov, A. Duch, M. García-Rubio, J. Clotet, J. Jimenez, A. Aguilera, F. Posas, The Stress-activated Protein Kinase Hog1 Mediates S Phase Delay in Response to Osmostress. *MBoC* **20**, 3572–3582 (2009).

52. E. Radmaneshfar, D. Kaloriti, M. C. Gustin, N. A. R. Gow, A. J. P. Brown, C. Grebogi, M. C. Romano, M. Thiel, From START to FINISH: The Influence of Osmotic Stress on the Cell Cycle. *PLoS ONE* **8**, e68067 (2013).

53. M. Guo, A. F. Pegoraro, A. Mao, E. H. Zhou, P. R. Arany, Y. Han, D. T. Burnette, M. H. Jensen, K. E. Kasza, J. R. Moore, F. C. Mackintosh, J. J. Fredberg, D. J. Mooney, J. Lippincott-Schwartz, D. A. Weitz, Cell volume change through water efflux impacts cell stiffness and stem cell fate. *Proc. Natl. Acad. Sci. U.S.A.* **114** (2017).

54. P. Jorgensen, M. Tyers, How Cells Coordinate Growth and Division. *Current Biology* **14**, R1014–R1027 (2004).

55. J. R. Broach, Nutritional Control of Growth and Development in Yeast. *Genetics* **192**, 73–105 (2012).

56. M. J. Brauer, C. Huttenhower, E. M. Airoldi, R. Rosenstein, J. C. Matese, D. Gresham, V. M. Boer, O. G. Troyanskaya, D. Botstein, Coordination of Growth Rate, Cell Cycle, Stress Response, and Metabolic Activity in Yeast. *MBoC* **19**, 352–367 (2008).

57. M. Schaechter, O. MaalOe, N. O. Kjeldgaard, Dependency on Medium and Temperature of Cell Size and Chemical Composition during Balanced Growth of Salmonella typhimurium. *Journal of General Microbiology* **19**, 592–606 (1958).

58. N. O. Kjeldgaard, O. MaalOe, M. Schaechter, The Transition Between Different Physiological States During Balanced Growth of Salmonella typhimurium. *Journal of General Microbiology* **19**, 607–616 (1958).

59. S. Jun, F. Si, R. Pugatch, M. Scott, Fundamental principles in bacterial physiology—history, recent progress, and the future with focus on cell size control: a review. *Rep. Prog. Phys.* **81**, 056601 (2018).

60. A.-C. Chien, N. S. Hill, P. A. Levin, Cell Size Control in Bacteria. *Current Biology* **22**, R340–R349 (2012).

61. J. T. Sauls, S. E. Cox, Q. Do, V. Castillo, Z. Ghulam-Jelani, S. Jun, Control of Bacillus subtilis Replication Initiation during Physiological Transitions and Perturbations. *mBio* **10**, e02205-19 (2019).

62. L. Pérez-Hidalgo, S. Moreno, Nutrients control cell size. *Cell Cycle* **15**, 1655–1656 (2016).

63. P. Fantes, P. Nurse, Control of cell size at division in fission yeast by a growth-modulated size control over nuclear division. *Experimental Cell Research* **107**, 377–386 (1977).

64. E. Metzl-Raz, M. Kafri, G. Yaakov, I. Soifer, Y. Gurvich, N. Barkai, Principles of cellular resource allocation revealed by condition-dependent proteome profiling. *eLife* **6**, e28034 (2017).

65. C. Waldron, F. Lacroute, Effect of growth rate on the amounts of ribosomal and transfer ribonucleic acids in yeast. *J Bacteriol* **122**, 855–865 (1975).

66. D. R. Kief, J. R. Warner, Coordinate control of syntheses of ribosomal ribonucleic acid and ribosomal proteins during nutritional shift-up in *Saccharomyces cerevisiae*. *Mol. Cell. Biol.* **1**, 1007–1015 (1981).

67. R. Loewith, M. N. Hall, Target of Rapamycin (TOR) in Nutrient Signaling and Growth Control. *Genetics* **189**, 1177–1201 (2011).

68. J. Rohde, J. Heitman, M. E. Cardenas, The TOR Kinases Link Nutrient Sensing to Cell Growth. *Journal of Biological Chemistry* **276**, 9583–9586 (2001).

69. H.-X. Yuan, Y. Xiong, K.-L. Guan, Nutrient Sensing, Metabolism, and Cell Growth Control. *Molecular Cell* **49**, 379–387 (2013).

70. W. Palm, C. B. Thompson, Nutrient acquisition strategies of mammalian cells. *Nature* **546**, 234–242 (2017).

71. A. González, M. N. Hall, Nutrient sensing and TOR signaling in yeast and mammals. *EMBO J* **36**, 397–408 (2017).

72. J. C. Rathmell, M. G. V. Heiden, M. H. Harris, K. A. Frauwirth, C. B. Thompson, In the Absence of Extrinsic Signals, Nutrient Utilization by Lymphocytes Is Insufficient to Maintain Either Cell Size or Viability. *Molecular Cell* **6**, 683–692 (2000).

73. D. A. Foster, P. Yellen, L. Xu, M. Saqcena, Regulation of G1 Cell Cycle Progression: Distinguishing the Restriction Point from a Nutrient-Sensing Cell Growth Checkpoint(s). *Genes & Cancer* **1**, 1124–1131 (2010).

74. L. H. Hartwell, J. Culotti, J. R. Pringle, B. J. Reid, Genetic Control of the Cell Division Cycle in Yeast: A model to account for the order of cell cycle events is deduced from the phenotypes of yeast mutants. *Science* **183**, 46–51 (1974).

75. P. Jorgensen, I. Rupeš, J. R. Sharom, L. Schneper, J. R. Broach, M. Tyers, A dynamic transcriptional network communicates growth potential to ribosome synthesis and critical cell size. *Genes Dev.* **18**, 2491–2505 (2004).

76. M. Saqcena, D. Menon, D. Patel, S. Mukhopadhyay, V. Chow, D. A. Foster, Amino Acids and mTOR Mediate Distinct Metabolic Checkpoints in Mammalian G1 Cell Cycle. *PLoS ONE* **8**, e74157 (2013).

77. G. Johnston, J. Pringle, L. Hartwell, Coordination of growth with cell division in the yeast. *Experimental Cell Research* **105**, 79–98 (1977).

References

78. R. M. Leitao, D. R. Kellogg, The duration of mitosis and daughter cell size are modulated by nutrients in budding yeast. *Journal of Cell Biology* **216**, 3463–3470 (2017).

79. F. Parviz, W. Heideman, Growth-Independent Regulation of *CLN3* mRNA Levels by Nutrients in *Saccharomyces cerevisiae*. *J Bacteriol* **180**, 225–230 (1998).

80. M. Fischer, A. E. Schade, T. B. Branigan, G. A. Müller, J. A. DeCaprio, Coordinating gene expression during the cell cycle. *Trends in Biochemical Sciences*, S0968000422001487 (2022).

81. M. L. Whitfield, G. Sherlock, A. J. Saldanha, J. I. Murray, C. A. Ball, K. E. Alexander, J. C. Matese, C. M. Perou, M. M. Hurt, P. O. Brown, D. Botstein, Identification of Genes Periodically Expressed in the Human Cell Cycle and Their Expression in Tumors. *MBoC* **13**, 1977–2000 (2002).

82. S. Dolatabadi, J. Candia, N. Akrap, C. Vannas, T. Tesan Tomic, W. Losert, G. Landberg, P. Åman, A. Ståhlberg, Cell Cycle and Cell Size Dependent Gene Expression Reveals Distinct Subpopulations at Single-Cell Level. *Front. Genet.* **8** (2017).

83. P. T. Spellman, G. Sherlock, M. Q. Zhang, V. R. Iyer, K. Anders, M. B. Eisen, P. O. Brown, D. Botstein, B. Futcher, Comprehensive Identification of Cell Cycle–regulated Genes of the Yeast *Saccharomyces cerevisiae* by Microarray Hybridization. *MBoC* **9**, 3273–3297 (1998).

84. Z. Bar-Joseph, Z. Siegfried, M. Brandeis, B. Brors, Y. Lu, R. Eils, B. D. Dynlacht, I. Simon, Genome-wide transcriptional analysis of the human cell cycle identifies genes differentially regulated in normal and cancer cells. *Proc. Natl. Acad. Sci. U.S.A.* **105**, 955–960 (2008).

85. M. T. Laub, H. H. McAdams, T. Feldblyum, C. M. Fraser, L. Shapiro, Global Analysis of the Genetic Network Controlling a Bacterial Cell Cycle. *Science* **290**, 2144–2148 (2000).

86. R. J. Cho, M. Huang, M. J. Campbell, H. Dong, L. Steinmetz, L. Sapinoso, G. Hampton, S. J. Elledge, R. W. Davis, D. J. Lockhart, Transcriptional regulation and function during the human cell cycle. *Nat Genet* **27**, 48–54 (2001).

87. P. R. Eriksson, D. Ganguli, V. Nagarajavel, D. J. Clark, Regulation of Histone Gene Expression in Budding Yeast. *Genetics* **191**, 7–20 (2012).

88. C. F. Kurat, J. Recht, E. Radovani, T. Durbic, B. Andrews, J. Fillingham, Regulation of histone gene transcription in yeast. *Cell. Mol. Life Sci.* **71**, 599–613 (2014).

89. K.-L. Claude, D. Bureik, D. Chatzitheodoridou, P. Adarska, A. Singh, K. M. Schmoller, Transcription coordinates histone amounts and genome content. *Nat Commun* **12**, 4202 (2021).

90. M. P. Swaffer, J. Kim, D. Chandler-Brown, M. Langhinrichs, G. K. Marinov, W. J. Greenleaf, A. Kundaje, K. M. Schmoller, J. M. Skotheim, Transcriptional and chromatin-based partitioning mechanisms uncouple protein scaling from cell size. *Molecular Cell* **81**, 4861-4875.e7 (2021).

91. M. C. Lanz, E. Zatulovskiy, M. P. Swaffer, L. Zhang, I. Ilerten, S. Zhang, D. S. You, G. Marinov, P. McAlpine, J. E. Elias, J. M. Skotheim, Increasing cell size remodels the proteome and promotes senescence. *Mol Cell* **82**, 3255-3269.e8 (2022).

92. R. K. Singh, D. Liang, U. R. Gajjalaiahvari, M.-H. M. Kabbaj, J. Paik, A. Gunjan, Excess histone levels mediate cytotoxicity via multiple mechanisms. *Cell Cycle* **9**, 4236–4244 (2010).

References

93. D. Maya Miles, X. Peñate, T. Sanmartín Olmo, F. Jourquin, M. C. Muñoz Centeno, M. Mendoza, M.-N. Simon, S. Chavez, V. Geli, High levels of histones promote whole-genome-duplications and trigger a Swe1WEE1-dependent phosphorylation of Cdc28CDK1. *eLife* **7**, e35337 (2018).

94. S. M. Burgess, T. Powers, J. C. Mell, "Budding Yeast *S accharomyces Cerevisiae* as a Model Genetic Organism" in *eLS*, John Wiley & Sons, Ltd, Ed. (Wiley, ed. 1, 2017; https://onlinelibrary.wiley.com/doi/10.1002/9780470015902.a0000821.pub2), pp. 1–12.

95. H. Karathia, E. Vilaprinyo, A. Sorribas, R. Alves, *Saccharomyces cerevisiae* as a Model Organism: A Comparative Study. *PLoS ONE* **6**, e16015 (2011).

96. S. Mohammadi, B. Saberidokht, S. Subramaniam, A. Grama, Scope and limitations of yeast as a model organism for studying human tissue-specific pathways. *BMC Syst Biol* **9**, 96 (2015).

97. A. A. Duina, M. E. Miller, J. B. Keeney, Budding Yeast for Budding Geneticists: A Primer on the *Saccharomyces cerevisiae* Model System. *Genetics* **197**, 33–48 (2014).

98. K. Forslund, F. Schreiber, N. Thanintorn, E. L. L. Sonnhammer, OrthoDisease: tracking disease gene orthologs across 100 species. *Briefings in Bioinformatics* **12**, 463–473 (2011).

99. P. K. Hanson, *Saccharomyces cerevisiae* : A Unicellular Model Genetic Organism of Enduring Importance. *CP Essential Lab Tech* **16** (2018).

100. G. A. Hoffman, T. R. Garrison, H. G. Dohlman, "Analysis of RGS Proteins in *Saccharomyces cerevisiae*" in *Methods in Enzymology* (Elsevier, 2002; https://linkinghub.elsevier.com/retrieve/pii/S0076687902447441)vol. 344, pp. 617–631.

101. A. Goffeau, 1996: a vintage year for yeast and Yeast. *Yeast* **12**, 1603–1605 (1996).

102. G. Giaever, A. M. Chu, L. Ni, C. Connelly, L. Riles, S. Véronneau, S. Dow, A. Lucau-Danila, K. Anderson, B. André, A. P. Arkin, A. Astromoff, M. El Bakkoury, R. Bangham, R. Benito, S. Brachat, S. Campanaro, M. Curtiss, K. Davis, A. Deutschbauer, K.-D. Entian, P. Flaherty, F. Foury, D. J. Garfinkel, M. Gerstein, D. Gotte, U. Güldener, J. H. Hegemann, S. Hempel, Z. Herman, D. F. Jaramillo, D. E. Kelly, S. L. Kelly, P. Kötter, D. LaBonte, D. C. Lamb, N. Lan, H. Liang, H. Liao, L. Liu, C. Luo, M. Lussier, R. Mao, P. Menard, S. L. Ooi, J. L. Revuelta, C. J. Roberts, M. Rose, P. Ross-Macdonald, B. Scherens, G. Schimmack, B. Shafer, D. D. Shoemaker, S. Sookhai-Mahadeo, R. K. Storms, J. N. Strathern, G. Valle, M. Voet, G. Volckaert, C. Wang, T. R. Ward, J. Wilhelmy, E. A. Winzeler, Y. Yang, G. Yen, E. Youngman, K. Yu, H. Bussey, J. D. Boeke, M. Snyder, P. Philippsen, R. W. Davis, M. Johnston, Functional profiling of the *Saccharomyces cerevisiae* genome. *Nature* **418**, 387–391 (2002).

103. G. M. Jones, J. Stalker, S. Humphray, A. West, T. Cox, J. Rogers, I. Dunham, G. Prelich, A systematic library for comprehensive overexpression screens in *Saccharomyces cerevisiae*. *Nat Methods* **5**, 239–241 (2008).

104. S. Ghaemmaghami, W.-K. Huh, K. Bower, R. W. Howson, A. Belle, N. Dephoure, E. K. O'Shea, J. S. Weissman, Global analysis of protein expression in yeast. *Nature* **425**, 737–741 (2003).

105. R. J. Cho, M. J. Campbell, E. A. Winzeler, L. Steinmetz, A. Conway, L. Wodicka, T. G. Wolfsberg, A. E. Gabrielian, D. Landsman, D. J. Lockhart, R. W. Davis, A Genome-Wide Transcriptional Analysis of the Mitotic Cell Cycle. *Molecular Cell* **2**, 65–73 (1998).

106. H. Zhu, M. Bilgin, R. Bangham, D. Hall, A. Casamayor, P. Bertone, N. Lan, R. Jansen, S. Bidlingmaier, T. Houfek, T. Mitchell, P. Miller, R. A. Dean, M. Gerstein, M. Snyder, Global Analysis of Protein Activities Using Proteome Chips. *Science* **293**, 2101–2105 (2001).

107. S. G. Villas-Bôas, J. F. Moxley, M. Åkesson, G. Stephanopoulos, J. Nielsen, High-throughput metabolic state analysis: the missing link in integrated functional genomics of yeasts. *Biochemical Journal* **388**, 669–677 (2005).

108. D. Botstein, G. R. Fink, Yeast: An Experimental Organism for 21st Century Biology. *Genetics* **189**, 695–704 (2011).

109. H. Feldmann, Ed., "Yeast Metabolism" in *Yeast* (Wiley, ed. 1, 2012; https://onlinelibrary.wiley.com/doi/10.1002/9783527659180.ch3), pp. 25–58.

110. B. Turcotte, X. B. Liang, F. Robert, N. Soontorngun, Transcriptional regulation of nonfermentable carbon utilization in budding yeast. *FEMS Yeast Research* **10**, 2–13 (2010).

111. J. A. Barnett, "The Utilization of Sugars by Yeasts" in *Advances in Carbohydrate Chemistry and Biochemistry* (Elsevier, 1976; https://linkinghub.elsevier.com/retrieve/pii/S0065231808603376)vol. 32, pp. 125–234.

112. T. Pfeiffer, A. Morley, An evolutionary perspective on the Crabtree effect. *Front. Mol. Biosci.* **1** (2014).

113. H. G. Crabtree, Observations on the carbohydrate metabolism of tumours. *Biochemical Journal* **23**, 536–545 (1929).

114. P. A. Frey, The Leloir pathway: a mechanistic imperative for three enzymes to change the stereochemical configuration of a single carbon in galactose. *FASEB J* **10**, 461–470 (1996).

115. M. Casal, H. Cardoso, C. Leao, Mechanisms regulating the transport of acetic acid in *Saccharomyces cerevisiae*. *Microbiology* **142**, 1385–1390 (1996).

116. J. García-Martínez, K. Troulé, S. Chávez, J. E. Pérez-Ortín, Growth rate controls mRNA turnover in steady and non-steady states. *RNA Biology* **13**, 1175–1181 (2016).

117. J. García-Martínez, L. Delgado-Ramos, G. Ayala, V. Pelechano, D. A. Medina, F. Carrasco, R. González, E. Andrés-León, L. Steinmetz, J. Warringer, S. Chávez, J. E. Pérez-Ortín, The cellular growth rate controls overall mRNA turnover, and modulates either transcription or degradation rates of particular gene regulons. *Nucleic Acids Res* **44**, 3643–3658 (2016).

118. D. O. Morgan, *The Cell Cycle: Principles of Control* (Published by New Science Press in association with Oxford University Press ; Distributed inside North America by Sinauer Associates, Publishers, London : Sunderland, MA, 2007) *Primers in biology*.

119. S. Sun, D. Gresham, Cellular quiescence in budding yeast. *Yeast* **38**, 12–29 (2021).

120. L. Merlini, O. Dudin, S. G. Martin, Mate and fuse: how yeast cells do it. *Open Biol.* **3**, 130008 (2013).

121. A. M. Neiman, Sporulation in the Budding Yeast *Saccharomyces cerevisiae*. *Genetics* **189**, 737–765 (2011).

References

122. I. Freidkin, D. J. Katcoff, Specific distribution of the *Saccharomyces cerevisiae* linker histone homolog HHO1p in the chromatin. *Nucleic Acids Research* **29**, 4043–4051 (2001).

123. M. A. Osley, THE REGULATION OF HISTONE SYNTHESIS IN THE CELL CYCLE. *Annu. Rev. Biochem.* **60**, 827–861 (1991).

124. L. M. Hereford, M. A. Osley, J. R. Ludwig II, C. S. McLaughlin, Cell-cycle regulation of yeast histone mRNA. *Cell* **24**, 367–375 (1981).

125. L. Hereford, K. Fahrner, J. Woolford, M. Rosbash, D. B. Kaback, Isolation of yeast histone genes H2A and H2B. *Cell* **18**, 1261–1271 (1979).

126. M. M. Smith, K. Murray, Yeast H3 and H4 histone messenger RNAs are transcribed from two non-allelic gene sets. *Journal of Molecular Biology* **169**, 641–661 (1983).

127. P. R. Eriksson, G. Mendiratta, N. B. McLaughlin, T. G. Wolfsberg, L. Mariño-Ramírez, T. A. Pompa, M. Jainerin, D. Landsman, C.-H. Shen, D. J. Clark, Global Regulation by the Yeast Spt10 Protein Is Mediated through Chromatin Structure and the Histone Upstream Activating Sequence Elements. *Molecular and Cellular Biology* **25**, 9127–9137 (2005).

128. P. R. Eriksson, D. Ganguli, D. J. Clark, Spt10 and Swi4 Control the Timing of Histone H2A/H2B Gene Activation in Budding Yeast. *Mol Cell Biol* **31**, 557–572 (2011).

129. E. M. Green, A. J. Antczak, A. O. Bailey, A. A. Franco, K. J. Wu, J. R. Yates, P. D. Kaufman, Replication-Independent Histone Deposition by the HIR Complex and Asf1. *Current Biology* **15**, 2044–2049 (2005).

130. J. Fillingham, P. Kainth, J.-P. Lambert, H. van Bakel, K. Tsui, L. Peña-Castillo, C. Nislow, D. Figeys, T. R. Hughes, J. Greenblatt, B. J. Andrews, Two-Color Cell Array Screen Reveals Interdependent Roles for Histone Chaperones and a Chromatin Boundary Regulator in Histone Gene Repression. *Molecular Cell* **35**, 340–351 (2009).

131. M. A. Osley, D. Lycan, *trans*-Acting Regulatory Mutations That Alter Transcription of *Saccharomyces cerevisiae* Histone Genes. *Molecular and Cellular Biology* **7**, 4204–4210 (1987).

132. C. Bruhn, A. Ajazi, E. Ferrari, M. C. Lanz, R. Batrin, R. Choudhary, A. Walvekar, S. Laxman, M. P. Longhese, E. Fabre, M. B. Smolka, M. Foiani, The Rad53CHK1/CHK2-Spt21NPAT and Tel1ATM axes couple glucose tolerance to histone dosage and subtelomeric silencing. *Nat Commun* **11**, 4154 (2020).

133. A. Gunjan, A. Verreault, A Rad53 Kinase-Dependent Surveillance Mechanism that Regulates Histone Protein Levels in *S. cerevisiae*. *Cell* **115**, 537–549 (2003).

134. S. Marguerat, J. Bähler, Coordinating genome expression with cell size. *Trends in Genetics* **28**, 560–565 (2012).

135. J. R. Wiśniewski, M. Y. Hein, J. Cox, M. Mann, A “proteomic ruler” for protein copy number and concentration estimation without spike-in standards. *Mol Cell Proteomics* **13**, 3497–3506 (2014).

136. K. M. Schmoller, J. M. Skotheim, The Biosynthetic Basis of Cell Size Control. *Trends Cell Biol* **25**, 793–802 (2015).

References

137. M. Bhagwat, S. Nagar, P. Kaur, R. Mehta, I. Vancurova, A. Vancura, Replication stress inhibits synthesis of histone mRNAs in yeast by removing Spt10p and Spt21p from the histone promoters. *Journal of Biological Chemistry* **297**, 101246 (2021).

138. L. A. Prado Barragán, J. J. B. Figueroa, L. V. Rodríguez Durán, C. N. Aguilar González, C. Hennigs, "Fermentative Production Methods" in *Biotransformation of Agricultural Waste and By-Products* (Elsevier, 2016; https://linkinghub.elsevier.com/retrieve/pii/B9780128036228000070), pp. 189–217.

139. M. Werner-Washburne, E. Braun, G. C. Johnston, R. A. Singer, Stationary phase in the yeast *Saccharomyces cerevisiae*. *Microbiol Rev* **57**, 383–401 (1993).

140. H. Inoue, H. Nojima, H. Okayama, High efficiency transformation of Escherichia coli with plasmids. *Gene* **96**, 23–28 (1990).

141. V. V. Kushnirov, Rapid and reliable protein extraction from yeast. *Yeast* **16**, 857–860 (2000).

142. V. Pelechano, J. E. Pérez-Ortín, The transcriptional inhibitor thiolutin blocks mRNA degradation in yeast. *Yeast* **25**, 85–92 (2008).

143. M. Örd, R. Venta, K. Möll, E. Valk, M. Loog, Cyclin-Specific Docking Mechanisms Reveal the Complexity of M-CDK Function in the Cell Cycle. *Molecular Cell* **75**, 76-89.e3 (2019).

144. F. Padovani, B. Mairhörmann, P. Falter-Braun, J. Lengefeld, K. M. Schmoller, Segmentation, tracking and cell cycle analysis of live-cell imaging data with Cell-ACDC. *BMC Biol* **20**, 174 (2022).

145. N. Dietler, M. Minder, V. Gligorovski, A. M. Economou, D. A. H. L. Joly, A. Sadeghi, C. H. M. Chan, M. Koziński, M. Weigert, A.-F. Bitbol, S. J. Rahi, A convolutional neural network segments yeast microscopy images with high accuracy. *Nat Commun* **11**, 5723 (2020).

146. S. van der Walt, J. L. Schönberger, J. Nunez-Iglesias, F. Boulogne, J. D. Warner, N. Yager, E. Gouillart, T. Yu, scikit-image: image processing in Python. *PeerJ* **2**, e453 (2014).

147. D. Shortle, J. E. Haber, D. Botstein, Lethal Disruption of the Yeast Actin Gene by Integrative DNA Transformation. *Science* **217**, 371–373 (1982).

148. J. E. Garbarino, I. R. Gibbons, Expression and genomic analysis of midasin, a novel and highly conserved AAA protein distantly related to dynein. *BMC Genomics* **3**, 18 (2002).

149. J. Schindelin, I. Arganda-Carreras, E. Frise, V. Kaynig, M. Longair, T. Pietzsch, S. Preibisch, C. Rueden, S. Saalfeld, B. Schmid, J.-Y. Tinevez, D. J. White, V. Hartenstein, K. Eliceiri, P. Tomancak, A. Cardona, Fiji: an open-source platform for biological-image analysis. *Nat Methods* **9**, 676–682 (2012).

150. A. Doncic, U. Eser, O. Atay, J. M. Skotheim, An Algorithm to Automate Yeast Segmentation and Tracking. *PLoS ONE* **8**, e57970 (2013).

151. D. Chandler-Brown, K. M. Schmoller, Y. Winetraub, J. M. Skotheim, The Adder Phenomenon Emerges from Independent Control of Pre- and Post-Start Phases of the Budding Yeast Cell Cycle. *Current Biology* **27**, 2774-2783.e3 (2017).

152. M. McLean, A. V. Hubberstey, D. J. Bouman, N. Pece, P. Mastrangelo, A. G. Wildeman, Organization of the *Saccharomyces cerevisiae* actin gene UAS: functional significance of

reiterated REB1 binding sites and AT-rich elements: REB1 and MCB control of the yeast actin promoter. *Molecular Microbiology* **18**, 605–614 (1995).

153. J. R. S. Newman, S. Ghaemmaghami, J. Ihmels, D. K. Breslow, M. Noble, J. L. DeRisi, J. S. Weissman, Single-cell proteomic analysis of *S. cerevisiae* reveals the architecture of biological noise. *Nature* **441**, 840–846 (2006).

154. J. Xia, B. J. Sánchez, Y. Chen, K. Campbell, S. Kasvandik, J. Nielsen, Proteome allocations change linearly with the specific growth rate of *Saccharomyces cerevisiae* under glucose limitation. *Nat Commun* **13**, 2819 (2022).

155. R. Milo, What is the total number of protein molecules per cell volume? A call to rethink some published values. *BioEssays* **35**, 1050–1055 (2013).

156. O. Griesbeck, G. S. Baird, R. E. Campbell, D. A. Zacharias, R. Y. Tsien, Reducing the Environmental Sensitivity of Yellow Fluorescent Protein. *Journal of Biological Chemistry* **276**, 29188–29194 (2001).

157. R. Higuchi-Sanabria, E. J. Garcia, D. Tomoiaga, E. L. Munteanu, P. Feinstein, L. A. Pon, Characterization of Fluorescent Proteins for Three- and Four-Color Live-Cell Imaging in *S. cerevisiae*. *PLoS ONE* **11**, e0146120 (2016).

158. P. Guerra, L.-A. Vuillemenot, B. Rae, V. Ladyhina, A. Milias-Argeitis, Systematic *In Vivo* Characterization of Fluorescent Protein Maturation in Budding Yeast. *ACS Synth. Biol.* **11**, 1129–1141 (2022).

159. K. A. Curran, A. S. Karim, A. Gupta, H. S. Alper, Use of expression-enhancing terminators in *Saccharomyces cerevisiae* to increase mRNA half-life and improve gene expression control for metabolic engineering applications. *Metabolic Engineering* **19**, 88–97 (2013).

160. Y. Ito, G. Terai, M. Ishigami, N. Hashiba, Y. Nakamura, T. Bamba, R. Kumokita, T. Hasunuma, K. Asai, J. Ishii, A. Kondo, Exchange of endogenous and heterogeneous yeast terminators in *Pichia pastoris* to tune mRNA stability and gene expression. *Nucleic Acids Research* **48**, 13000–13012 (2020).

161. J. E. Pérez-Ortín, P. M. Alepuz, J. Moreno, Genomics and gene transcription kinetics in yeast. *Trends in Genetics* **23**, 250–257 (2007).

162. S. Das, D. Sarkar, B. Das, The interplay between transcription and mRNA degradation in *Saccharomyces cerevisiae*. *Microb Cell* **4**, 212–228 (2017).

163. A. Jimenez, D. J. Tipper, J. Davies, Mode of Action of Thiolutin, an Inhibitor of Macromolecular Synthesis in *Saccharomyces cerevisiae*. *Antimicrob Agents Chemother* **3**, 729–738 (1973).

164. T. Trcek, D. R. Larson, A. Moldón, C. C. Query, R. H. Singer, Single-Molecule mRNA Decay Measurements Reveal Promoter- Regulated mRNA Stability in Yeast. *Cell* **147**, 1484–1497 (2011).

165. D. Zenklusen, D. R. Larson, R. H. Singer, Single-RNA counting reveals alternative modes of gene expression in yeast. *Nat Struct Mol Biol* **15**, 1263–1271 (2008).

166. B. Futcher, G. I. Latter, P. Monardo, C. S. McLaughlin, J. I. Garrels, A Sampling of the Yeast Proteome. *Mol Cell Biol* **19**, 7357–7368 (1999).

References

167. M. A. Osley, J. Gould, S. Kim, M. Kane, L. Hereford, Identification of sequences in a yeast histone promoter involved in periodic transcription. *Cell* **45**, 537–544 (1986).

168. M. Costanzo, J. L. Nishikawa, X. Tang, J. S. Millman, O. Schub, K. Breitkreuz, D. Dewar, I. Rupes, B. Andrews, M. Tyers, CDK Activity Antagonizes Whi5, an Inhibitor of G1/S Transcription in Yeast. *Cell* **117**, 899–913 (2004).

169. A. Amoussouvi, L. Teufel, M. Reis, M. Seeger, J. K. Schlichting, G. Schreiber, A. Herrmann, E. Klipp, Transcriptional timing and noise of yeast cell cycle regulators—a single cell and single molecule approach. *npj Syst Biol Appl* **4**, 17 (2018).

170. I. V. Kukhtevich, N. Lohrberg, F. Padovani, R. Schneider, K. M. Schmoller, Cell size sets the diameter of the budding yeast contractile ring. *Nat Commun* **11**, 2952 (2020).

171. K. M. Schmoller, J. J. Turner, M. Kõivomägi, J. M. Skotheim, Dilution of the cell cycle inhibitor Whi5 controls budding-yeast cell size. *Nature* **526**, 268–272 (2015).

172. R. A. M. de Bruin, W. H. McDonald, T. I. Kalashnikova, J. Yates, C. Wittenberg, Cln3 Activates G1-Specific Transcription via Phosphorylation of the SBF Bound Repressor Whi5. *Cell* **117**, 887–898 (2004).

173. F. Mueller, A. Senecal, K. Tantale, H. Marie-Nelly, N. Ly, O. Collin, E. Basyuk, E. Bertrand, X. Darzacq, C. Zimmer, FISH-quant: automatic counting of transcripts in 3D FISH images. *Nat Methods* **10**, 277–278 (2013).

174. S. Dvir, L. Velten, E. Sharon, D. Zeevi, L. B. Carey, A. Weinberger, E. Segal, Deciphering the rules by which 5′-UTR sequences affect protein expression in yeast. *Proc. Natl. Acad. Sci. U.S.A.* **110** (2013).

175. L. W. Barrett, S. Fletcher, S. D. Wilton, Regulation of eukaryotic gene expression by the untranslated gene regions and other non-coding elements. *Cell. Mol. Life Sci.* **69**, 3613–3634 (2012).

176. P. R. Araujo, K. Yoon, D. Ko, A. D. Smith, M. Qiao, U. Suresh, S. C. Burns, L. O. F. Penalva, Before It Gets Started: Regulating Translation at the 5′ UTR. *Comparative and Functional Genomics* **2012**, 1–8 (2012).

177. F. Mignone, C. Gissi, S. Liuni, G. Pesole, Untranslated regions of mRNAs. *Genome Biol* **3**, reviews0004.1 (2002).

178. T. Tuller, E. Ruppin, M. Kupiec, Properties of untranslated regions of the *S. cerevisiae* genome. *BMC Genomics* **10**, 391 (2009).

179. G. Pesole, F. Mignone, C. Gissi, G. Grillo, F. Licciulli, S. Liuni, Structural and functional features of eukaryotic mRNA untranslated regions. *Gene* **276**, 73–81 (2001).

180. M. Kozak, Point mutations define a sequence flanking the AUG initiator codon that modulates translation by eukaryotic ribosomes. *Cell* **44**, 283–292 (1986).

181. Y. Yun, T. M. A. Adesanya, R. D. Mitra, A systematic study of gene expression variation at single-nucleotide resolution reveals widespread regulatory roles for uAUGs. *Genome Res.* **22**, 1089–1097 (2012).

182. W. Ding, J. Cheng, D. Guo, L. Mao, J. Li, L. Lu, Y. Zhang, J. Yang, H. Jiang, Engineering the 5′ UTR-Mediated Regulation of Protein Abundance in Yeast Using Nucleotide Sequence Activity Relationships. *ACS Synth. Biol.* **7**, 2709–2714 (2018).

183. P. Eisenhut, A. Mebrahtu, M. Moradi Barzadd, N. Thalén, G. Klanert, M. Weinguny, A. Sandegren, C. Su, D. Hatton, N. Borth, J. Rockberg, Systematic use of synthetic 5′-UTR RNA structures to tune protein translation improves yield and quality of complex proteins in mammalian cell factories. *Nucleic Acids Research* **48**, e119–e119 (2020).

184. H. A. Meijer, A. A. M. Thomas, Control of eukaryotic protein synthesis by upstream open reading frames in the 5′-untranslated region of an mRNA. *Biochemical Journal* **367**, 1–11 (2002).

185. M. P. Swaffer, G. K. Marinov, H. Zheng, A. W. Jones, J. Greenwood, A. Kundaje, A. P. Snijders, W. J. Greenleaf, R. Reyes-Lamothe, J. M. Skotheim, RNA polymerase II dynamics and mRNA stability feedback determine mRNA scaling with cell size. *bioRxiv*, 2021.09.20.461005 (2021).

186. R. K. Singh, M.-H. M. Kabbaj, J. Paik, A. Gunjan, Histone levels are regulated by phosphorylation and ubiquitylation-dependent proteolysis. *Nat Cell Biol* **11**, 925–933 (2009).

187. X. Zhao, E. G. D. Muller, R. Rothstein, A Suppressor of Two Essential Checkpoint Genes Identifies a Novel Protein that Negatively Affects dNTP Pools. *Molecular Cell* **2**, 329–340 (1998).

188. B. Smets, R. Ghillebert, P. De Snijder, M. Binda, E. Swinnen, C. De Virgilio, J. Winderickx, Life in the midst of scarcity: adaptations to nutrient availability in *Saccharomyces cerevisiae*. *Curr Genet* **56**, 1–32 (2010).

189. R. J. Duronio, W. F. Marzluff, Coordinating cell cycle-regulated histone gene expression through assembly and function of the Histone Locus Body. *RNA Biology* **14**, 726–738 (2017).

190. W. F. Marzluff, R. J. Duronio, Histone mRNA expression: multiple levels of cell cycle regulation and important developmental consequences. *Curr Opin Cell Biol* **14**, 692–699 (2002).

191. X.-M. Sun, A. Bowman, M. Priestman, F. Bertaux, A. Martinez-Segura, W. Tang, C. Whilding, D. Dormann, V. Shahrezaei, S. Marguerat, Size-Dependent Increase in RNA Polymerase II Initiation Rates Mediates Gene Expression Scaling with Cell Size. *Current Biology* **30**, 1217-1230.e7 (2020).

192. P. Shah, Y. Ding, M. Niemczyk, G. Kudla, J. B. Plotkin, Rate-Limiting Steps in Yeast Protein Translation. *Cell* **153**, 1589–1601 (2013).

193. D. Greenbaum, C. Colangelo, K. Williams, M. Gerstein, Comparing protein abundance and mRNA expression levels on a genomic scale. *Genome Biol*. **4**, 117 (2003).

194. P.-J. Lahtvee, B. J. Sánchez, A. Smialowska, S. Kasvandik, I. E. Elsemman, F. Gatto, J. Nielsen, Absolute Quantification of Protein and mRNA Abundances Demonstrate Variability in Gene-Specific Translation Efficiency in Yeast. *Cell Systems* **4**, 495-504.e5 (2017).

195. S. P. Gygi, Y. Rochon, B. R. Franza, R. Aebersold, Correlation between Protein and mRNA Abundance in Yeast. *Mol Cell Biol* **19**, 1720–1730 (1999).

196. N. Selevsek, C.-Y. Chang, L. C. Gillet, P. Navarro, O. M. Bernhardt, L. Reiter, L.-Y. Cheng, O. Vitek, R. Aebersold, Reproducible and Consistent Quantification of the *Saccharomyces*

cerevisiae Proteome by SWATH-mass spectrometry *. *Molecular & Cellular Proteomics* **14**, 739–749 (2015).

197. M. Choder, mRNA imprinting: Additional level in the regulation of gene expression. *Cellular Logistics* **1**, 37–40 (2011).

198. N. Dahan, M. Choder, The eukaryotic transcriptional machinery regulates mRNA translation and decay in the cytoplasm. *Biochimica et Biophysica Acta (BBA) - Gene Regulatory Mechanisms* **1829**, 169–173 (2013).

199. L. Harel-Sharvit, N. Eldad, G. Haimovich, O. Barkai, L. Duek, M. Choder, RNA Polymerase II Subunits Link Transcription and mRNA Decay to Translation. *Cell* **143**, 552–563 (2010).

200. A. Bregman, M. Avraham-Kelbert, O. Barkai, L. Duek, A. Guterman, M. Choder, Promoter Elements Regulate Cytoplasmic mRNA Decay. *Cell* **147**, 1473–1483 (2011).

201. V. Goler-Baron, M. Selitrennik, O. Barkai, G. Haimovich, R. Lotan, M. Choder, Transcription in the nucleus and mRNA decay in the cytoplasm are coupled processes. *Genes Dev.* **22**, 2022–2027 (2008).

202. S. Richard, L. Gross, J. Fischer, K. Bendalak, T. Ziv, S. Urim, M. Choder, Numerous Post-translational Modifications of RNA Polymerase II Subunit Rpb4/7 Link Transcription to Post-transcriptional Mechanisms. *Cell Reports* **34**, 108578 (2021).

203. R. Lotan, V. G. Bar-On, L. Harel-Sharvit, L. Duek, D. Melamed, M. Choder, The RNA polymerase II subunit Rpb4p mediates decay of a specific class of mRNAs. *Genes Dev.* **19**, 3004–3016 (2005).

204. I. Gupta, Z. Villanyi, S. Kassem, C. Hughes, O. O. Panasenko, L. M. Steinmetz, M. A. Collart, Translational Capacity of a Cell Is Determined during Transcription Elongation via the Ccr4-Not Complex. *Cell Reports* **15**, 1782–1794 (2016).

205. M. Catala, S. Abou Elela, Promoter-dependent nuclear RNA degradation ensures cell cycle-specific gene expression. *Commun Biol* **2**, 211 (2019).

206. N. Kaplan, I. K. Moore, Y. Fondufe-Mittendorf, A. J. Gossett, D. Tillo, Y. Field, E. M. LeProust, T. R. Hughes, J. D. Lieb, J. Widom, E. Segal, The DNA-encoded nucleosome organization of a eukaryotic genome. *Nature* **458**, 362–366 (2009).

207. R. V. Chereji, T. D. Bryson, S. Henikoff, Quantitative MNase-seq accurately maps nucleosome occupancy levels. *Genome Biol* **20**, 198 (2019).

208. L. Y. Chan, C. F. Mugler, S. Heinrich, P. Vallotton, K. Weis, Non-invasive measurement of mRNA decay reveals translation initiation as the major determinant of mRNA stability. *eLife* **7**, e32536 (2018).

209. J. D. Barrass, J. E. A. Reid, Y. Huang, R. D. Hector, G. Sanguinetti, J. D. Beggs, S. Granneman, Transcriptome-wide RNA processing kinetics revealed using extremely short 4tU labeling. *Genome Biol* **16**, 282 (2015).

210. S. Kwon, Single-molecule fluorescence in situ hybridization: Quantitative imaging of single RNA molecules. *BMB Reports* **46**, 65–72 (2013).

References

211. L. Cai, B. M. Sutter, B. Li, B. P. Tu, Acetyl-CoA Induces Cell Growth and Proliferation by Promoting the Acetylation of Histones at Growth Genes. *Molecular Cell* **42**, 426–437 (2011).

212. N. T. Ingolia, J. A. Hussmann, J. S. Weissman, Ribosome Profiling: Global Views of Translation. *Cold Spring Harb Perspect Biol* **11**, a032698 (2019).

213. P. Zhou, “Determining Protein Half-Lives” in *Signal Transduction Protocols* (Humana Press, New Jersey, 2004; http://link.springer.com/10.1385/1-59259-816-1:067) vol. 284, pp. 067–078.